A COMPARISON OF BRINE EVAPORATION RATES UNDER CONTROLLED CONDITIONS IN A LABORATORY

by

Denzil Bent

Department of Earth Sciences

Faculty of Natural Sciences, University of the Western Cape

Supervisors

Prof. L.F, Petrik and Mr A, Scheepers

DECLARATION

I declare that "**A COMPARISON OF EVAPORATION RATES UNDER CONTROLLED CONDITION IN A LABAROTORY"** is my own work and has under no circumstances been submitted for any degree or examined in any other university. All sources or quotes used have been indicated and acknowledge by complete references.

Full name: Denzil Bent Date: 19 October 2017

Signed  …….

ACKNOWLEDGEMENT

- I am forever in debt by Professor Leslie Petrik for her unconditional support as a supervisor and for providing all the necessary funding for the completion of my qualification. I am grateful to Prof Petrik for her continuous motivation and for the exposure to other learning opportunities during my studies.

- I would like to thank Mr Theo Scheepers for his role as a supervisor during his tenure in the Environmental and Water Science Department at University of the Western Cape. I fully enjoyed your company and appreciate all your contribution towards my undergraduate and postgraduate qualifications.

- A special mention is reserved for Dr Jacobus Nel who has set everything in motion. Thank you for the support and contribution towards my studies and for my initial involvement with the WRC project.

- I thank Dr Ojo Olanrewaju Fatoba and Dr Godfrey Madzivire from the Environmental Nanoscience Department at the University of the Western Cape for their guidance and input throughout my studies.

- I would like to thank Rallston Richards, Ilse Wells and Shamiel Davids for their technical input and assistance. My sincerest gratitude goes the administrative staff Many Naidoo, Averil Abbott and Vanessa Kellerman for their contribution at the at the University of the Western Cape.

- I want to thank Clinton Naicker from Anglo-American at the water reclamation plant in eMalahleni, Mpumalanga South Africa, for the provision of samples for my studies.

- I also like to thank the Water Research Commission for their funding and collaborative effort with the University of the Western Cape especially the Environmental Nanoscience Group and Environmental and Water Science Group.

I would like to thank the Almighty God for providing me with the knowledge, strength and perseverance to complete my daily tasks during my studies. I thank my entire family and friends for their prayers, unconditional support and patience during my studies. Your motivation and words of encouragement has not gone unnoticed.

ABBREVIATIONS

AMD Acid Mine Drainage

Cp Specific Heat (Constant pressure)

DWAS Department of Water Affairs and Sanitation

EC Electrical conductivity

EFC Eutectic Freeze Crystallisation

EWRP eMalahleni Water Reclamation Plant

Ksp Solubility constant product

IR Infrared

*m*S milli-Siemens

RO Reverse Osmosis

RWQOs Resource Water Quality Objectives

SANS South African National Standards

SAWS South African Weather Service

UNEP United Nation Environmental Program

USGS United States Geological Survey

*u*S Micro-Siemens

WMA Water Management Area

GLOSSARY

DESALINATION

Desalination is the process where water molecules are separated from a saline water source. This process can be executed by means of either a phase change or using a membrane recovery system. Common examples of desalination plants that are set up for phase change can be vapour compression (VC) and multi stage boiling (MSB). Reverse osmosis and Electrodialysis is popular for the liquid phase process (Ahmed et al, 2000).

MONOATOMIC AND POLYATOMIC IONS

Monoatomic ion such as NaCl is a charged particle that consists of a single atom. The charge on the ion can either be positive or negative. Polyatomic ions contain more than one atom and are known as molecular ions. Acting as a one unit, the covalently bond atoms will have a single charge. Most common polyatomic ions found in aqueous solutions are SO_4, NO_3, CO_3 and PO_4 (Beran, 2014).

TEMPERATURE

Temperature is defined as a system property which is linked to the quantity of thermal energy of an object. In general it is a measurement of how cold or hot the measured object is relative to the environment or measuring instrument. There are mainly 3 common scales, Fahrenheit (°F), Degree Celsius (°C) and Kelvin (K) which is the SI unit for temperature (Sandler, 1989).

RELATIVE HUMIDITY

Relative humidity (h) is referred to as the amount of moisture in the air. Under the same temperature it is the ratio between the saturated vapour pressure (e) and the actual vapour pressure (e) (Monteith and Unsworth, 2008). The SI unit for relative humidity is as percentage in ratio difference.

$$h = \frac{e}{e_s} \times 100\% \quad \text{.....Equation 1}$$

ABSTRACT

There are growing concerns around the environmental issues related to processed water as the demand for potable water is on the increase in South Africa. Effluents discharged from various sectors such as water treatment facilities pose a constant threat to the environment and natural water resources, including rivers and groundwater due to their poor chemical and physical composition. As a result, the demand for predicting the elevated concentrations of salts in a spatial and temporal dimension is constantly growing. The effluent at the eMalahleni water reclamation plant in Mpumalanga, South Africa, is being processed through a triple reverse osmosis that improves the water quality of the mine water to potable standards. Two water quality streams emerge from this process, i.e. a potable standard and the other a brine concentrate which is stored in ponds. Brine ponds are used for inland brine disposal in the eMalahleni water reclamation plant. The large volumes and limited capacity to store brines has placed great emphasis on enhanced evaporation rates to increase the efficiency of the ponds. In order to improve the rate of brine evaporation in the pond, an understanding of the effect of brine salt content and other parameters affecting the rate of evaporation is required. This study aimed at establishing the physical and chemical behaviour of the brine from the eMalahleni plant in a controlled environment. The investigation incorporated actual brine from the eMalahleni plant as well as synthetic salts typical of the major components of the eMalahleni brine.

An experimental unit (controlled environment) was designed to accommodate and manipulate the parameters that influenced the evaporation rate of the original and synthetic brines. The eMalahleni brine was analysed for major ions and was significantly high in Mg^{2+}, K^{+}, Ca^{2+}, Na^{+}, SO_4^{2-}, Cl^{-}. These major ions are associated with the coal formation in the region of eMalahleni (Witbank). The effects of these ions on the rate of evaporation were investigated using synthetic salts such as; NaCl, KSO_4, $MgSO_4$, $CaSO_4$, $NaNO_3$, $NaSO_4$.

The rate of evaporation was found to be a function of physical parameters including the air`s humidity, wind speed, radiation, salinity and the temperature. The chemical parameters investigated showed that the type of salt solution and its concentration were significant contributors to the brine evaporation rate in the laboratory. Applying forced convection (approximately 2m/s wind force) to the experiments, yielded increases in evaporation rates of more than 25% for both the eMalahleni and synthetic brines. The salinity factor was highlighted in experiments when the molar concentrations of the synthetic salt solutions were systematically increased from 0.125 to 4 M. Based on the salinity experiments, the higher concentrated salt solutions (4 M) showed a reduction in evaporation rates of nearly 50%. The eMalahleni brine is dominated by sodium and sulphate ions. However less soluble salts such as CaSO4 and MgSO4 collectively contribute only 6% of the total brine composition. The solubility of the synthetic salts was significant as precipitated salts showed potential as a heating storage component. The findings from the eMalahleni brine in the laboratory were expressed in the Oroud model as a real environment scenario. Based on the assumptions for more arid regions, the Oroud model depicted more realistic outputs for the summer season in the eMalahleni area.

KEY WORDS

Acid mine drainage

Activity coefficient

Boundary layer

Environmental

Infrared radiation

Ions

pH

Precipitation

Salinity

Solubility

Vapour pressure

Water quality

TABLE OF CONTENTS

TABLE OF FIGURES

TABLES

CHAPTER 1

1.1 INTRODUCTION

Water is a great necessity to humans and the ecosystem. Hence the quantity and quality is fundamental to the survival of all species (Rosegrant, 1997). World water is facing a crisis where the demand to maintain the quality of water needed for human and habitat remains a growing challenge (Halder at al, 2015). Freshwater resources have been under constant threat of being polluted which has placed a strain on human and ecosystems wellbeing (Furumai, 2008). With more than half of Africa`s population without safe drinking water it is imperative that all exiting water resources are protected (UNESCO, 2005). Worldwide the demand for potable water has led to the increase of desalination plants to address the issue of water shortage and decrease of salinity. Mining is a worldwide activity where it is always accompanied by environmental issues, especially those related to water quality. A significant margin of environmental related issues is associated with mining. In the eastern USA an estimate 1100 streams and rivers were polluted in the Appalachian states which endangered potable water supply (Zhu &Anderson, 2002). The estimate remediation for this pollution was between $32 and $72 billion (Zhu &Anderson, 2002).

South Africa forms is one of the most water scarce regions in Africa and the demand for reasonable quality water is on the rise. Finding a balance between growing our economy and addressing the demand for potable water can be quite challenging. With various desalination installations along the coast of water scarce regions, the mining sector has adopted an approach to minimise their environmental footprint by purifying their wastewater (Hobbs at al, 2008). South Africa has laws which protect its natural water resources and habitats. The disposal of waste water is particularly emphasized in the SA Water Act, 1998. In particular section 22 (2) (c) of the Act, clearly stipulates the standards and management practices to be observed by any party responsible for discharging wastewater (effluent). The guidelines for disposal of wastewater are described in the South African National Standards (SANS). However many sectors still contribute towards pollution and pose a threat to environment and natural water resources like rivers and groundwater. South Africa is seen as an emerging economy and a need for energy and clean water is always going to be a major issue. With any growing economy there is a degree of waste that is produced. However the disposal of the waste generated usually raises some concern amongst environmentalist and the general public. The mining sector for instance, is a major factor in the economy and it is also one of the main contributors towards pollution. Acid mine drainage (AMD) has been identified as a

major problem in recent times, which is the result of mining. The most noticeable effect of AMD is the negative affecting it has upon the water resources and the aquatic life thereof (Zhu &Anderson, 2002). The oxidation of sulphide minerals is a process where mine waste is exposed to oxygen and water during mining activities. In addition ore processing can also lead to this problem (Zhu &Anderson, 2002). The constant degrading of natural arable land and the quality of water resources will have a long term effect on the natural resources. Problems which have been identified today are the result of mining activities in the 1930`s and 1940`s (Furumai, 2008). Evidence in the most recent recorded data during the period between (1999-2008) of the Resource Water Quality Objectives (RWQOs) suggest that the increasing levels of sulphate and Electrical Conductivity, is directly linked to the mining and energy utilities in the northern parts of the water management area (Comrie, 2011).

Evaporation is the process by which a substance in the liquid state is transformed into a vapour. Evaporation is an important process in the hydrological cycle. It is a link between water on the surface of the earth and the atmosphere which operates continuously with no specific origin or ending (Monteith and Unsworth, 2008). The rate of evaporation however varies around the world where many factors play an important role. Evaporation from a free water body is different from that which evaporates from a water body with vegetation. This makes evaporation estimates quite challenging in a natural environment (Brutseart, 1982). The seepage from a natural water body can add to the complexity of measuring evaporation rates (Singh, 1989). The ambient temperature, the air`s humidity, radiation and wind speed are the major components which contribute towards the rate of evaporation (Dama-Fakir et al., 2012).

The application of evaporation in the modern era requires a more accurate prediction as it incorporates the energy and economic factors into the entire system (Sartori, 2000). Evaporation in the modern era is required to address quite a number of issues in hydrology, forestry, irrigation management and river flow predictions (Xu et al.,1997). These contributing elements were tested in an environment, where some of the parameters were changed to resemble conditions in reality. Brines are considered to have greater than 10 000 ppm of salt and hyper salinity found to be above 35 000 ppm according to United States Geological Survey. Evaporation of industrial brines is an important aspect in all processes when managing saline effluents. A greater evaporation rate of brines will subsequently lead to a greater rate in mineral precipitation. The efficiency of managing brine ponds makes a difference as a reduction in salts can improve the quality of our natural water resources.

1.2 ENVIRONMENTAL IMPACT

1.2.1. The AMD impact

Mining activity in South Africa has been around since the late 1800`s when gold was discovered. Environmental policies were not evident or less effective at that stage. The influence that mining has on the environment is always made evident long after the guilty party was operating. These mining practices always influenced the quantity and quality of water which adds to the problem of water scarcity (Bell et al., 2001).

Mines were decommissioned but continue to be a major environmental risk (Hobbs et al, 2008). Acid mine drainage (AMD) in particular coal mining discharge, is associated with high sulphate concentrations that are likely to be detrimental to the ecosystem (Dama-Fakir et al., 2012). In India for example, brine contamination has caused an increase in the hardness of groundwater. Elevated levels of sodium, chloride and boron can increase the soil salinity and reduce the level of productivity Maas &Tanji, 1990). South Africa is regarded as a water scarce country, with arid to semi-arid regions in the southern parts of the country. An increase in the soil salinity in regions with less arid conditions will elevate the problem of water shortage in the country. The Wilge, Bronkhorstspruit, Klein Olifants and Olifants Rivers are being polluted in the quest to mine coal (Van Veelen & Dhemba, 2011). The accumulative impact of the AMD problem transcends the environmental, political and financial sectors (Adler, 2007 & Hobbs et al, 2008). The low pH of the acid mine drainage can be a threat to most plant and other life forms as the high hydrogen ions concentration is related to inactivation of enzyme systems, limits respiration and the intake of nutrients (Bradshaw, 1982). The low pH values are attributed to the formation of sulphuric acid during the reaction of pyrite with air and water (Bell et al., 2001).

1.2.2. Desalination impact

The approach in the past to brines viewed saline water as a waste problem and not as a viable economical water resource. Sectors like agriculture, fishing, algae and mineral production have to some extent changed the perception towards brines. The concern is that brine is a waste problem and the fact is that the brines are generally broken down into their respective basic compounds. This perception however, makes the outlook to reclaim water very unappealing (Koening, 1958; Ahmed et al., 2000).

It is a common occurrence for brines to be pre-treated prior to processing in a reverse osmosis (RO) system. The pre-treatment consists of acidification, anti-scalants and chlorination while the pre-treatments for a lower water quality may use filtration, coagulation, ion exchange and carbon adsorption as a viable option (Ahmed et al., 2000). Brine is associated with high total dissolved solids (TDS) and requires minimal further processing with the addition of chemicals (Ahmed et al., 2000). The measurement for brine concentrate is known as the concentration factor (CF).

$$CF = \frac{1}{1-R} \quad (1)$$

Where C*F* is the concentration factor and R is the fractional water recovery.

Desalination is an important component in water management to reduce the impact of human activity on water resources. The desalination process reduces the impact across the industrial, municipal and agricultural sector (Macedonio et al., 2011). This adds more water to the reserve which is vital for living plants and animals. In particular the mining industry used a desalination installation to remedy the impact of their effluents on the environment and natural resources. The coal mining activity near eMalahleni uses a reverse osmosis (RO) system which is capable of treating saline waters from 3 collieries in the area. The Kleinkoppie, Greenside and South Witbank Collieries feed their respective mine water to the eMalahleni desalination plant which is capable of a 20 ML day treatment capacity (Gunther, 2006). The plant was designed to maintain a water standard equivalent to SANS 0241 Class 0 potable standards (Gunther, 2006).

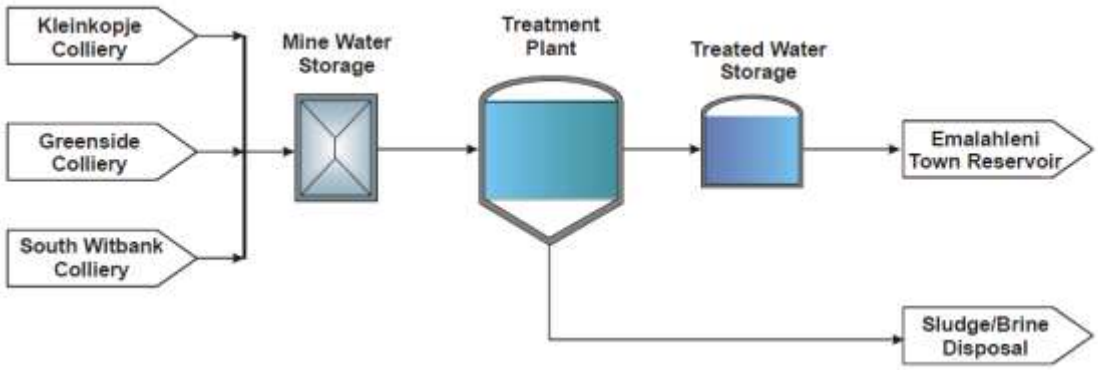

Figure 1.1Representation of the eMalahleni water reclamation system (Günther, 2006).

1.2.3 Brine pond problem statement

The mining sector contributed towards the salinity and the turbidity of the Olifants Catchment (Comrie, 2011). This problem has led to dam sedimentation, increased cost of water treatment and brine ponds are certainly an option for inland waste brine disposal resulting from desalination. It is a cost effective means to store brine concentrate from an inland source. The major problems associated with brine ponds is membrane leaks. Any leak will subject the surrounding environment to high levels of saline solutions. The biggest threat will be groundwater contamination and salinity increases in the soil. An even bigger issue is land acquisition as the size of the pond will incur large costs to construct (Ahmed et al., 2000).

Although a large number of issues are associated with the installation of brine ponds, it is still a viable means to minimize the brine footprint especially in the mining industry. Inland desalination plants produce brines as main by-product with a concentration of around 7500 mg/L (Halder at al, 2015). With high levels of sulphates and metal content, brine is likely to affect surface and groundwater resources. Other methods such as deep well injection are considered a high risk to groundwater contamination, (Dama-Fakir et al., 2012). The government approval of high risk methods is stringent especially when groundwater is a factor (Dama-Fakir et al., 2012). Controlled discharge was explored by the Department of Water Affairs (DWA) and Anglo American which showed promising results in terms of policy framework.

High temperatures and low rainfall is associated with the ideal solar brine pond conditions. The added advantage to the solar brine pond system is the fractional evaporation process where pre-separation of brines can occur (Schultheis, 2001). Forced energy and convection systems are a cost bearing factor which can make solar ponds economically unattractive (Dama-Fakir et al., 2012). Measuring evaporation requires consideration of a number of variable factors that influence the evaporation rate which is a challenging task. In a natural pond the density of the brine, ambient temperature, wind speed variation and fauna impact can affect the evaporation rate (Schultheis et al, 2001).

Evaporation ponds are suitable for salt storage under the following conditions (Mickely, 2006):

- A suitable climate where the solar energy is sufficient (especially arid regions)
- Conditions where the insulation system is adequate to contain the energy
- The volume and type of brines which suits the design of the pond.

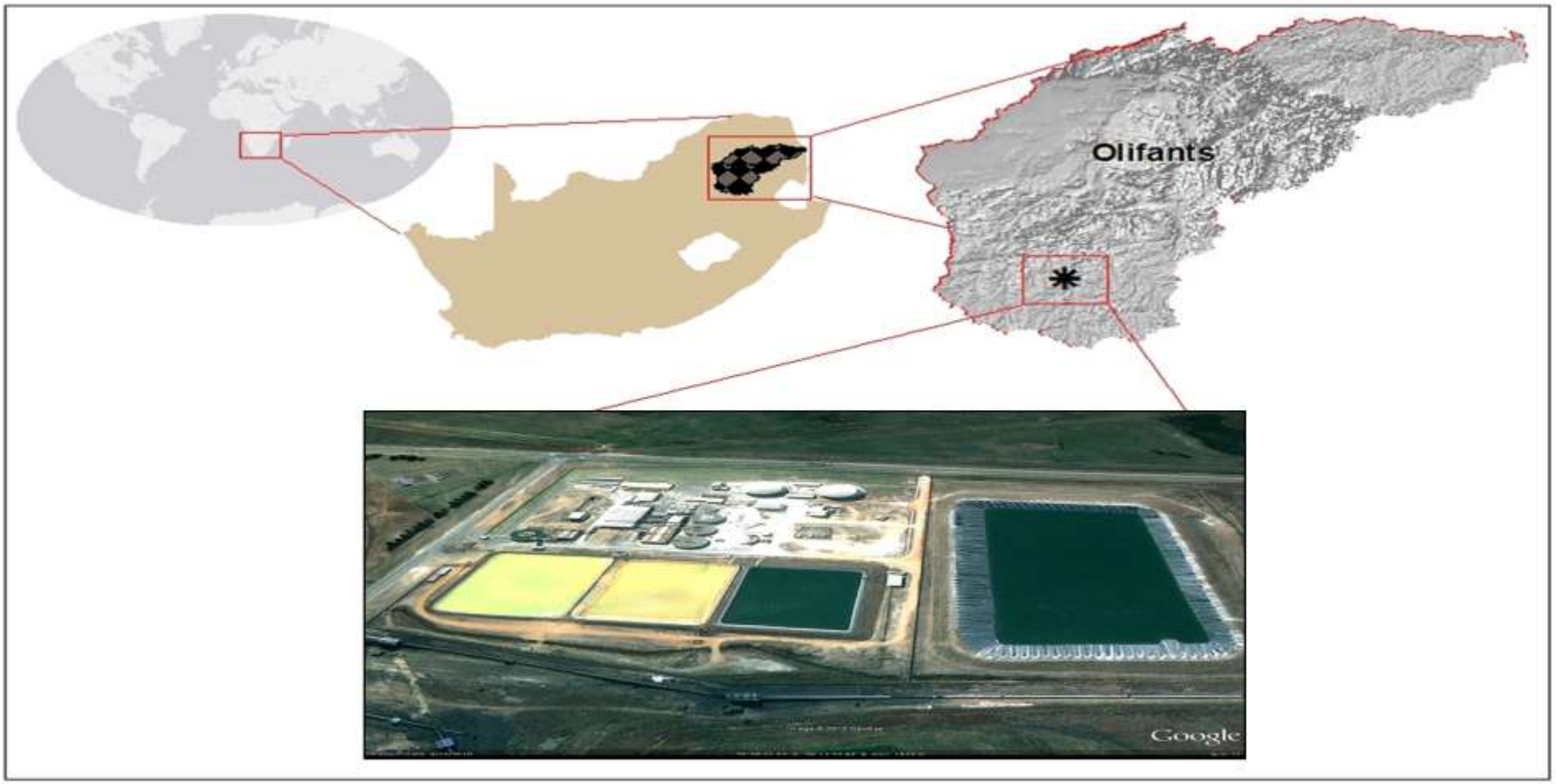

Figure 1.2 The geographical area of the evaporation ponds in eMalahleni, Mpumalanga. The eMalahleni water reclamation ponds are located within the Olifants Catchment. (Picture retrieved from Google Earth, 2013)

1.3 THE AIM

The aim of this study was to simulate the rate of evaporation of synthetic salts and processed brine in a controlled environment and to observe the effect of physical and chemical parameters of the different salts solutions throughout the salinity and forced convection experiments.

1.4 RESEARCH QUESTIONS

- What conditions are necessary for a controlled environment to maximize the evaporation rates?
- What major factors play a significant role in the rate of evaporation of water under a controlled environment?
- What type of variations of the meteorological components can be expected in a controlled environment?

THE OBJECTIVES

- To subject various components in synthetic brines to conditions that incorporate, radiation, temperature, humidity and the wind component under a controlled environment;
- To establish the effects of the synthetic brines with similar molar concentrations under a controlled environment that resembles natural day and night rhythmic cycles on evaporation rates.
- To subject the brines to specific, scaled energy inputs under free and forced convection and determine the different evaporation rates thereof, and ;
- To express the eMalahleni brine in a mass transfer equation that incorporates salinity.

1.6 SCOPE AND OUTLINE OF THE THESIS

Chapter 1

Introduction

Chapter 1 provides a general overview of the thesis, and problem statement, highlights the main objectives, research questions, and main objectives.

Chapter 2

Literature review

This chapter is directed towards reviewing the body of knowledge to find procedures and background information for the experimental setup and the measuring devices for the experimental cycles. The chapter also focused on the background of data collection and the data comparison of a real environment. This chapter elaborates on the physical factors associated with evaporation in a natural environment. In addition, this chapter briefly discussed the different models to estimate the evaporation rate based on their respective assumptions.

Chapter 3

Study area and brine analysis

This chapter is directed towards detailing the materials and methods for the experimental setup and the measuring devices for the experimental cycles. The chapter also focus on the data collection and the data comparison of a real environment. This chapter also compared data from the laboratory and real environment. It also explains the analytical techniques used with the sampling procedures and the characterization of the eMalahleni brine.

Chapter 4

Laboratory preparation and simulation methodology

This chapter focuses on the salinity experiments in particular the synthetic salt solutions and the eMalahleni brine. The lower and higher salinity experimental setup is also discussed and the main differences are highlighted.

Chapter 5

Results and discussion

This chapter focuses on the results from the salinity experimental cycles. This chapter also discusses the main differences between the free and forced convection experiments. It also highlights the limitations of this particular study.

Chapter 6

This chapter deals with the energy budget in particular the energy being absorbed by the brine in a controlled environment. In addition, the chapter also focuses on the suggested model for this study to express the eMalahleni brine from a salinity perspective.

Chapter 7

Conclusion

In this chapter the main conclusions are discussed from the convective and saline experiments. The chapter also focused on the appropriate model application for the real environment. The chapter also highlights the recommendations, challenges and possible future studies.

1.7 LIMITATIONS AND CHALLENGES

1.7.1 Humidity control limitation.

The air`s relative humidity is a major factor in evaporation rate in general. The vapour pressure can increase the rate or decrease the rate of evaporation. In this study the humidity was not explored to its full extent. The humidity inflow from the building was approximately set for a 60% ratio with some minor variations at times. The control of higher or lower humidity settings can potentially add value to future studies.

1.7.2 Turbulent effect

The main effects of the forced convection experiments were to remove the saturated air above the container but indirectly the wind force also generated a wave pattern on the brine surface. This was evident in the temperature graphs during the forced convection experiments. The temperature graphs indicated a distortion in the temperature profile when the wind energy was applied. A better design of the experimental setup can limit this effect to a certain degree. Experiments conducted by Jodat (2012a) claimed a reduction in the turbulent effects of the fans by implementing a draw-through system.

1.7.3 Energy from the lamps changes

The expected life span of the infrared lamps was approximately 6000 hours recommended by the manufacture per lamp. With a deterioration of the lamps, it will always be a challenge to factor in the changes over an extensive period of several weeks. The compound effect by the infrared lamps contributed towards slight elevation in ambient temperature. The extent of the small impacts on the ambient temperature was not considered for this study.

1.7.4 Optical challenges

The coefficient of expansion was noted when the brine surface level raised the brine by a 1 mm for certain salts when the infrared lights applied energy to the system. The coefficient of expansion of the container was neglected since it was exposed to the same heat source as the brine and was a concern for the manual readings. The manual data collection had some challenges during the experiments. The meniscus that formed near the sides of the Perspex container caused a level of discrepancy with certain measurements. The angle at which the data recordings were read was critical as the refractive indices affected the accuracy of the measurement to a certain degree. The clear Acrylic Perspex was insulated with a silver Aerolite blanket and obscured vision from the outside of the container. The colour of the infrared light contributed to the challenges especially if the incremental markings have a similar red appearance when used as a datum.

1.7.5 White water mould

Mould in general was not very prominent in this study. However, a very small amount did appear in the container with distilled water which served as a control measure for the experiments. Sterilising the control (distilled water) can eliminate the mould but might have implications when classified as fresh water.

1.7.6 Up-scaling

The incorporation of precipitation to the system remains a challenge. The unpredictable rain variation (spatial and temporal) can be a challenge but could add significant value to the study. Specific boundaries may be set based on the assumptions of a specific model to accommodate this feature. The annual rainfall was not considered in this study although the rain does affect the level changes, but can be significant in the development of a holistic approach.

1.7.7 Ambient temperature

The ambient temperature indicated a fairly limited range but was sufficient to perform the related tasks. A greater range in ambient temperature would have been beneficial to serve a greater region. The overwhelming effect of the ambient temperature was more evident in the free convection experiments where the brine temperature was slowly altered to the same temperature as the room as soon as the lights were switched off. Best practice to mimic the annual fluctuation of a brine pond would be if all the seasons of a specific study area with a complete temperature range were incorporated.

CHAPTER 2

Literature review

This chapter elaborates all the major components necessary for evaporation in a natural environment. In addition, this chapter briefly discusses the different models to measure the evaporation rate based on their respective assumptions. This chapter also emphasises the different application to measure evaporation and the advancements of brine experiments in a controlled environment.

2.1 INTRODUCTION

The ambient temperature, humidity, density of the liquid and the energy input are major components that contribute towards the rate of evaporation (Karimi-Googhari, 2012). The application of evaporation in the modern era requires a more accurate prediction as it incorporates the energy and economic factors into an entire system (Sartori, 2000). In this study these contributing elements will be tested in an enclosed environment (laboratory), where some of the parameters will be changed to resemble conditions in a real environment.

2.1.1 UNITS OF MEASUREMENTS

The standard evaporation measurements were expressed in mm /day. At constant pressure at 20°C the energy input to evaporate one mm layer of water over a $1m^2$ (1 kg) is equal to 2.5 MJ (FOA,1992; Monteith and Unsworth, 2008). The electrical conductivity (EC) of the brine is measured in micro Siemens (mS) and indicated the ion activity of the brine solutions. The energy from the infrared lamps however are measured in Watts/m^2 but converted to Joules per unit time to relate the energy balance of the system. The density of the brine was measured in g/cm^3 especially for the salinity experiments. The water temperature of the experiments was measured in degrees Celsius (°C). Evaporation rate is measured by water level changes and expressed in mm. In addition, the water level changes are also captured by pressure changes expressed in kilopascal (kPa).

2.2 METEOROLOGICAL COMPONENTS

Evaporation with transpiration of a well vegetated area with ample supply of water to be transferred to the atmosphere is known as potential evaporation (PE). Actual evaporation is referred to as the volumetric amount of water transferred to the atmosphere under natural conditions. Several components form the basis of the meteorological system which drives the hydrological cycle as are described in the following subsections:

2.2.1 The boundary layer

The air near the surface of the earth is known as the atmospheric boundary layer (ABL). The humidity, temperature and the wind speed show greater amount of change near the surface than at higher elevations (Brutsaert, 1982). The boundary layer near a water surface therefore has a greater influence on the evaporation rate than surrounding elements. Water vapour being transported away from the surface layer by turbulent eddies is a function of surface roughness and wind shear (Arya, 1998).

2.2.2 Thermal radiation

All objects with a temperature above 0 K emit energy in the form of electromagnetic waves. The major factors influencing incoming solar radiation are the atmospheric scattering, absorption, reflection and cloud cover and latitude (Calver and Finch, 2008). Convection and conduction requires the presence of molecules and atoms to relay the energy from a higher to a lower energy medium. However radiation can transfer energy from one medium to another without the presence of any physical medium.

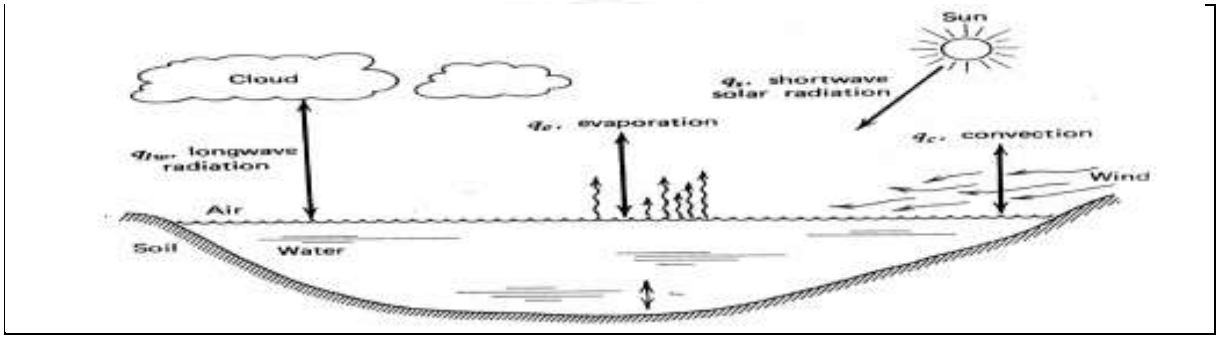

Figure 2.1 The mechanisms related to the evaporation process (Adapted from Al-Khlaifat, 2008)

2.2.3. Long and short-wave radiation

The radiation directly from the sun is known as short-wave radiation and varies with geo-location on the surface of the earth. The exchange of irradiative energy of the surroundings, especially the water and the air is regarded as long wave radiation. The total balance between the short and long-wave radiation (shown in Figure 2.1) is referred to as the net radiation (Monteith and Unsworth, 2008).

2.2.4 Heat flux

Energy conveyed per unit area over a surface unit is referred to as the heat flux. The heat energy storage capacity is directly related to the temperature profile of a water body and can

be determined through empirical data (Brutsaert, 1982). The SI unit for heat flux density is measured in W/m^2.

2.2.5 Boltzmann equation

Long-wave radiation is highly affected by the cloud formation and subsequently affects the amount of radiation a water body receives. With a portion of the incoming long-wave radiation affected by the environment, a small amount of solar energy is reflected away from the surface of the water body (Monteith and Unsworth, 2008). The air temperature and humidity above a water body plays a significance role. Boltzmann formulated a model to calculate the reflection.

$$\boldsymbol{E = \varepsilon\sigma T^4} \quad \text{(2)}$$

Where E is the energy, σ is the Boltzmann constant, T is the temperatures in K and ε is the emissivity of the surface.

2.2.6 Solar radiation

The amount of solar radiation received by a surface area of the earth is known as irradiance and expressed in W/m^2. The radiation from the sun, known as the solar flux, reaches the outer atmosphere at around $1368W/m^2$ called the solar constant (Arya, 1998). The solar power is measured as irradiance when it reaches the earth`s surface (Monteith and Unsworth, 2008). The solar radiation at the surface of the earth can be lower than the amount received by the outer atmosphere as result of interference of cloud cover and air pollution (Brutsaert, 1982). From a spatial perspective the radiation intensity from a point source can be expressed as:

$$\boldsymbol{I = d^4/dw} \quad \text{(3)}$$

I = Intensity of the radiation

d^4 =Change in flux emitted from the source

dw =Change in solid angle

The heat flux penetrating water can be determined by measuring the water temperatures at various depths of the water. At the surface the radiation can be measured using a pyranometer (Brutseart, 1982). The depth of a solar pond along with the surface area is highly significant in the rate of crystalline salt production. The radiated energy from the sun can dissipate in deeper waters and consequentially influence the thermal stratification of the pond. A shallow pond may have the ability to increase the evaporation rate and crystalized salts at a faster rate.

This however might have an adverse effect on the production of salts over a longer term if the salts are not removed. Salt production in a shallow pond with a large enough surface area can reflect the radiated energy back into the atmosphere (Coleman, 2000).

2.2.7 AIR CURRENT DYNAMICS

2.2.7.1 Wind

One of the main functions of the wind is to remove the saturated air above the water surface during evaporation. The wind has a major influence in maintaining the atmospheric moisture gradient to allow consistent evaporation of the water. A water body exposed to a wind force greater than 2 m/s is considered to be dynamic (Marek and Straub, 2001). The experimental design for this study on the evaporation rates of a brine solution (see paragraph 1.3) incorporated a forced convection segment of 2 m/s with the saturated air above a water body constantly being removed. A higher evaporation rate can be anticipated if all other factors affecting evaporation are equal.

2.3.7.2 Impact on surface layers

The impact from wind blowing over a water body is highly dependent on many variable factors. The wind speed, flow direction and wave breaking of the water, play significant roles in the rate of evaporation (Duan et al., 2009). A shear stress is developed when wind comes into contact with the surface of a water body which results in a surface roughness that consist of three segments. The surface roughness is proportional to thickness of the viscous layer during the initial shear velocity (O'Connor, 1983). The second segment of the shear velocity is raised to the exponential power to be proportional of the viscous layer. In the third segment the shear force breaks through the viscous layer and remains constant (O'Connor, 1983).

Within the boundary of the air-water interface the air flow and the stream flow can reduce the turbulence of the water resulting in a viscous layer between the water as demonstrated in figure 2.2 (Duan et al., 2009). Turbulence generated in a stagnant pond, is mainly wind driven and promotes gas transfer through diffusion. The viscous layer strength is highly dependent on impurities and temperature of the water (Duan et al, 2009). With an increase of the water temperature the strength of the viscous layer decreases and vice versa. For a liquid to evaporate successfully, it requires enough energy to overcome the cohesive forces between the molecules generated by the viscous layer (Duan et al., 2009). To improve evaporation, the dependence can be extended to the air density along with the vapour pressure of the saturated air (Jodat, 2012a).

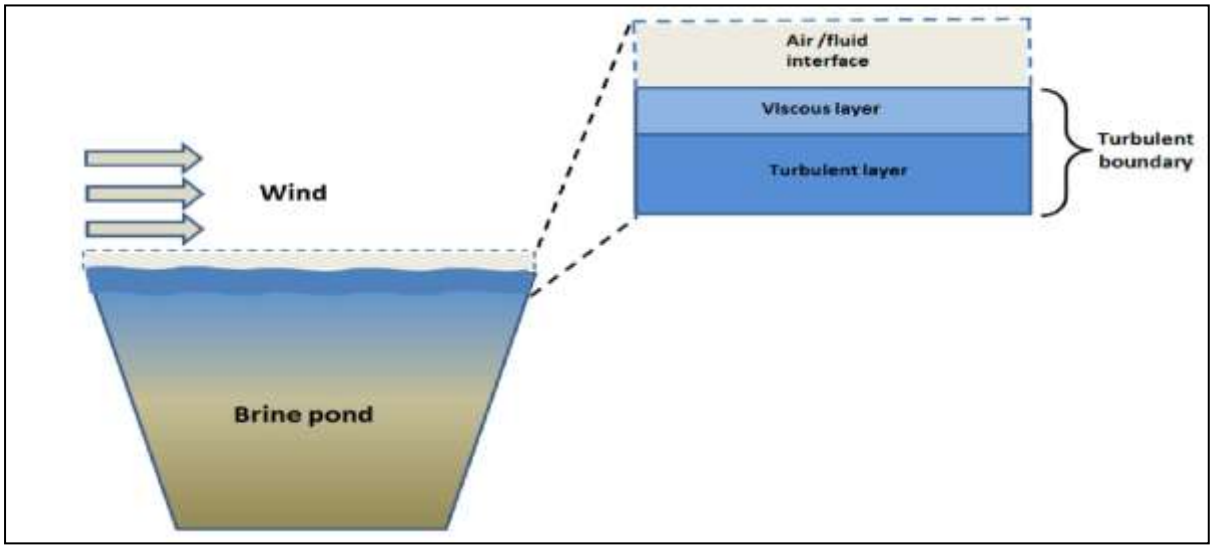

Figure 2.2 The wind interaction with a fluid surface (adapted from Duan et al, 2009)

2.3.5.3 Friction drag with forced convection

Under conventional circumstance when a liquid is subjected to air currents with forced convection, it is prone to shear stress at the surface (Wang et al., 2013). Drag coefficient is mainly a function of surface roughness (Kondo., 1975). The molecular property of liquid is a function of heat and mass transfer when subjected to surface roughness (Kondo., 1975).

2.3 PHYSICAL LIQUID PROPERTIES

2.3.1 Latent heat of vaporization

The latent heat of vaporization refers to the amount of heat energy needed to convert a specific unit mass in liquid form into a vapour without any change in the temperature (Brutsaert, 1982). It is the amount of heat required to break the intermolecular bonds of the liquid. The latent heat of vaporization for pure water is 2500 J g^{-1} at standard temperature and pressure (Monteith and Unsworth, 2008). The more volatile the substance is, the less the energy required to evaporate it. The energy available has a direct influence on the evaporation, subsequently leading to more vapour being released into the atmosphere (Calver and Finch, 2008). The energy transforming water into vapour can be classified as a two part energy release system. The first stage is to heat the liquid surface and the second part of the energy is directed to transform the actual liquid to vapour (Calver and Finch, 2008). The latent heat of vaporization is an important factor in the psychometric calculation and plays a significant role in the evaporation model.

2.3.2 Thermal stratification

Water has the potential to transport stored heat and usually associated with large and deep water bodies (Calver and Finch, 2008). Thermal stratification affects the water of lakes and is related to eutrophication in lakes (Yu et al., 2010). In addition, it is also prone to have a time lag between the radiation input and the total evaporation rate (Calver and Finch, 2008). In a natural water body, thermal stratification can have an adverse effect on the water quality if not functioning within certain limits (Shaw, 1983). In the context of water quality, the chemical stratification is dependent on the thermal stratification (Yu et al., 2010).

2.3.3 Specific Heat Capacity

The specific heat capacity of a substance is referred to as the energy requirements to elevate or lower the temperature of 1 kg unit mass by 1 degree Celsius (Arya, 1998). At constant pressure the specific heat capacity can be determined by temperature. The specific heat capacity is significant in the thermal stratification and the energy absorption of a particular substance.

2.3.4 Vapour pressure

Vapour pressure is a state of a liquid which has a tendency to change into a gas phase when the molecules have the ability to separate, hence have greater kinetic energy (Monteith and Unsworth, 2008). Vapour pressure is an important component in the liquid to gas phase transition (Brutsaert, 1982). The temperature plays a significant role when the lower boundary layer is saturated (Brutsaert, 1982). The Clausius-Clapeyron equation was suggested for the rate of change of the saturated vapour pressure above the liquid (Monteith and Unsworth, 2008). From a saline solution perspective, the activity coefficient is one of the main governing factors regarding the ratio of the saturated vapour pressure above a liquid compared to a freshwater plane with the same temperature. (Oroud, 1999).

2.3.5 Capillary effect

The capillary effect is demonstrated by the rising of liquid through narrow tubes that enables the liquid to flow in opposite direction against gravity (Atkins, 1978). The energy is significantly reduced when a liquid is spread thin, but the upward movement along a dense surface such as glass signifies that the pressure below the surface area of the meniscus is lower than the atmospheric pressure (see Figure 2.3). This movement will continue until hydrostatic pressure has reached equilibrium (Atkins, 1978). This can be expressed in the following equation:

$$\boldsymbol{p = \frac{\pi \rho r^2 hg}{\pi r^2} = 2\gamma / r} \quad \text{..... (4)}$$

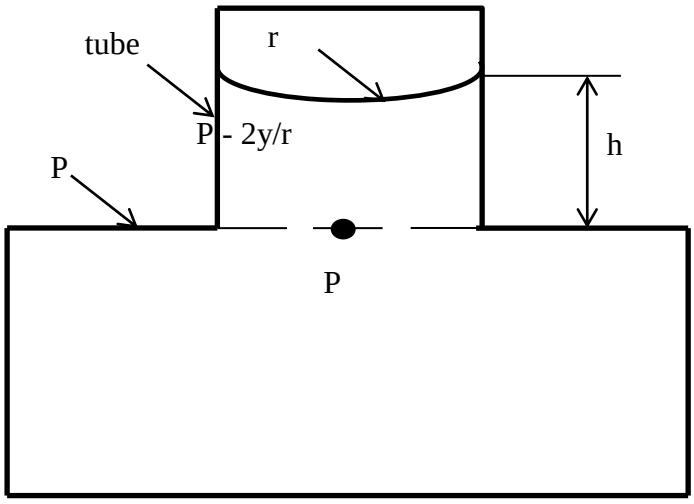

Figure 2.3 Illustration of the capillary effect (Atkins, 1978).

Where r is the radius of the capillary tube and p is the pressure outside the tube. ρ is the density of the liquid, g is the gravitational force, h is the height,γ is the surface tension

2.3.6 Surface tension

The surface tension is referred to as the cohesive forces that appear at the surface of a liquid. The strength of the cohesive forces is temperature dependent and time sensitive since relatively newly formed water bodies possess greater surface tension strength (Marek and Straub, 2001). This theory constitute towards a stagnant ponds being more susceptible towards releasing water molecules into the atmosphere as result of diminished cohesive forces.

2.4 THE MEASURING COMPONENT OF POTENTIAL EVAPORATION

Evaporation rates can be measured using different methods. Examples are the change in humidity in the air stream, above a water body, or changes in water level of the water body, heat and mass balances, can all be used to determine the evaporation rate (AI-Shammiri.M, 2002). A brief discussion of various methods developed to measure evaporation rate is explained in this section.

2.4.1 A pan measurement

A number of evaporation pans are on the market for standardization of measurement of evaporation. The US Class A–pan has been regarded as the most commonly used amongst farmers and water resource managers (Cobaner, 2013). The US Class A-pan is approximately

1.207 m in diameter and 255 mm deep (see Figure 2.4). Measurement of evaporation loss is recorded by measuring the change in the water level of the pan. Water level changes can be recorded on a daily basis. The measurement for all pans incorporates a pan coefficient factor for the final result. The coefficient is necessary as the sun`s intensity varies according to geo-locations. The sun's rays heat up the sides of the pan resulting in an increase of evaporation rates. An environment where the A pan is placed that is dry might lead to the evaporation rate of the A-pan to increase (Calver and Finch, 2008).

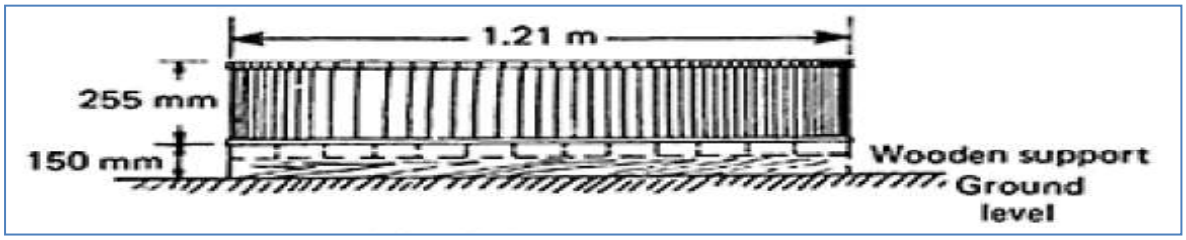

Figure 2.4 Dimensions of a typical US Class pan (Shaw, 1983).

2.4.2 Weighing lysimeter

The lysimeter can be utilised for measuring the actual evapotranspiration from a vegetated surface At operational capacity the soil is kept at field capacity by sprinkling a recorded volume of water on the tank filled with soil. The percolation of the water ensures that the constant field capacity is maintained. Evapotranspiration from the system can only be anticipated from the top surface area of the lysimeter system (Shaw, 1982).

2.4.3 Atmometer

The atmometer consists of a cylinder with a water reservoir and with a porous ceramic cup mounted on top of the cylinder. In order to simulate crop canopy, a shaded fabric material is used to cover the ceramic cup. The fabric has an underlining that resembles a membrane preventing rain from seeping through. The Atmometer works on a principle that allows distilled water from the reservoir to evaporate by extending a tube from the bottom of the cylinder that feeds into the ceramic cup where the water transfers into the air (Knox et al, 2011).

2.4.4 Eddy Covariance method

Another direct method for the measurement of evaporation from an open reservoir is the Eddy Covariance technique used by Tanny et al, (2008). It evaluates fluctuations of vertical velocity in air currents and vapour densities at high frequencies over short periods (Tanny et al, 2008). The system consists of a 3 dimensional sonic anemometer that records the wind

speed in all possible directions. It also consists of a krypton hygrometer accounting for the humidity of the air. One notable feature of the system is that it must be mounted on a support structure at a certain height above the water surface to improve the accuracy of the system. The Eddy Covariance system is one of the most reliable methods in the modern era under prescribed criteria (Itier et al., 1996).

2.5 EQUATIONS OF POTENTIAL EVAPORATION

2.5.1 Empirical equations

A number of equations have actively been used to estimate evaporation (see Table 2.1) often without the necessary consideration of the conditions under which these formulas apply (Sartori, 2000). A large amount of energy of a free water surface is lost as a result of evaporation and it is critical to apply the correct model based on its respective assumptions. As much as 50% of the energy would be considered lost during the transfer from liquid to vapour (Sartori, 2000).

2.5.2 Methods of measuring evaporation

The method of measuring evaporation has evolved over the years. In the early days, the tiled pit was one of the first methods to measure evaporation where water is refilled daily from the previous evaporation. The modern quantitative theories were developed during the nineteenth century by (Dalton, 1802) and others. The Penman, (1948) equation combined the energy balance, mass transfer formulas for open water bodies and saturated land surfaces (Arya, 1998). The formula has undergone many modifications to assist with different scenarios. Today the Penman–Monteith model is a common method that is widely used to estimate evapotranspiration.

Table 2.1 Equations used for calculating evaporation (Hassani et al., 2008)

Methods	Equation	Reference	Application
Combination group Priestley-Taylor	$E = \propto \frac{s\,Q_n - Q_x}{s+\gamma} * 86.4$	Stewart and Rouse (1976)	10 days or greater
deBruin-Keijman	$E = \frac{s}{0.85s + 063\gamma}\,\frac{(Q_n - Q_x)}{L\rho} x86.4$	deBruin and Keijman (1979)	Daily
Penman	$E = \frac{s}{s+\gamma}\left(\frac{Q_n - Q_x}{\lambda\rho}\right) x\ 86.4 + \frac{\gamma}{s+\gamma}(0.26(0.5 + 0.54\ U_2)(e_s - e_a)$	Brutsaert (1982)	Greater than 10 days
deBruin	$E = 1.192\ \left(\frac{\alpha}{\alpha - 1}\right)\left(\frac{\gamma}{s+\gamma}\right)\frac{(2.9 + 2.1\ U_2)(e_{s-}\ e_a)}{L\rho} x86.4$	deBruin (1978)	Period of 10 d or greater
Dalton Group Mass transfer	$E = (\mathrm{NU2}(e_0 - e_a)\mathrm{x}10$	Harbeck et al.,(1955)	Depends of the calibration N
Temperature group Papadakis	$E = 0.5625(e_s\ \max - (\mathrm{es} - \min - 2))(\frac{10}{d})$	McGuinness and Bordne (1972)	Monthly

α=1.26 =Priestley-Taylor empirical constant

S =slope of the saturated vapour pressure- temperature curve at mean air temperature (Pa °C^{-1})

γ= psychometric constant (subjected to temperature and atmospheric pressure) (Pa °C^{-1})

Q_n=net radiation (Q_s-Q_{r+} Q_{ar} –Q_{bs})(Wm^{-2})

Q_x =change in heat stored in the water body (Wm^{-2})

λ= latent heat of vaporization (MJ kg^{-1})

ρ = density of the water (998 kg m^{-3} @ 20 °C)

N= mass transfer coefficient
U_2 = wind speed at 2 m/s
e_0 = saturated vapour pressure of at the water surface temperature
e_s = saturated vapour pressure of air above the water surface
e_a = vapour pressure at the air temperature and relative humidity of the air (mb)
T_a = air temperature
d =days
e_s max e_s min = saturated vapour pressure at daily and minimum air temperatures (Pa)
10 or 86.4 to be converted to mmd^{-1}

Over an extensive period evaporation models were developed for very specific regions. Table 2.1 summarises various methods that were developed under certain assumptions where an empirical coefficient had to apply in order to make the model more functional and accurate. On the basis of comparing the various methods, the combination methods were perceived as being more accurate in comparison with the Bowen Ratio Energy Budget (BREB) method (Hassani et al., 2008). The more cost effective methods such as the temperature methods of Papadakis are also well within the range of the BREB method (Hassani et al, 2008). The Bowen Energy method is a more energy orientated budget equation that is related to the energy loss and gains during the evaporation process.

The conventional Penman (1948) and the Ferguson (1952) equations are designed to calculate the evaporation over an open water surface. The equation incorporates the energy budget as well as the aerodynamics of an environment to account for the loss of evaporation. Penman (1948) and Ferguson, (1952) incorporated four meteorological variables in the initial equation to determine the evaporation loss. This includes the wind speed, humidity, air temperature and net radiation (Calder and Neal, 1984).

Penman equation

$$\boldsymbol{E = \frac{\Delta}{\Delta+\gamma} Rn + \frac{\gamma}{\Delta+\gamma} fu)(e_s - e)} \quad \text{..... (5)}$$

E is the evaporation rate expressed in mm, Rn is the net radiation, γ is the latent heat of vaporization, *f* is the coefficient and *u* is the wind speed expressed in m/s. Furthermore, e_s is the saturated vapour pressure and *e* is the vapour pressure of the air. Δ is the rate of change of saturation specific humidity with air temperature.

2.5.3 Mass-transfer method

The mass-transfer method is regarded as one of the first methods applied to model evaporation (Penman, 1948; Rohwer, 1931). It is still a useful method in the modern era as its accuracy and simplicity make it a viable option today. This method is extensively used in the estimation of evaporation of large fresh water bodies such as lakes (Singh, 1989: Sartori, 2000).

$$\boldsymbol{E = Cu(e_{sat} - e_{air})} \quad \text{..... (6)}$$

Where E is the evaporation, *C* is considered the coefficient of the mass transfer, *u* is the wind speed exposed to the water body, e_{sat} is the saturated vapour pressure above the water body

surface and e_{air} is the vapour of the air in the room. It is rather implausible to apply one coefficient that can be applied to all assumptions (Finch, 2001).

2.5.4 Energy budget of water surface

Evaporation is the process which transcends the water and the energy budget (Brutsaert, 1982). When a water body is subjected to energy it can transform into a different phase, from liquid to gas for example. The energy budget method is considered to be the most reliable in terms of a practical approach (Calver and Finch, 2008). The equation to demonstrate this is:

$$R_n = L_e \mathrm{E} + \mathrm{H} + \mathrm{G} \quad \ldots\ldots\ldots\ldots\ldots\ldots\ldots\ldots\ldots\ldots (7)$$

R_n = flux of net radiation

L_e= latent heat of vaporization

E = evaporation rate

H= sensible heat flux

G = heat flux into the earth

A large amount of energy is being absorbed by the earth's surface and this energy drives various cycles like the hydrological cycle. A considerable amount of this energy is converted into long-wave radiation. Nearly half of the sun's rays are converted into infrared energy that is responsible for the heating of water bodies (Brutsaert, 1982). Part of this energy is used to convert large amounts of water into vapour where it drives atmospheric process. This forms an integral part of the hydrological system shown in Figure 2.1 and it also highlights the importance of the evaporation process along with the other processes that play a vital role in weather patterns and climatic processes. The latent heat and sensible heat fluxes are quite important in the consideration of energy plants on a micro scale and have the potential to influence the global energy budget (Brutsaert, 1982). With the change in seasons, the absorption of radiation energy varies and subsequently affects the evaporation rate. During the stratification of a water body the energy absorbed from the sun is slowly released and results in the cooling of the water body (Calver and Finch, 2008). The major disadvantages of the energy budget that it requires a vast amount of data over a high frequency. The

importance of measuring the net radiation forms a major component in the accuracy of this method (Calver and Finch, 2008)

2.5.5 The Bowen Ratio

Evaporation cannot be isolated with reference to other aspects and sensible heat cannot be singled out as the only factor. Sensible heat is the heat energy required to change the temperature of the air This relationship can be expressed as in equation 8 below.

$$\mathbf{B_o = H/}\boldsymbol{L_e}\mathbf{E}\text{.....} \quad (8)$$

B_o=Bowen Ratio

H = Sensible heat flux

L_e E= Latent heat flux

2.6 EVAPORATION AS A FUNCTION OF SALINITY

The general focus for estimating evaporation from a saline water body is not very well known. Using standard models to calculate evaporation from hyper saline water bodies may impact the representation of the measurement (Asmar and Ergenzinger, 1999). With water scarcity being a major challenge, it is appropriate to pursue different approaches to understand the saline water body from a holistic perspective. Models predict a decrease in water resources in the southern African region that will subsequently elevate the salinity levels of our resources. In recent times significant progress has been made in the development of models relating to evaporation from saline water sources.

2.7 CHEMICAL ASPECT

2.7.1 Activity Coefficient

The activity coefficient is referred to as a thermodynamic notion for liquid mixtures governed by temperature, pressure and composition (Sandler, 1989). In the past the activity coefficient was calculated using the Davies equation along with along the Debye-Hückel equation (Crawford, 1999). The activity coefficient is related to the margin the system expands from the ion and solvent interaction. The activity coefficient concept is based on the Pitzer ion-ion-interaction model that aids the computing of ionic strengths (Risacher and Clement, 2001). The activity coefficient is regarded as a limit of an equation derived for an activity that is a factor with no units. It has been suggested that the activity coefficient plays a significant role in the temperature, radiation and evaporation of saline solutions which subsequently affect the boundary layer (Oroud, 1999). The vapour pressure is another related factor in ion activity and activity coefficient (Kokya and Kokya, 2008).

Pitzer Equation

$$\frac{G^{ex}}{n_w RT} = f(u) + \sum_i \quad \sum_j \lambda_{ij}(u) M_i M_j + \sum_i \sum_j \sum_k \delta_{ijk} M_i M_j M_k \quad \ldots\ldots\ldots\ldots\ldots\ldots\ldots\ldots\ldots\ldots \quad (9)$$

Where G^{ex} is the free Gibbs energy that is available in 1 kg of solution, R is the number of moles, T is the absolute temperature, *M* is the molality of the ions, *f(u)* is the Debye-Hückel, λ is dependent on the ionic strength of the species. δ_{ijk} is referred to as the respective third viral coefficient while λ_{ij} is the second within the species (Sandler, 1989).

2.7.2 Alkalinity

The neutralisation of an acid is referred to as the alkalinity. To determine the alkalinity or acidity a titration is needed by means of a buffer like HCl or NaOH (Zhu, 2002). Factors which influence alkalinity are bicarbonates, carbonates and hydroxides (Du Plessis et al., 2006). In terms of geochemical modelling the carbonate aspect is regarded as the one of the most important parameters (Zhu and Anderson, 2002).

2.7.3 pH

The pH is the – Log of H^+ (Atkins, 1978). The pH can be a valuable tool to assess mining impacts in water and the variability in a natural water body (Van Veelen and Dhemba, 2011). The pH of a solution can be altered by the addtion of H_2SO_4 for a acidic solution or NaOH

for a alkaline solution (Al-Jibbouri et al., 2002). The pH factor is associated with the solubility of toxic heavy metals and the addition or removal of hydrogen from other ions (Fatoba, 2010).

2.7.4 Ion interaction

Ions in a solution are fundamentally determined by measuring conductivities and by the determination of colligative properties (Atkins, 1978). The conductive motion is based on the movement of charged ions while the colligative properties however are based on the empirical evidence of the vapour pressure characteristics and the osmotic pressures (Atkins, 1978).

The stoichiometric ionic strength is centred on the assumption that all ions are dissociated. The ionic strength of NaCl is virtually the same strength as the molality based on the single charge of each ion and the minimal presence of neutral species (Zhu, 2002). The thermodynamic of an ion depends on chemical potential μ (Atkins, 1978). In the case where I molar NaCl solution has a stoichiometric value of 1.00 molal and $CaCl_2$ has a stoichiometric value of 3.00 molal (Zhu, 2002). This relates to the deliquescence of $CaCl_2$ and the ability to attract moisture from the atmosphere (Molenda et al., 2013).

2.7.5 Evaporation models developed for saline application

Ali et al., (2001) developed a computer model for saline water bodies best suited for a monthly and annual application. The model modified the energy budget method to account for the salinity effect. In the early development models, Lee (1927) and Young, (1947) investigated evaporation models by experimenting with the salinity of lakes in comparison with clean water (Kokya and Kokya, 2008). Harbeck (1958) focused extensively on studies that involved the effects of total dissolved solids in a lake. Calder and Neal (1984) developed a model to accommodate salinity using the Penman method (Kokya & Kokya, 2008). See equation below.

$$\mathbf{E}= \frac{H+ \rho C_p \frac{e_g(T_a)-e/a}{r}}{\lambda(\frac{de_s}{dT_a}+\frac{\gamma p}{a})} \ldots\ldots \quad (10)$$

E is the evaporation, H is the sensible heat, ρ is the density of the water, C_p is the specific heat of air at constant pressure, e_s is the saturated air above the water surface, T_a is the air temperature, e_a is vapour pressure of the air, λ is the latent heat of evaporation, *eg* γp constant

of the psychometric equation and *r* is aerodynamic resistance to the transport of water vapour from the surface into the atmosphere

Other researchers developed models which focused directly on the density of water bodies. Stanhill (1994) used the energy budget method to highlight density in the vapour pressure gradient (Asmar and Ergenzinger., 1999). According to Stanhill (1994) the input energy is distributed in two ways, where 2\3 is consumed to establish the vapour pressure gradient and the remaining 1/3 as the radiation balance. Oroud, (1999) and Salhotra et al., (1985, 1987) experimented with the mass transfer method. In addition to this approach the wind speed, surface roughness and atmospheric stability is considered for the transfer coefficient Asmar and Ergenzinger, (1999).

Oroud (1999) pursued other possibilities and derived an equation where the activity coefficient can be expressed as a function of density but placed little emphasis on the ionic strength of the water. The modified Dalton model is;

$$\boldsymbol{E = f(u,\phi)[ae_s(T_w) - e]} \quad \text{..... (11)}$$

The *E* refers to the evaporation rate, *f (u,ϕ)* expresses the wind factor, *a* expresses the activity coefficient, e_s is the saturated air above the water body and *e* represents the air of the environment. T_w is used for water temperaure (Oroud, 1995)

The Penman equation enshrines an aerodynamic and thermodynamic combination. Oroud, (1999) suggested that calculation with the Penman equation rated the aerodynamic component very high for saline evaporation.

$$\mathbf{E=}\frac{\boldsymbol{\beta\Delta H}}{\boldsymbol{\beta\Delta+\psi}} + \boldsymbol{\psi f(u)}\frac{\boldsymbol{\beta e_a^* - e_a}}{\boldsymbol{\beta\Delta+\psi}} \quad \text{..... (12)}$$

Where E is the evaporation rate, β is referred to as the activity coefficient, *H* is the energy input, Δ is the gradient of saturated vapour pressure relative to temperature, ψ is the psychometric constant, *f(u)* is the wind speed, e_a^* is the saturated air above the brine and e_a is the vapour pressure of the air.

Summary

Table 2 displays different models to measure evaporation from a temporal perspective. Each model formulated by the author was applied with specific assumptions and limitations to be more effective. Investigators like Stanhill (1984) focused on the energy budget method to develop a model while Salhotra (1985) had a strong focus for the mass transfer application. These models focus on different methods to achieve a specific outcome. However the initial formulation was directed towards fresh water bodies and not a saline water bodies. In relation to this study, researchers like Oroud (1999) adapted his model to be more useful in saline environments. The incorporation of the activity coefficient into the model enables the model to incorporate the ion-ion interaction. Research regarding these types of studies especially with a saline application is very limited.

2.8 CONTROLLED EXPERIMENTS

2.8.1 Controlled environment limitations

Absolute control of individual parameters in an enclosed artificial environment can be very complex and challenging. A partial controlled environment allows the secondary effects of a controlled process to be factored in the experimental design. Apart from conducting experiments in the real environment there are several assumptions pending. In a real environment the parameters change partially or quite vigorously in a temporal and spatial environmental setting. To mirror fluctuations in a controlled environment is a challenge, especially controlling all the parameters at once to resemble a real environment. To put in motion a controlled experiment which represents the evaporation rate when conducting an indoor experiment can trigger a secondary effect. For instance, the humidity may fluctuate with respect to the temperature of the surroundings and the brine. The control factor has certain assumptions and the greater the need to control the environment, the greater the cost to construct and maintain the climate chamber.

Several authors conducted experiments in a controlled environment to mimic conditions in a real environment. Each assumption made, had limitations and subsequently influenced the end results and restricted the range of the controlled experiments. In the following paragraphs, a comprehensive overview highlights these limitations.

2.8.2 Wind tunnel experiment

The aerodynamic influence was highlighted by Oroud (1999) regarding the surface area of a liquid and wind effect. Various experiments were conducted with restricted parameters in a wind tunnel. Chu et al., (2010) conducted experiments in a wind tunnel using a standard Class A pan with water being exposed to different wind velocities along with different water depths. The average temperature and humidity was kept constant to determine the vapour pressure, because of the fluctuation in the laboratory. The evaporation was measured using a water level sensor with a resolution of 0.097 mm and the net radiation was kept to approximately 10 W/m^2. With an increase in wind velocity the evaporation rate increased at higher water levels Chu et al., (2010). At extreme high wind velocities the water was physically removed from the Class A pan. This relates to the entire water loss shared between evaporation and spillage. At lower water levels of the Class-A pan, the results were fairly different from the high wind velocities. Initially a steady increase in the evaporation rate was

observed with an increase in the wind velocity until the evaporation rate remained constant even at much higher wind speeds exceeding 7 m/s for the duration of 10 minutes Chu et al., (2010). Based on their experiments, the side wall of the container acted as a shield for the lower water levels against the high velocity winds Chu et al., (2010). Some of the experiment`s duration ranged between 4 to 15 hours based on the evaporation rates. With experiments conducted outside a wind tunnel, variations in wind speed are highly significant to pan evaporation Rayner (2009).

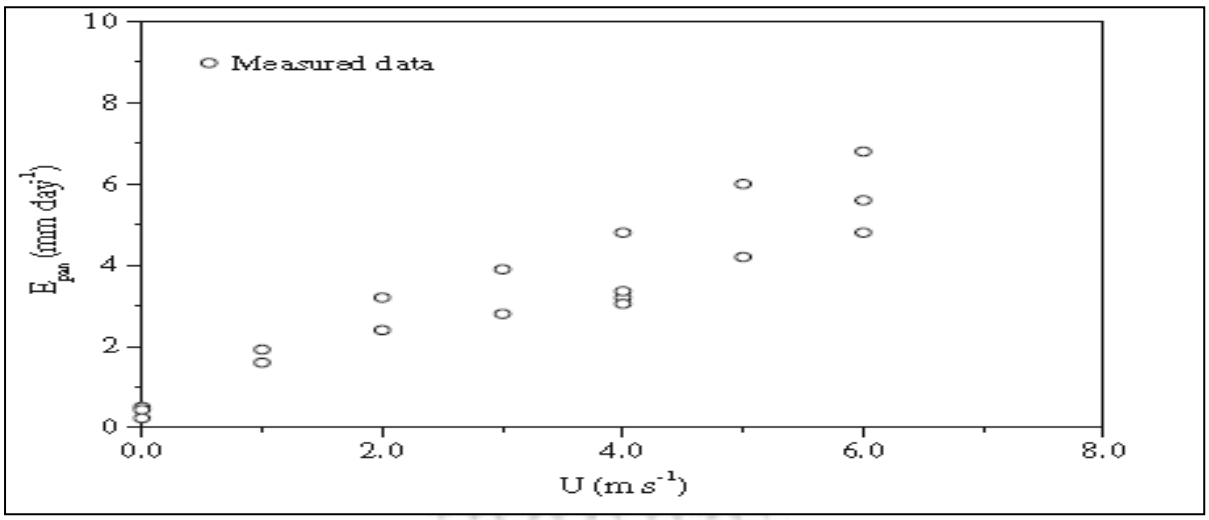

Figure 2.5 The results from Chu et al., (2010) of various wind speeds and different depths at 10 W/m 2.

2.8.3 Salinity and density experiments

Moore and Runkles (1968) investigated the impact of NaCl brines on evaporation rates in a climate chamber where it was tested under several different variations. Two models were compared during the experiment, a physical and a statistical model. Moore and Runkles (1968) varied the salinity along different wind speeds and concluded that the difference between pure water and the saline solution was greater at higher velocities.

Mao (1999) focused on the density of three salts NaCl, KCl and MgCl under the same environmental conditions. Each experiment had a pure water system as a control. Furthermore wind was generated and applied in additional experiments. The wind effect was compared with the natural observed evaporation rates. According to Mao (1999), the effect of the intermolecular forces of the salts was based on the Raoults law concept. Mao (1999) findings suggested that the evaporation rate of the salts was subjected to a different molecular weight. This particular study by Mao (1999) stated that the ionic composition of a saline

solution played a major role in the quest to determine the evaporation rate of saline water. Distilled water was used which was free from total dissolved solids (TDS) in place of ordinary potable water. The day and night temperature fluctuations were not considered in the experimental design.

Young (1947) investigated the difference in evaporation from between natural lakes and evaporation pans. Young`s study was mainly focused on salt lakes of the western parts of the United States. The investigation was directed towards developing coefficients for evaporation pans. The focus was on the shade variations of the evaporation pans which altered the heat storage capacity of the pan. Findings from Young (1947) stated that the absorption reduction based on the colour of the evaporation pans affected the evaporation rates. Key findings suggested that the water level of the lakes was of greater importance in the evaporation rate as it was inversely proportional to the density. In addition, Young (1947) varied the concentration of the NaCl in an evaporation pan to observe the salinity effect on evaporation. One of the main findings from the salinity experiments suggested that the increase in salinity from 5% to 20 %, reduced the overall evaporation rate of the brine.

The Dalton base models were examined by Jodat (2012b) under free and forced convection scenarios. The evaporation rate was determined by air flow rate and digital weighing of volume loss. Jodat (2012b) stated that an increase in vapour pressure difference or air velocities increase the evaporation rate. The main findings of their study, in particular at high evaporation rates was the behaviour of data that is nonlinear association as a result of the increased vapour pressure. Under free convection the density difference and vapour pressure difference played a significant role in the evaporation rate. Under forced and free convection the prediction of non-linearity between vapour pressure and evaporation rates was not projected.

The limitations of this particular study were the natural thermal stratification of the brine. The artificial heating source was located at the bottom of the container (see Figure 2.6) where a reverse thermal stratification might have occurred.

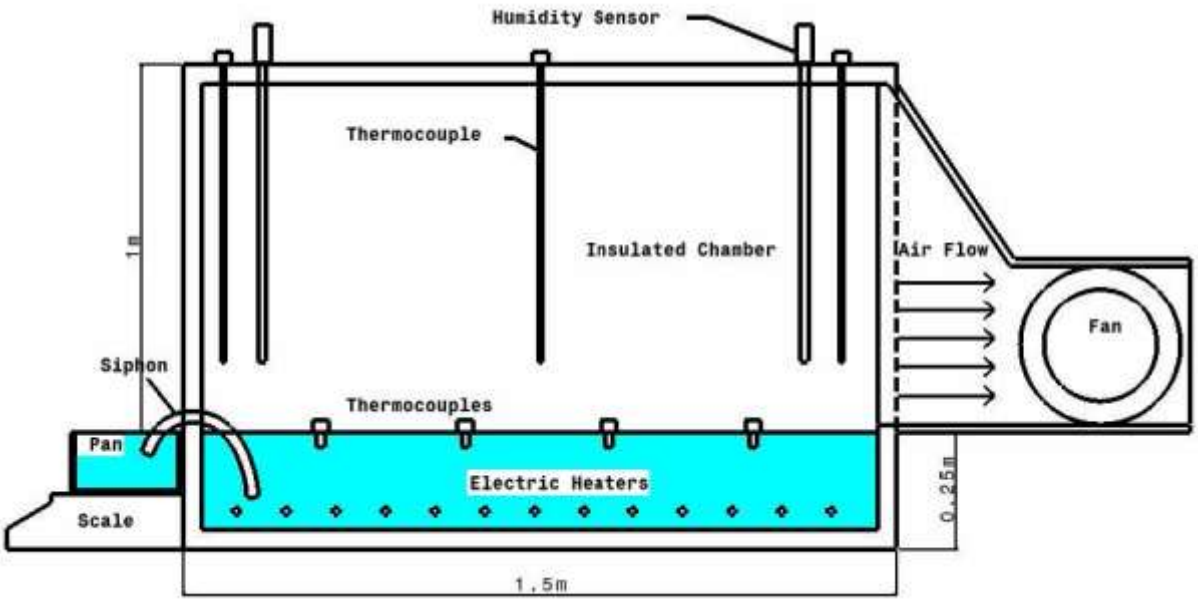

Figure 2.6 A scaled model of the experimental design by Jodat (2012b)

Schultheis et al., (2001) experimented with different brine types and densities with an indoor pilot plant. The crystallisation sequence with respect to brine composition was particular examined under artificial conditions. Schultheis et al (2001) adopted quite a unique setup to accommodate highly technical experiments. The system was able to constantly monitor and record changes in the parameters by implementing a floatable platform which housed the main temperature sensors. The wind generated by electrical fans was conveyed via flexible pipes. The pipes were mounted on the side of the containers and had limitation of maintaining a constant height above the brine surface. Schultheis et al., (2001) was able to design an experimental setup that incorporated a thermal stratification with along the depth of the container and the ability to record small fluctuations over the experimental period. The design is fairly simple to set up and the energy input was highly consistent for easy repeats.

A limiting factor to this set up was the inability to account for the humidity changes during the experiments. The positioning of the containers could influence the cascading of humidity accumulation and have influence the evaporation rate. The radiation input was not directly measured and the output of the infrared bulbs could have fluctuated in the intensity and subsequently impacted the evaporation rate. In addition, the ambient temperature play a major role in the controlled experiments was not accounted for throughout their experiment. Overall Schultheis et al., (2001) experimental design was more realistic and was best suited for this study.

Kirabira et al, (2015) experimented with the crystallised sequence of Lake Katwe through natural evaporation. The investigators applied the geochemical simulation by using computer simulated software. The researchers applied the Pitzer thermodynamic model in the PhreeqC 3.0 software application. The modelling assumed that the lake had no replenishing sources such as rainfall. In addition, the model also assumes that the evolution pathways become the carbonated type brine rich in Na+, K+, Cl-, $SO_{4,}$ CO_3^2, $HCO_{3,}$ and HCO_3^- prior to mineral precipitation. Their results suggested that halite was the dominating mineral during precipitation while the carbonated minerals remained in the solution after 60% evaporation. The limiting factor for their simulation was to identify the specific geochemical pathways and known time for the brine solution to reach equilibrium.

2.8.4 Nanotechnology in evaporation experiments

The manipulation of the evaporation rates in the modern era is being pursued at a micro level. Moghiman and Aslani (2013) experimented with base fluids with the addition of nanoparticles to manipulate the evaporation rate (see experimental setup shown in Figure 2.7). The objectives of their study focused particularly on the behaviour of 5 nanofluids and compared the results thereof. The main outcome of the experiment was the reduction of the surface tension of the deionised water with the inclusion of the nano particles. Moghiman and Aslani (2013) stated that the concentration of nano particles influenced the evaporation efficiency. A factor of approximately 1.1 was achieved in evaporation rates when 1% of Povidone (PVP) was applied to the system.

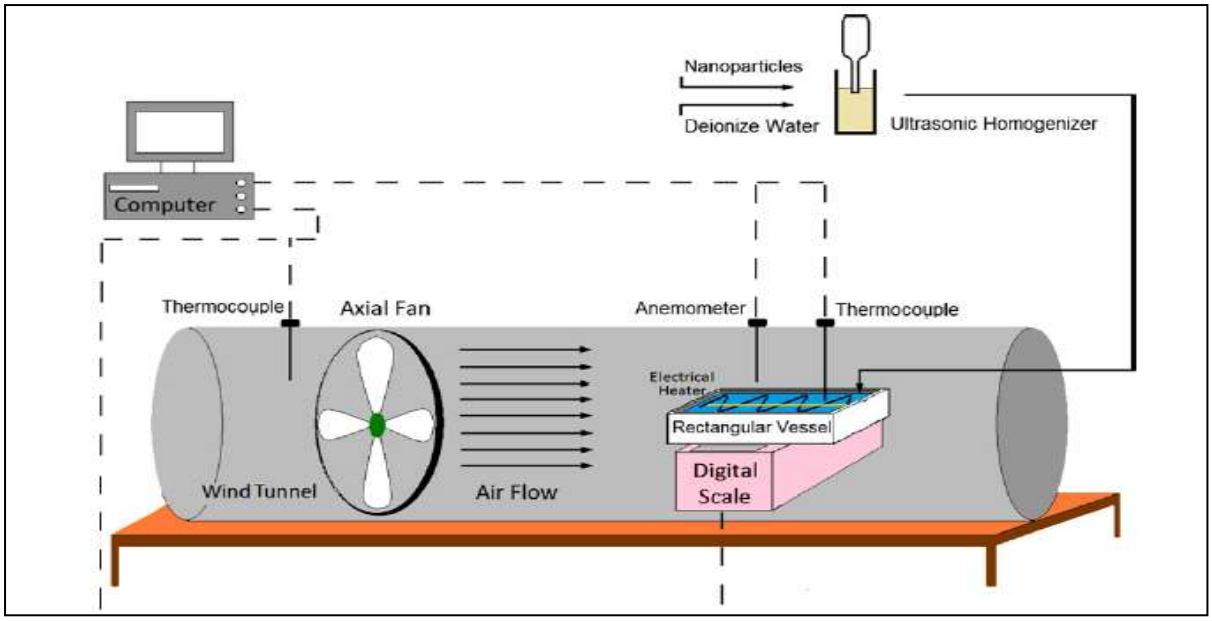

Figure 2.7 Layout of the experimental setup of Moghiman and Aslani (2013).

2.9 MITIGATION MEASURES

2.9.1 Brine disposal

Brine is also referred to as reject brine, wastewater and membrane concentrate (Ahmed et al., 2001; Khordagui, 1997). The disposal of brine can be economically viable or influence the environment (Ahmed et al., 2001). Surface disposal of brine increases the possibility for groundwater pollution. The highly saline solution can increase the salinity of the groundwater. Other toxic chemicals such as anti-scalent can also add to environmental degradation Ahmed et al., 2001).

Zayani et al., (1999) conducted brine experiments where the samples of a saline source in the south of Tunisia were subjected to conditions similar to a real environment in a laboratory. Various ions were exposed to climatic conditions similar to the summer season in the Tunisia region. The observations were focused on the variations in densities and molar concentration of different ions. The ions used in the experiment were Na+, Mg^{+2}, K^{+1}, $Cl^{-1}$and SO_4^{-2} ions from precipitated salts that had their respective densities measured according to their natural sequence of precipitation. The precipitated salts were NaCl, ($MgSO_4 \cdot KCl \cdot H_2O$) and $MgSO_4 \cdot 7H_2O$ and suggested a change in density of the various brines during the crystallisation of the salts.

2.9.2 Desalination

The desalination era started in the early 1960`s with limited application and technology (Ahmed et al., 2000). Desalination has since been developed to service the needs for a broader spectrum of uses. Currently there are two types of desalinations systems. The first type is subjected to a phase change where the solution is deliberately forced to evaporated or freeze. These systems are usually associated with the multi-stage flash (MSF) system, vapour compression (VC), freezing and finally solar distillation. The second type is a single phase system where the brine does not undergo any phase changes. Electrodialysis (ED) and reverse osmosis (RO) are considered to be such systems. Despite the difference in the design between the single and multiphase systems, the waste saline concentrate product still remains an issue. A number of factors influence the volume of waste product (brine concentrate), including the status of the feed water into the plant and the applied system. The reverse osmosis (RO) system delivers approximately 25% of waste product (brine concentrate) during the desalination process while systems like (MSF) and multi-effect boiling (MEB) achieve far lower water recoveries (Awerbuch et al., 1990).

Desalination of brackish water such as seawater, groundwater and mine water is gaining popularity. Desalination is a process which helps improve the quality of wastewater discharged into our rivers and streams. It is certainly a big contributor to alleviate water shortage with supply to various sectors, such as municipalities, industries and agriculture. Desalination processes are highly energy intensive and require highly skilled personnel to operate desalination plants. The desalination industry acknowledges that desalting seawater consumes the least energy (Ahmed et al., 2000). Inland desalting can be more challenging as it is subjected to a different environment with limited water options and strict regulations (Ahmed et al., 2001). However several other good initiatives have developed from desalination. One example is an uranium mine in Namibia where desalting seawater was considered for the mine and potable water for the local municipalities (Ruffini, 2009).

It is a common occurrence for brines to be pre-treated prior to the processing in a RO system. The pre-treatment may consist of acidification, anti-scalants and chlorination while the pre-treatments for a lower water quality may use filtration, coagulation, ion exchange and carbon adsorption as a viable option (Ahmed et al., 2000). Brine is associated with high total dissolved solids (TDS) and requires minimal further processing with the addition of chemicals (Ahmed et al., 2000). It has been found that the cost of disposing brine from an

inland area is far greater than a desalination plant along a vast water body such as the ocean (Williamson et al., 1982; Glueckstem and Priel, 1996). The measurement of brine concentrate is known as the concentration factor (CF).

$$\boldsymbol{CF = \frac{1}{1-R}} \quad \text{(13)}$$

CF= concentration factor

R= fractional recovery

2.9.3 Eutectic freeze method

Eutectic freeze is one of the most advanced technologies in brine treatment as a mitigation measure. Eutectic Freeze Crystallisation (EFC) has a lower energy output in comparison to vaporization energy. The Eutectic point of a mixture is the actual minimal point of freezing. The technology is not an entirely new concept where the by-products are produced for different applications. This method works on the basis of a salt crystallising as it cools below its freezing temperature. Along with salt development ice crystals form as well and float to the surface since ice is less dense than brine. The salt crystals that form will continue to precipitate at the bottom of the solution (Günther and Mey, 2006). Crystallisation of complex salt solutions allows easy separating by this method. Each individual salt has its own eutectic freeze point and can be easily separated from the remaining brine by altering the brine concentration. The energy required to execute this method is less intensive than thermal evaporation methods but freezing demands a significant amount of energy (Günther and Naidu, 2008). The energy required to produce ice is approximately (6.01 kJ/mol) while the energy to vaporise water is (40.65 kJ/mol) but in contrary the overall cooling process is more energy intensive (Lewis et al., 2010). In a broader perspective impurities within the brines have a significant effect on the EFC process in terms of efficiency (Lewis at al., 2010). Eutectic Freeze Crystallisation (EFC) research is still developing but shows promising results when assisted by reverse osmosis treatment (Randall et al., 2011).

2.9.4 Dye application

The concept of dying brines is not entirely a new phenomenon. The application is very popular in mining table salt (NaCl) where it utilises a natural colour mechanism to enhance the absorption of heat energy to improve evaporation**.** In the case of NaCl harvesting the raw brine undergoes a physical and a biological (Halophiles**)** process. Methylene blue is a

common substance used to enhance the evaporation rate in industrial practices. Furthermore Methylene blue can be decolourised and be less prominent when subjected to titania-based photocatalysis (Houas et al., 2001)

2.9.5 Mechanical sprayers

The use of mechanical sprayers can enhance the evaporation rate of brine ponds. Nozzles are used to disperse the brine in a form of a mist over the ponds. This method uses nozzles that are connected via pipes to compressors that condense the brine and feed the system. In this system a large amount of the energy is used to power the compressors. The drawback of this system is the extensive energy consumption needed to maintain the high pressure for this system. Another potential drawback might be that strong winds can blow the mist away from the pond and onto riparian vegetation and surrounding soil. The use of mechanical evaporators can be a costly exercise based on high energy consumption (Ahmed et al., 2000). According to Mickley, (1995) mechanical evaporators meet certain criteria for irrigation. Some of the main factors are the location of the proposed plant, the land requirements, vegetation selection and the surface runoff regulation.

Temperature plays a significant role in the evaporation process and is directly related to the energy costs. Further investigation on the effect of temperature and salinity on absorption must then be known in order to interpret the measured absorption specific heat (*Cp)* values. To rectify the thermal stratification of a traditional pond, a layer of coal cinder can be placed at the bottom of the pond to increase the temperature closer to the bottom of the pond and subsequently increase the evaporation rate (Wang et al, 2015).

2.9.7 Deep well injection

This option is ideal for hazardous waste in particular from municipalities (El-Naas, 2011). Deep well injection is certainly not one of the most cost effective methods by todays standards (Mickley, 2006). The main drawbacks of this method are acquisitioning of a geologically stable site, adjusting the brine composition and transportation (El-Naas, 2011). The application of this method is not very prominent in the South Africn context as a result of the risk factor to groundwater (Du Plessis, 2006).

2.9.8 Bio-remediation

The bio-remediation process was developed from the idea based on microorganisms producing alkalinity which counters the actions of AMD (Barrie Johnson and Hallberg.,

2005). Developments in the field of biological environmental research can play a significant role in the reduction of brine impact on the environment. Algae like Spirulina have some level of success in the reduction of brine originating from coal mining activity (Günther and Naidu, 2008 ; Barrie Johnson and Hallberg, 2005). Active biological systems such as the implementation of wetlands are familiar waterways to filter effluent originating from wastewater treatment plants. In coal mining activity the application of algae such as *Spirulina* had a certain level of success in the reduction of brine streams (Rose, 2002; Günther and Naidu, 2008). The assistance from biological systems is applicable to remediation, but the exact contribution from iron oxidation or microorganisms leaves room for some dispute (Barrie Johnson and Hallberg, 2005).

2.9.10 Zero discharge

The concept of zero discharge refers to the reduction in the waste generated by desalination (Mohamed et al., 2005). In recent times most desalination plants are associated with waste products as 100 % water recover remains a challenge (Giwa et al., 2017). In the past the general perception viewed brine as a waste by-product and damaging to the environment. This concept however is changing and brines are seen as a saline resource in the modern world (Ahmed et al., 2000). Zero liquid or near liquid discharge is under constant development to improve the recovery of potable water and reject brines with a greater focus towards pressurised and electrical potential membranes (Giwa et al., 2017).

2.10 MODELLING

2.10.1 Geochemical aspect

In 1887 there were experiments conducted by the Colorado Agricultural Experimental Station on a sunken pan. They realised the complexity of the evaporation process and the need to develop it further. As early as the 1930`s evaporation experiments were conducted and deemed an important tool to predetermine the effect on reservoirs and lakes from an economic view point.

The very fundamental law that governs the evaporation from a free water surface was brought to the fore by James Dalton in 1802 (Rohwer, 1931). Moreover, Fritzgerald realised the value of controlled experiments where he documented a series of empirical data for both laboratory condition and natural environments (Rohwer, 1931). Modelling is regarded as a vital tool to expose geochemical processes, analyse laboratory experiments and use as a mechanism to

predict and monitor for the future (Crawford, 1999). Despite all the accolades associated with geochemical modelling, it remains rather a tool for the preserve of research groups and not in the public domain (Crawford, 1999). The factor which has a greater influence in determining geochemical processes in the modern era is the processing speed of a computer (Risacher and Clement, 2001).

2.10.2 Solubility

A solute dissolved in a solvent until saturation status translates to the solubility of a solution (Atkins, 1978). The mechanism which drives solubility is the Gibbs free energy concept (Zhu, 2002). When a solution has reached is maximum dissolved capabilities, it is known to reach its solubility limit (Connell, 2005). A number of factors can influence the solubility of a salt. Temperature is one of the most important factors as it is almost a certainty that it will have a significant impact on the solubility of a salt. The pH can affect the solubility of particularly compounds like carbonates and silicates (Shukla et al., 2008).

2.11 COMPUTER APPLICATION FOR GEOCHEMICAL ANALYSIS

Several components are required for the application of geochemical modelling. A database and a computer code are required to combine the thermodynamics, the kinetic ability of the database and concentrations as an input file (Zhu et al., 2002).

2.11.1 The code

Codes are a set of mathematical processes activated by a computer on demand to enable a number of equations to solve various chemical reactions. The demand to predict elevated concentrations of salts in a spatial and temporal dimension is high especially in the quest to solve environmental problems associated with contamination and water resource problems (Zhu and Anderson, 2002).

2.11.2 The database

Equilibrium constants are not fixed into the coding of the software that is designed to accommodate the change of the equilibrium constants (Zhu and Anderson, 2002). PhreeqC and EQ3/6 enables the user to change the database and input file to manipulate the equilibrium constant.

2.11.3 Computer programs available

MINTEQA2 Version 3.11 is a free application sponsored by the US EPA. The latest known version is 4.03 recognised in 2006 and is a free application. It is able to perform very complex surface models (Zhu and Anderson, 2002). Speciation, redox and ion exchange can be computed using this particular software.

The Geochemist Workbench has a wide range of programs that was developed by Aqueous Solutions LLC. The program focuses on the thermodynamic equilibrium constant that is used to compute the equilibra in the range of (0°C -300°C). This is proprietary software which limits the usage to a smaller fraternity although it can perform more functions than the other software.

PhreeqC software was developed by the US Geological Survey which featured speciation and reaction path programs (Zhu and Anderson, 2002; Parkhurst and Appelo., 2013). The software makes use of a C language where it can perform speciation, solubility, reaction pathways and inverse mass balance modelling The program can consider the analytical uncertainties. PhreeqC has no licence obligations hence it is very popular to a wider audience and ideal for this particular study.

2.12. CLIMATE CHANGE

2.12.1 Temperature

Studies project an increase of approximately 3°C for the Southern region of Africa based on climate change impacts (Malisawa and Rautenbach, 2012). The southern region of Africa is known to be a water scarce area and aridity is set to increase based on the warming effects resulting from climate change (Morishima and Akasaka, 2010; Kusangaya et al., 2014). However, the increasing temperature has the potential to enhance evaporation of water bodies (Warburton and Schulze, 2005). This could negatively impact natural water resources as salt loads are expected to grow with increasing evaporation.

2.12.2 Rainfall

The rainfall fluctuations are expected to surge in South Africa associated with increased rainfall intensity (Kane, 2009; Kusangaya et al., 2014). A large number of models suggested that southern African will experience lower rainfall, as well as an increase in runoff and evaporation by 2050 (IPCC, 2007). It is expected that the southern African region will have a

projected decrease of 3-23% in rainfall due to climate change. This however should encourage greater efforts towards water saving and efficient practices (Mazvimavi, 2011).

2.12.3 Evaporation forecast

A projected increase of approximately 40% in evaporation based on climate change can influence the outflow of reservoirs significantly as a result of temperature increases (Kusangaya et al., 2014). As a collective, the projected increase in temperatures would result in dryer region for South Africa but may be ideal for the solar evaporation ponds.

2.12.4 Study of this paper

Evaporation is a very important component of the hydrological cycle. The Penman-Monteith method is one of the most used models to determine evapotranspiration. However, the vast growing industrial sector is facing challenges with waste by-products such as brines from various activities. During the early 1900`s the brine factor was neglected because of limited environmental laws and concerns. In addition, monitoring of these harmful activities only occurred well after many environmental disasters were discovered. Today these activities are a major concern and waste disposal must be accounted for as it is highly regulated by government through more stringent laws.

As part of the remedial efforts, brines are stored in ponds and subsequently occupy valuable space and the lifespan of these ponds are paramount from a sustainability perspective. Evaporation plays a significant role throughout the entire process when it concerns the fluctuating brine levels of these ponds. This makes monitoring a key requirement.

Pond level changes require a greater consideration for predictions over an extensive period. Models are being used to predict current and future outcomes. Most available models focus on freshwater bodies and often neglect the saline factor. With almost certainty this limitation restricts the accuracy of models when predicting evaporation from saline water bodies.

With the incorporation of salinity, the accuracy of the model increases as more parameters are considered for a certain application. Saline water bodies have a tendency to show lower evaporation rates than fresh water bodies based on the lower vapour pressure. The concentration factor and salts selection are key variables in developing saline evaporation models.

Most evaporation models are based on the energy balance and mass transfer. However, these applications are very limited with the more complex saline adaptations. Computer generated models such as PheerqC that are based on the ion-ion equations are being utilised to determine aqueous speciation of elements (Baptist 2014).

CHAPTER 3

STUDY AREA AND CHARACTERISATION OF EMALAHLENI BRINE

In Chapter 1 the problems associated with brine ponds in mining areas were identified and the aim of this study was to highlight these challenges. In the previous chapter the concept of evaporation, its measurement and modelling were in particular discussed. To achieve a good simulation of brine evaporation in the laboratory, it is important to characterise certain components of the eMalahleni area. Both the climatic conditions of the area and the chemical composition of the brines are major components and Chapter 3 focuses on these aspects.

3.1 Climate of the study area

Climatic data for the study area was obtained and used as a guideline for the laboratory simulations. The eMalahleni (Witbank) area is part of the Highveld region and is normally associated with moderate temperatures and cold winters (see Figure 3.1 and 3.2). The region in Figure 3.3 is known for a summer rainfall occurrence and a severe frost appearance throughout winter.

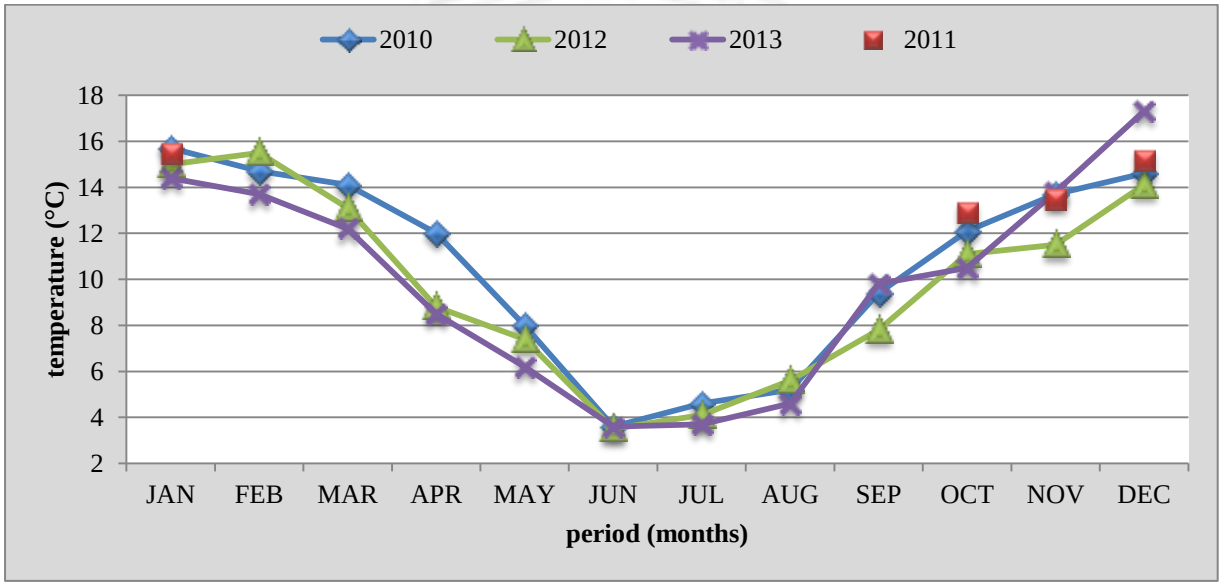

Figure 3.1 The monthly minimum temperatures (for the period 2010 to 2013) of the relevant secondary Olifants Catchment where the study area is situated. The 2011 is not a complete data set and contains several missing data points (Courtesy of South African Weather Service, 2013).

The average minimum temperatures in the Olifants Catchment ranged between 3 and 18°C over the last four years according to South African Weather Services data (SAWS). The lowest temperatures occurred in winter during the June and July period. The highest

minimum temperatures occurred during the January and December period where the temperatures exceeded 14 °C. Although the higher temperatures could contribute to higher evaporation rates, the high precipitation expected during the summer period (Figure 3.3) could counter the higher temperature and as a result also higher evaporation rates.

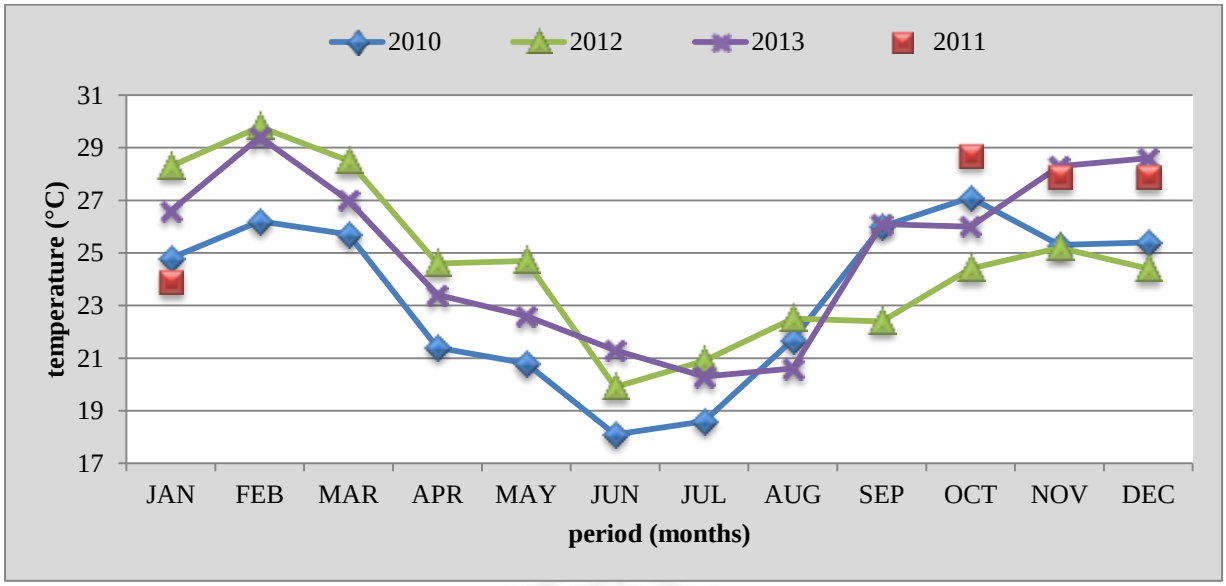

Figure 3.2 The monthly average maximum temperatures of eMalahleni area for the period 2010 to 1013. The 2011 data set is not completed and contains several missing data points. (Courtesy of SAWS 2013)

The data from the South African Weather Service suggests that the average maximum temperatures portray the eMalahleni area as a real environment. Figure 3.2 shows that the highest monthly temperatures occurred during the 2010 and 2013 session. This occurred during the summer period between October and February that coinciding with the highest rainfall period.

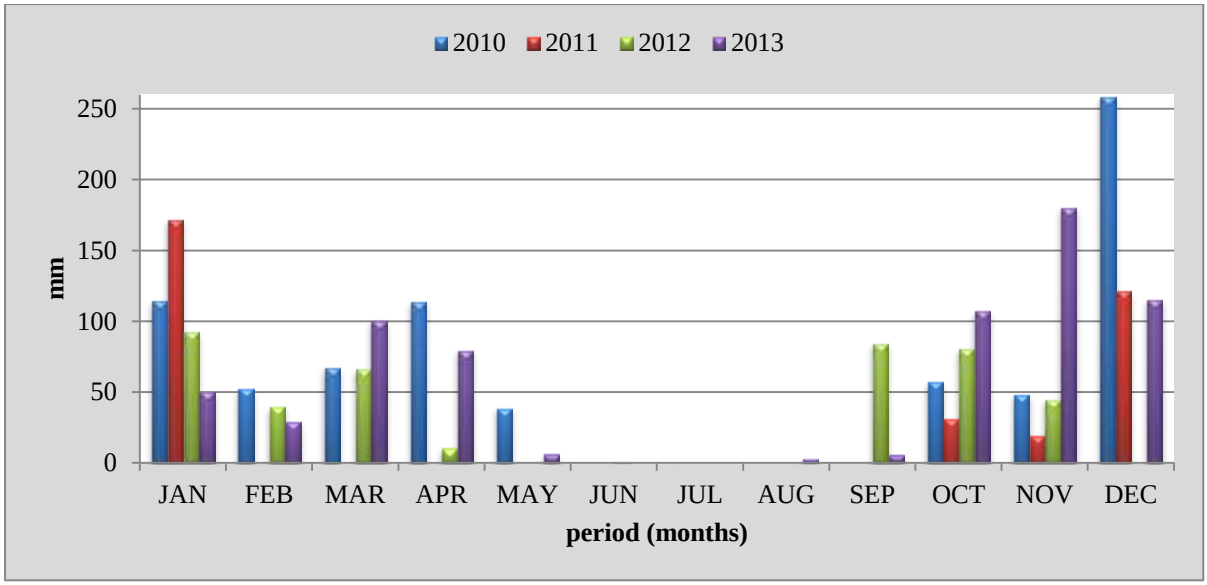

Figure 3.3 The monthly rainfall of the eMalahleni area for the period 2010 to 2013. (Courtesy of South African Weather Service, 2013)

Total rainfall varied between 550 and 750 mm/annum for the Highveld and eastern Lowveld (Van Veelen and Dhemba, 2011). Figure 3.3 shows that the highest rainfall occurred during December and January for the period 2010 – 2013.

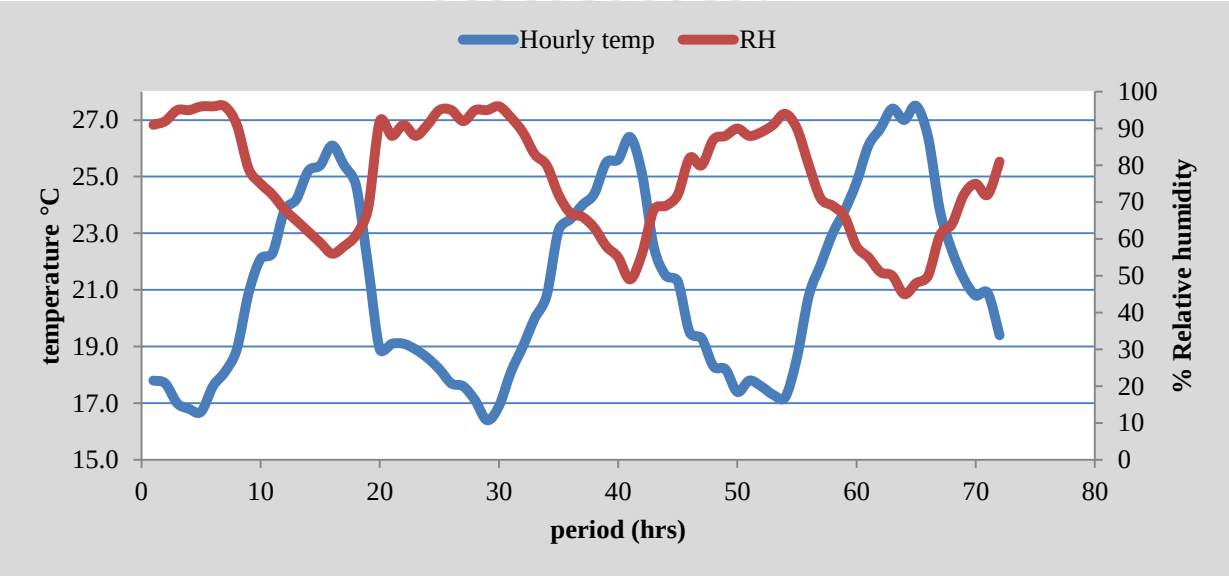

Figure 3.4 The average air temperature and the relative humidity of the eMalahleni area for 3 days. (17 to 19) February 2009. (Courtesy of SAWS, 2013)

Figure 3.4 shows the typical temperature and humidity variations in the eMalahleni area over 3 days during the summer period. Humidity varies between 48% and 55% during the warmest part of the day and exceeded 90% at night.

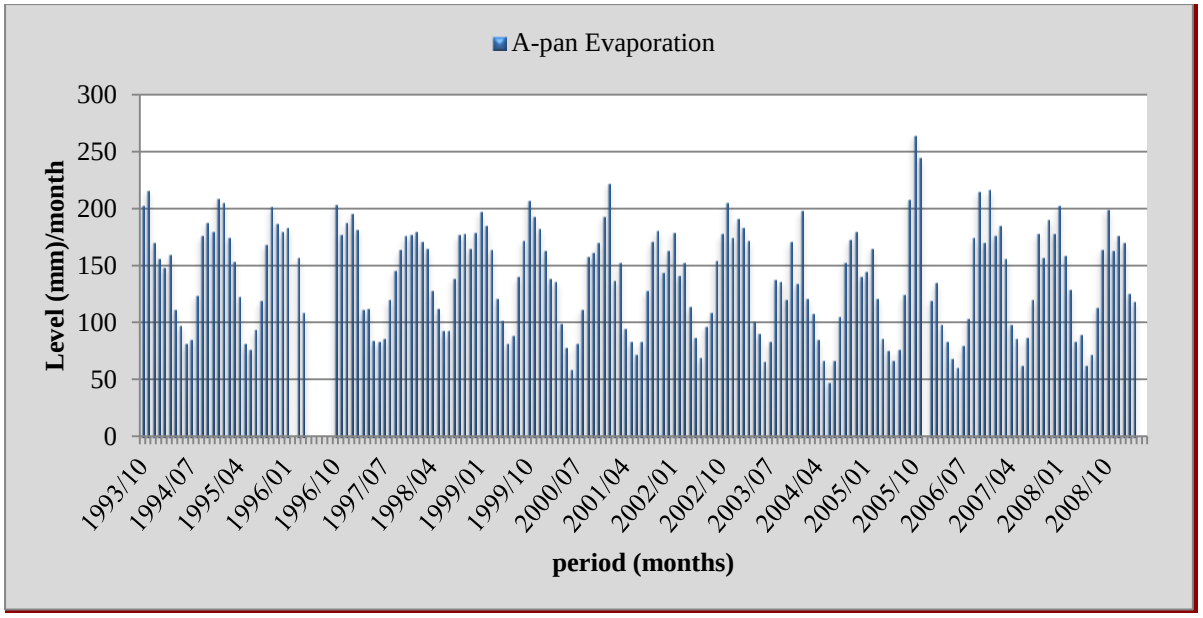

Figure 3.5 The pan evaporation data of the Witbank Dam in Mpumalanga, is in close proximity to the brine ponds. (The data obtain from DWS website, retrieved 2015)

Evaporation in the study area was assumed to be similar to the evaporation reported by the Department of Water and Sanitation (DWS) at the nearby Witbank Dam in Mpumalanga (Figure 3.5). The reported evaporation data over an extensive period of several years exhibits the evaporation rates of the region where the eMalahleni brine ponds are located. However, Figure 3.5 highlights the evaporation over a fresh water body in the absence of a salinity factor. A fresh water body is expected to have higher evaporation rates than a saline water source and based on certain anomalies.

3.2 The eMalahleni brine

The main objective for the characterization of the brine is to identify all the major ions of the eMalahleni brine and subsequently simulate the evaporation over various concentrations of certain major ions represented by using synthetic salts in the laboratory. Analytical tools and techniques such as mass spectroscopy (ICP) and ion chromatography (IC) were used to examine the brine. This provided the necessary information needed to identify the major ions of the eMalahleni brine. Comparing the results with an earlier study (Dama-Fakir et al., 2012), the analysis also served as a basis to verify whether the characteristic of the eMalahleni brine have changed over the past few years.

The original brine for this study was collected from the water reclamation plant in eMalahleni, Mpumalanga South Africa, after a triple reverse osmosis treatment process occurred. The sample was stored in several 25 L containers sealed with Plastiform and only the samples for geochemical analysis were refrigerated at approximately 4 °C. The $NaSO_4$, NaCl, $CaSO_4$, $MgSO_4$, $NaNO_3$, K_2SO_4 synthetic salts were obtained from Kimix Chemical & Lab Supplies (see Table 2 below).

Table 2.2 Summary of the synthetic salts used for the experiments

Formula of synthetic salts	Purity (%)	Supplier
NaCl	99	Kimix
$Na_2SO_4.10H_2O$	99.5	Kimix
$NaNO_3$	98.5	Kimix
KCl	99.5	Kimix
$CaSO_4.2H2O$	99	Kimix
$MgSO_4.7H2O$	99.5	Kimix

During each experimental cycle, the relevant salts were weighed and then gradually added to a container with distilled water to make 0.5 M salt solutions. The solution was stirred with a hollow PVC pipe until all the salts have dissolved in the water. To resemble a natural pond, the solution was then left undisturbed for several hours to allow for natural precipitation. This process was repeated for all the synthetic salts in Table 2.2 and the control unit with distilled water was refilled to a specific water level.

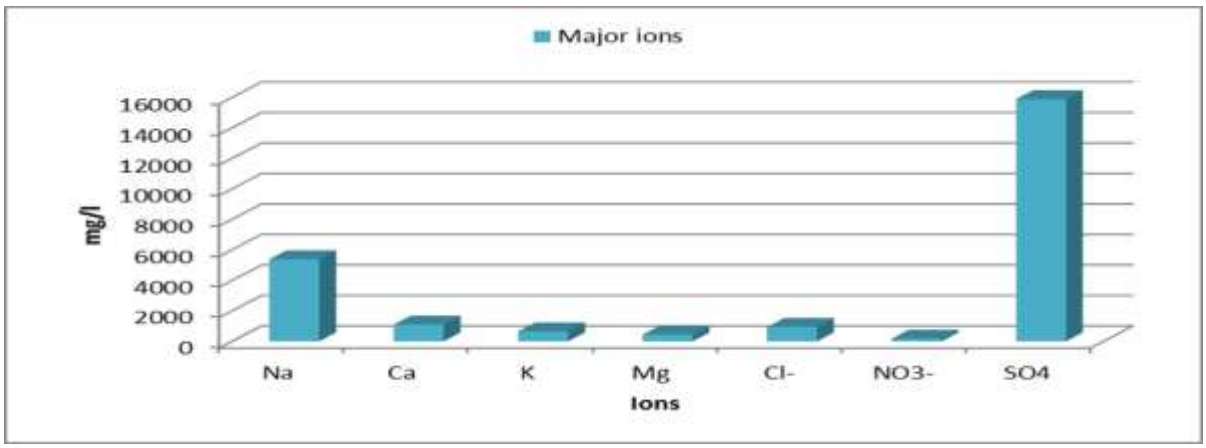

Figure 3.6 Major ions of the eMalahleni brine were analysed in 2013 using an Inductive Coupled Plasma with a mass spectrometer.

The eMalahleni brine had a slightly alkaline pH of 7.23 as a result of pre-treatment with lime prior to the reverse osmosis process. According to Du Plessis et al., (2006), lime softening is a normal procedure to raise the pH levels of predominantly acidic brines. The lower pH prior to desalination results from the contribution of sulphuric acid, a direct product of the oxidation of pyrite occurring in the coal (Bell et al., 2001). The cation-anion balance error from the eMalahleni brine was less than 5%. The total alkalinity (HCO_3, CO_3) was determined using HCl titration and methyl orange to indicate the changes.

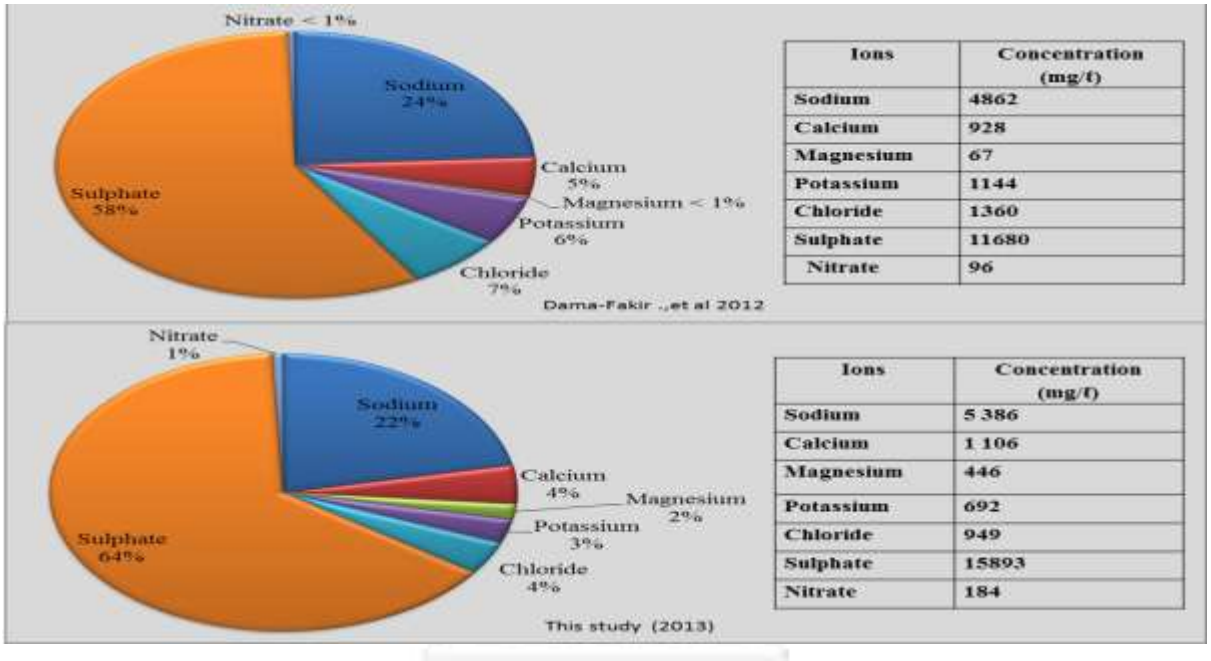

Ions	Concentration (mg/l)
Sodium	4862
Calcium	928
Magnesium	67
Potassium	1144
Chloride	1360
Sulphate	11680
Nitrate	96

Ions	Concentration (mg/l)
Sodium	5 386
Calcium	1 106
Magnesium	446
Potassium	692
Chloride	949
Sulphate	15893
Nitrate	184

Figure 3.7 A comparison of the present eMalahleni brine composition with an analysis by Dama-Fakir et al. (2012).

The analyses of the eMalahleni brine that is shown in both pie-charts (Figure 3.7) indicated the dominance of sulphate and sodium in the composition of the brine. The eMalahleni brine composition suggests a marginal change over the last few years. The brine analysis conducted by Dama-Fakir et al (2012) was presumably analysed in 2010 while the brine used in the current study was analysed in 2013. In the current study the brine composition shows a slight increase in sodium and a decrease in sulphate. Another notable change was the increase in magnesium. A 6% sulphate increase and 2% decrease in sodium could likely improve the evaporation rate because of the slight change in solubility.

By using PhreeqC, a computer modelling program developed for simulating chemical reactions and processes in natural water (Parkhurst and Appelo, 1999), a speciation analysis

was conducted to determine the composition of the brine (see Appendix 2). This was then compared with the results obtained by Dama-Fakir et al., (2012). The results are summarized in Table 3.1

Table 3.1 A comparison of the output files of the eMalahleni brine in PhreeqC

Parameter	This study	Dama-Fakir et al, (2012)
pH	7.32	7
pe	4	4
Specific Conductance (µS/cm,25°C)	23656	21566
Density (g/cm^3)	1.01979	1.01506
Volume (L)	1.00604	1.00585
Activity of water	0.992	0.993
Ionic strength	4.19E-01	3.466E-01
Mass of water (kg)	1.00E+00	1.00E+00
Total CO_2 (mol/kg)	7.00E-03	7.50E+00
Temperature (°C)	25	25
Electrical balance (eq)	-1.25E-02	3.05E+00
Percentage error 100*(Cat)	-2.2	0.62
Interactions	7	8
Total H	1.11E+02	1.110190E+
Total 0	5.62E+01	5.602906E+

The analysis was completed using PhreeqC 3.1 and it indicates a negligible change in certain parameters, in particular the ionic strength of the brine solutions. The previous study by Dama-Fakir et al., (2012) was poised slightly towards the cation side while this study shows a balance towards the anion side. In theory, this particular study has a marginal higher ionic strength compared to the brine solution from the Dama-Fakir et al, (2012) study.

Subsequently the activity of the brines suggested the difference was very small in terms of interactions. The analysis from the brines shown in Figure 3.7 suggests a small change in the composition, but the analysis conducted by using PhreeqC (Table 3.1) indicates a very similar ionic strength related to almost similar evaporation rates from the same study area. If the present small difference in composition indicated by the two analyses should change vastly in future, the brine composition could have greater implications over a longer period.

Knowing the relevant climatic conditions in the study area and the composition of the eMalahleni brine, it is more applicable that the following chapter focuses on simulating these conditions in a laboratory and measuring the evaporation associated with these conditions.

CHAPTER 4
MATERIALS AND METHODS

LABORATORY PREPARATION AND SIMULATION METHODOLOGY

Measuring evaporation from a brine surface in a laboratory can be challenging, mainly due to the many variables that are playing a role as been discussed earlier. Creating a laboratory environment that is similar to reality and equipped with the right instrumentation can be a costly undertaking. These aspects will be discussed in more detail in this chapter.

The main objectives for the study were set out in Chapter 1. The first two of these objectives, namely identifying the main climatic factors influencing evaporation rates in general and determining the eMalahleni brine composition were addressed in the previous two chapters. To address objective three and four, the focus is firstly on determining the effect of varying molal concentrations of the brine components on its evaporation. Secondly, to compare the evaporation rate of the synthetic brines with a known starting concentration under forced convection conditions. Two experimental operations were required firstly, a setting where the salinity can be altered under normal room temperature conditions and another where a wind force can be applied to simulate environmental conditions of the eMalahleni.

4.1 SALINITY EXPERIMENTAL SETUP

The main purpose of an incremental change in molality was to highlight the effect of salinity on the evaporation rate with respect to the different salt solutions. The potential change in evaporation rates of the major salts is an indication of its diverse interaction between a liquid to air interphase.

To investigate the salinity aspect, a smaller volume of brine was necessary to demonstrate changes in the evaporation rates. Higher evaporation rates are generally achieved with shallow water (Ai-Shammiri, 2002). Relatively uniform environmental conditions were needed for these experiments in order to verify their effects under similar conditions. The laboratory was air-conditioned with the temperature set to approximately 20˚C and the humidity close to 60% (but fluctuating between 55% and 75%). The windows were covered with a fire blanket to prevent any additional thermal radiation from the outside to interfere with the experiments (see Chapter 2). Two metal frames were placed in the centre of the room to ensure even air distribution. Each metal frame had a surface area of approximately 150 x 42 cm and was 70 cm from the ground (Figure 4.1).

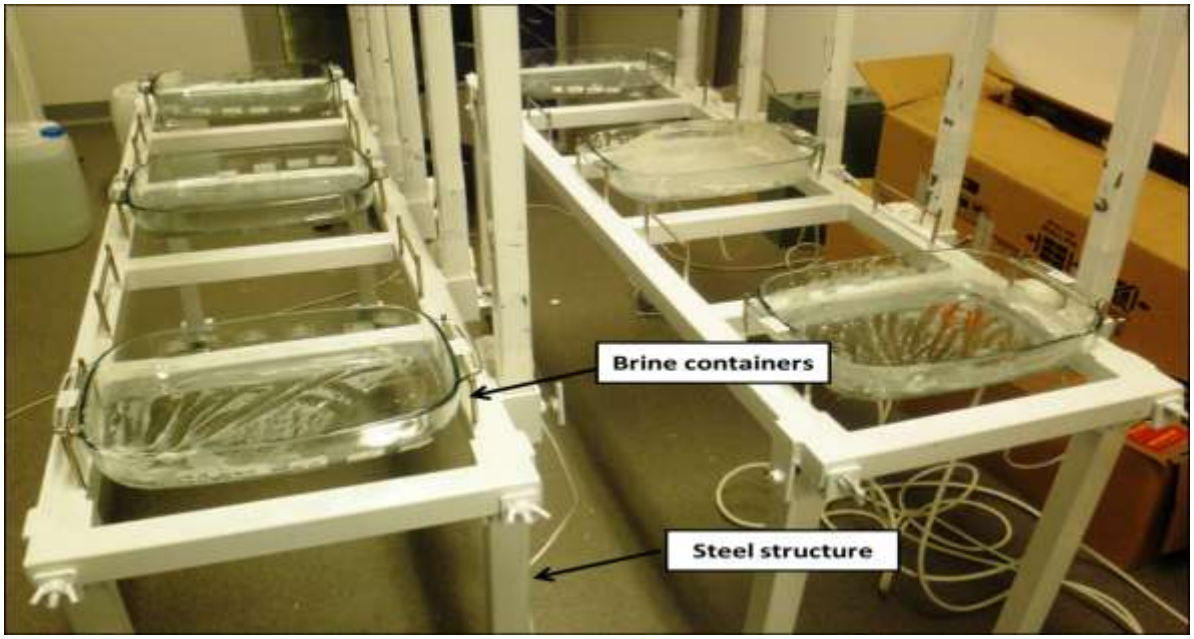

Figure 4.1 The experimental setup with different molality from the same salt solution was subjected to evaporation during the salinity experiments.

A preliminary experiment was conducted to eliminate any irregularities and to establish a baseline. Six glass containers were placed evenly apart in the metal frame. Each of these was filled with a volume of 500 cc distilled water and left to evaporate over a four day period. The volume of water remaining in each container after four days was decanted into a 500 cc measuring cylinder to record the changes in evaporation. This served as a validation that the same volume of water will evaporate from similar containers under similar conditions and when the salinity effect was determined.

The salinity experiments were conducted using eight glass containers, six of which were filled with a fixed volume (500 cc) of a solution containing one of the major salts in the eMalahleni brine and having a specific molality. The other two were filled with 500cc distilled water and eMalahleni brine, respectively. The six main synthetic salts used were calcium sulphate, sodium sulphate, potassium sulphate, sodium nitrate, magnesium sulphate and sodium chloride. The containers were evenly spaced to about 35 cm apart permitting an even vapour pressure difference between the salt solutions at the start of each experiment. Parameters such as volume, pH, EC, and density were measured to establish change. The parameters were recorded on a 24-hour cycle over 4 days of evaporation to illustrate the salinity effect. Ai-Shammiri (2002) considered a 2 to 3 day period as adequate for achieving experimental significance based on changes in water volume.

After four days the brine solutions were changed and the procedure repeated with solutions having a molality of 0.125, 0.5, 1.0, and 4.0. A molality of 0.125 is considered as a fairly low concentration while one with a molality of 4.0 is viewed as extremely concentrated. The calcium sulphate has a low solubility but this study still followed similar molar increments as the other salts. Previous experiments showed that the concentration of $CaSO_4$ decreased rapidly as a result of the low solubility and subsequently leading to salts accumulating at the bottom of the brine (Zayani et al., 1999).

4.2 ENVIRONMENTAL EXPERIMENTAL SETUP

The second experiment was setup to accommodate a larger volume of brine. A container was filled with a 0.5 M synthetic brine solution (125 L) while a similar container was filled with 125 L distilled water to serve as a control. In the first scenario, a typical summer`s day/night temperature and humidity distribution equivalent to the eMalahleni area was simulated under free convection conditions (no added wind force). In the other scenario, the experiment was repeated with the addition of a light wind force to simulate a windy day. This process was repeated until all the six major salts from the eMalahleni brine were determined. Besides the evaporation of the salts, a number of other significant parameters in the evaporation process were also determined. These parameters were configured to capture information similar to that of a natural pond. The parameters considered were similar to those of the Schultheis et al., (2001) experimental setup and are summarised in Table 4.1.

Table 4.1.Summary of the parameters, units and logging intervals used in the experimental setup.

Parameters	**Units**	**Logging periods**
Ambient temperature	˚C	Continuous
Water thermal stratification	˚C	Continuous
Humidity of the room	%	hourly
Humidity 10mm above	%	Continuous
Evaporation	mm	Hourly per cycle (24hrs)
Wind	m/s	Once per cycle

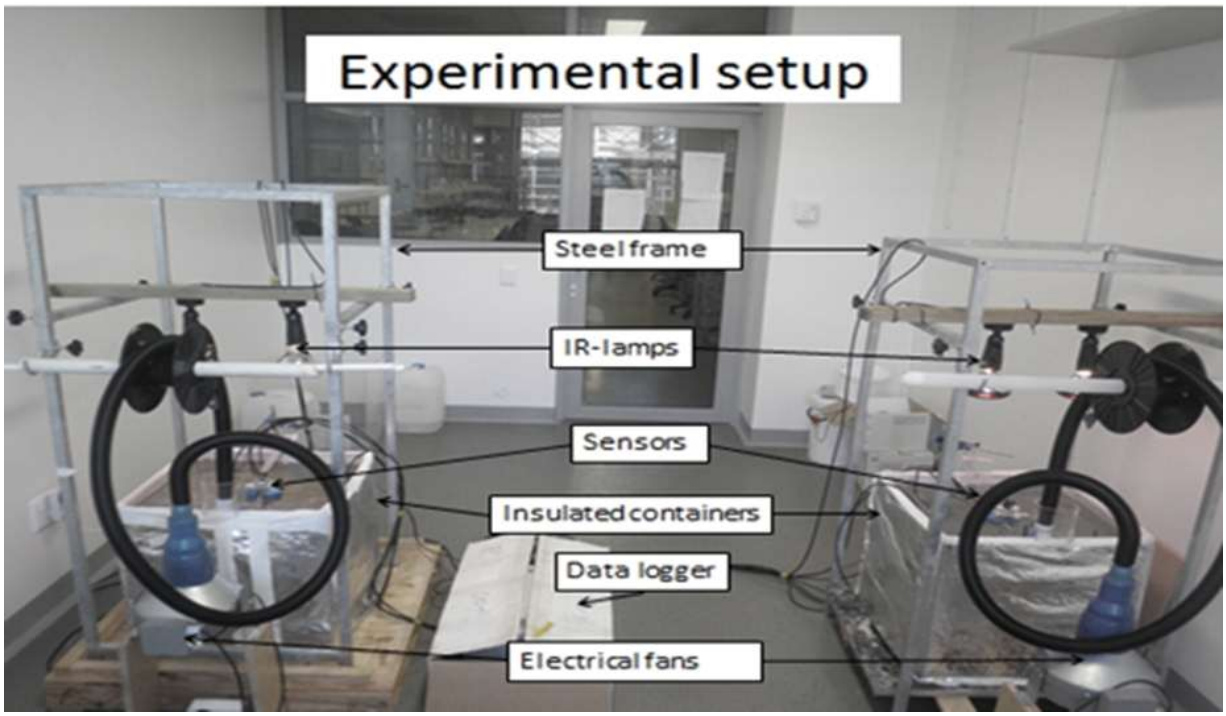

Figure 4.2 The experimental setup in the laboratory, showing the main components.

4.2.1 Brine containers

Evaporation can be observed from the two Perspex containers with sides of 0.5 m x 0.5 m and with a similar level. To prevent a potential leaking problem, the sides were seamless and had a thickness of 8 mm for better durability. The top surface was open to the atmosphere to allow evaporation and had a surface area of 0.25 m^2. The container was well insulated with a fibre blanket which served as a substitute material for the rock blanket used in the Schultheis et al., (2001) experiments. This ensured that the majority of the energy input for the brine and water was only derived from the infrared lighting source above the containers. The containers had to be deep enough (0.5 m) to account for thermal stratification of the brine, simulating a real pond environment. The surface area had to be large enough to absorb most of the radiated energy emitted from the infrared energy source above the container. The scattered energy reflected from the brine surface was not accounted for in this particular study.

The steel frame around the Perspex containers (see Figure 4.2) was erected to support the equipment suspended above the containers with minimal impact on the various processes. The stable structure erected allowed easy adjustments to be made to the system throughout the experiments. In addition, the steel structure was coated with a non-corrosive material, galvanised with a protective layer of zinc to prevent rust.4.2.2 Energy source

The average energy from the sun is about 1368 Watts of per m^2 before it enters the atmosphere (Arya, 1998). A further reduction in the energy due to scattering occurs before it reaches the earth surface. Energy for the experimental setup was supplied by 2 infrared lights with an energy output of about 250 Watt per bulb. The infrared bulbs were suspended above the containers to simulate the maximum temperature of a high summer's day. Trial experiments were conducted prior to the main experiments to determine the optimal settings of the infrared lamps to mimic the real environment. Several adjustments were therefore made to observe changes in the evaporation rate. These included height adjustments of the heating source and the reduction in the irradiative energy source as well as the wind exposure. The optimum distance between the infrared lights and the brine was important to express a suitable temperature range that resembles the study area. The optimum distance also aided the minimizing of the horizontal convection at the surface of the container during the experiments. Although the ambient temperature and humidity ranges indicated certain restriction, the variations were still within temperature and humidity ranges of the study area. During the preliminary experiments and test runs, two 175 Watts lamps were used to simulate a cooler day-maximum temperature but the temperature range was very limited. The lamps could be adjusted in a vertical and horizontal manner making it easy to obtain variation in the radiation reaching the brine surface of the containers as well as ensuring an even distribution of energy over the whole surface area. Wåhlin et al., (2010) experienced problems with the distance between the infrared lamps and the water bodies during their experiments which eventually affected the evaporation rates. In order to simulate a day and night setting the energy source was controlled by a timer switch that allowed a continuous supply of electricity to the infrared lamps for twelve hours in a 24-hour cycle. The total duration of each experiment was about 72 hours for each salt solution.

4.2.3 Electrical fan

The main purpose of the fan was to generate a wind force to remove the saturated air above the containers during the evaporation of the brines. A key feature for the attachment of the fan was to demonstrate the increase in the evaporation rate when subjected to air currents. To achieve equal distribution of air currents over the surface area of the container, the air currents were funnelled through a pipe with equally spaced holes mounted on the side of the containers. The wind speed could be varied, but was kept constant throughout the experiments at 2 $m.s^{-1}$. The wind speed was determined by using an anemometer near the ventilated areas of the cylinder.

4.2.4 Water temperature sensors

Since evaporation is an endothermic process, it requires energy to conduct the phase change. Firstly, energy is used to elevate the temperature of the water and secondly to change the phase (Young, 1947). The dissipation and flow of energy inside the water body is therefore important. To monitor this, five temperature sensors were mounted inside the containers to automatically record the water temperature at depths of 25 mm, 50 mm, 75 mm, 125 mm and 355 mm below the water surface. Besides temperature, the bottom sensor (355mm depth) also recorded the pressure of the water column directly above it thereby making it possible to determine the water level during the evaporation process at any specific time. Temperatures were logged every 10 minutes by means of a datalogger over the full duration (72 hrs) of each experiment. To achieve and maintain the depth of a specific sensor, the top four sensors were mounted on a floating device in such a manner that they had the freedom to fluctuate with changes of the water level. The continuous monitoring of all the temperature sensors formed a thermal stratification for better interpretation of evaporation losses.

4.2.5 Ambient temperature /humidity measurements

Room temperature could potentially influence the brine and water temperatures especially when it fluctuates. Jodat (2012b) conducted laboratory experiments and confirmed that the ambient temperature do play a significant role towards the evaporation rate. The experimental area for this study had a pre-set humidity of 60% and could not be altered to accommodate vigorous changes. The heating, ventilation and air conditioning (HV/AC) system was limited in its capacity to modify the humidity below or higher than 60% for the experiment, hence the exact simulation concerning the humidity was merely monitored.

The room temperature and humidity were recorded manually near the centre of the laboratory by using a portable temperature probe (Lutron HT 315). The measurements were recorded hourly during the first two hours of each experiment and then every 2 hours afterwards for the rest of the 72 hrs period. The device was factory calibrated and checked on a regular basis for battery fatigue. Continuous temperature and humidity measurements (every 10 minutes) were furthermore taken by a sensor installed 10 cm above the brine surface to monitor the changes of the air temperature and humidity directly above the water surface.

4.2.6 Data logger

A data-logger was installed to record all the measurements that were continuously recorded. The datalogger is the device that simultaneously collects and records all the different parameters that has been setup around the container. The datalogger (CR 1000) was obtained from Campbell Scientific ® (South Africa). All the sensors relayed the information to the datalogger simultaneously and can be monitored in real time with laptop. The recording interval for the data was every 10 minutes. The data was retrieved from the datalogger using Loggernet ® software loaded on a Windows 7 Microsoft Windows ® operating system. The data collected were analysed by means of time series plots. The continuously logged data from the datalogger and manual logged data were combined to validate and identify the changes in the evaporation rates of the experiments.

4.2.7 Measuring evaporation rates

The initial evaporation loss was recorded manually by measuring the brine level with a ruler. The changes in water level were recorded over a fixed time interval (hourly) although there were isolated periods where no data was recorded. Over a 72 hour period the volume loss was then calculated by multiplying the area of the water surface by the difference in depth that occurred over the total experimental period. At the start of the experiment the water temperature was approximately the same as the room temperature. The coefficient of expansion of the water and the container was small and this factor was neglected for this study.

The brine meniscus occurring near the sides of the Perspex container made the reading challenging with certain brines and caused a level of discrepancy in the measurements. The accuracy was limited to 1 mm depending on the type of salt used during the experiments. This was as result of the capillary action between the brine and the Perspex container. Overcoming the above-mentioned problem and still able to account for the loss of liquid, the systems were equipped with a pressure transducer placed at the bottom of the container. The pressure transducer works on the principle that it records any pressure changes of the liquid column above the transducer when the weight of the liquid changes. The pressure transducer was factory calibrated and the accuracy was approximately 0.1% at a temperature range between 0 and 60 °C.

4.2.8 Measuring pH and Electrical conductivity.

An Eijkelkamp model 18.21 portable pH/EC meter was used to measure the change in both pH and electrical conductivity (EC) of the brines during the experiments. Prior to any measurements the handheld device was calibrated using buffers 4 and 10 for pH since the different salt solutions never exceeded these values.

4.2.9 Measuring density of the solution

The density of the different salt solutions was verified using a portable density/specific gravity meter [DA-130N]. The suitable operating temperature for this device is between 0°C and 40°C. The operating density range is approximately 0.0000 to 2.0000 g/cm^3. The accuracy had a factory set accuracy of approximately ±0.001 g/cm^3. Calibration was performed during each solution change.

The laboratory setup and methodology are described as such in this particular chapter, the results obtained for the various experiments will be discussed in detail in the next chapter.

CHAPTER 5

RESULTS AND DISCUSSION: SALINITY

This chapter reports on the results obtained from experiments. It firstly focuses on the evaporation of relatively small volumes of single salt solutions that represents the major salts in the eMalahleni brine. For the molar concentration experiments, each experimental cycle had different salt solution with the same molality.

Secondly, it also focuses on the evaporation occurring from containers with larger volumes of synthetic salt solutions with 0.5 M concentrations and typical eMalahleni brine with free and forced convection in a controlled environment. The experimental setup for this study is presented in Chapter 4, section 4.3.

5.1 RESULTS OF SALINITY EXPERIMENTS

Prior to conducting experiments with different salt solutions with different molar concentrations, the evaporation of similar volumes from six similar glass containers with distilled water were determined as described in Chapter 4.2. The main reason for the preliminary experimental run was to establish a baseline. The temperature range over the containers acted as an indicator for any environmental changes during the baseline experiment. The results are shown in Figure 5.1 below.

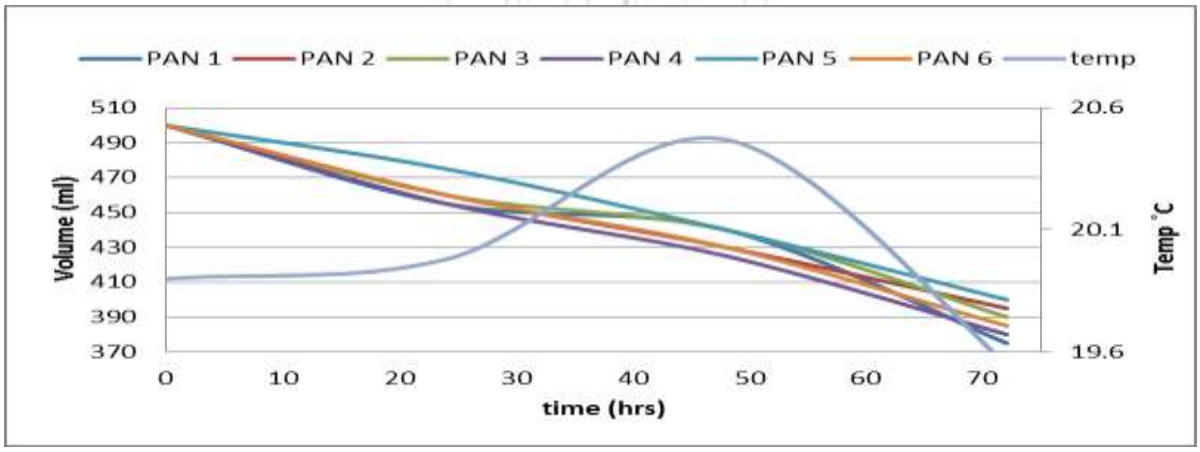

Figure 5.1 Graph illustrating the evaporation rate from the surface of similar containers, each with the same volume of distilled water.

As observed from Figure 5.1, the curves vary slightly indicating a small difference in the evaporation rate of the distilled water. After approximately 70 hours the difference between the maximum and minimum evaporation (Pan 4 and Pan 1) was about 20 mL or a 4% difference over the 72 hours. The difference is within the margin of 5% error for determining

the volume loss as a result of evaporation but small differences in the exposed surface area of each container can also play a role. The difference is therefore small enough to be ignored.

To determine the effect of salinity on evaporation, several major synthetic brines were subjected to a controlled environment in a laboratory. The molar concentrations of the synthetic brines systematically increased as depicted in Figure 5.2 below.

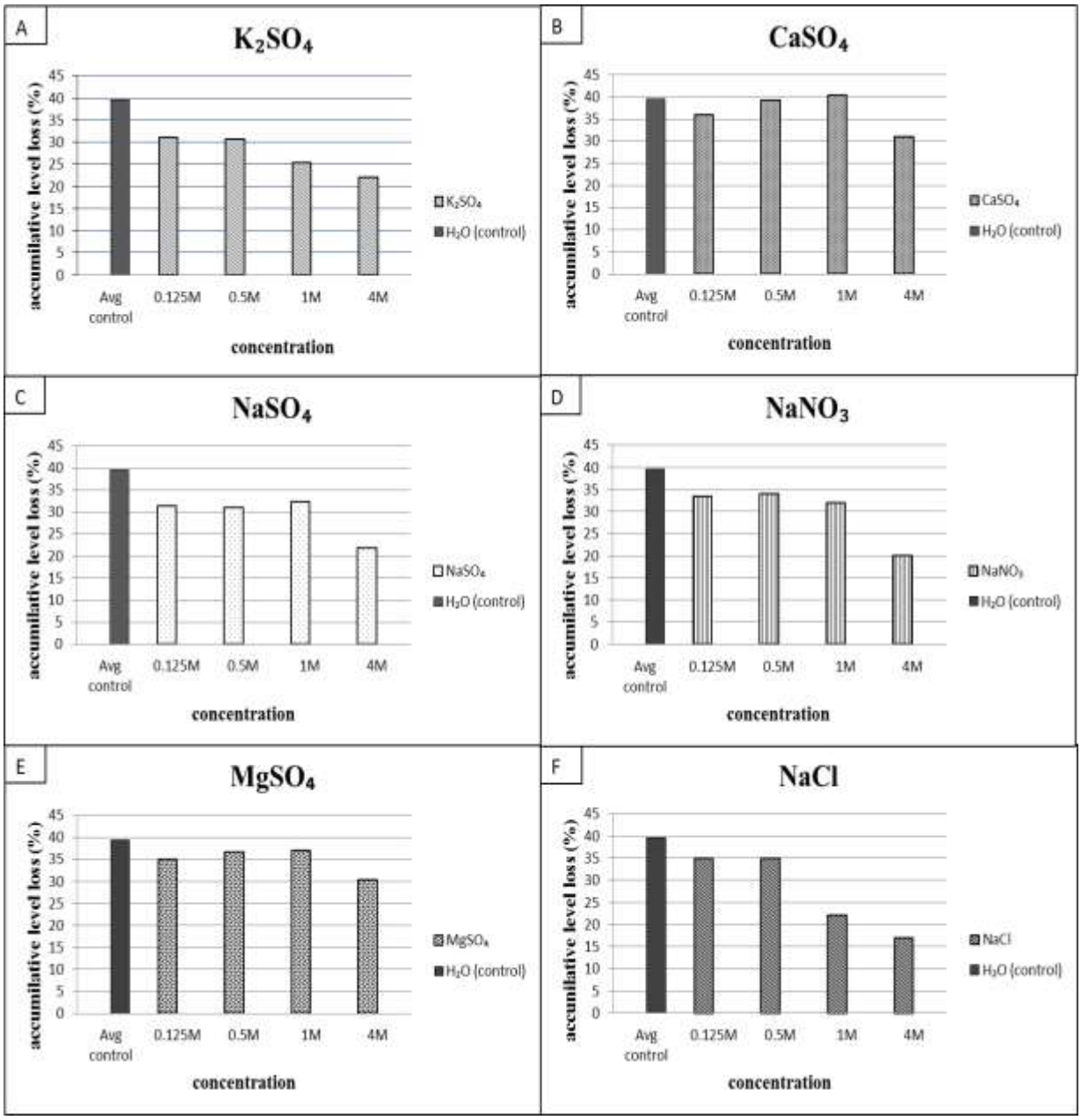

Figure 5.2 The volume loss (%) over a 4 day period for the control (H_2O) as a control measures along with different molar concentrations for each of the main synthetic salts occurring in the eMalahleni brine.

5.1.1 Potassium sulphate

At a molality of 0.125 M (Figure 5.2 A), the volume loss over 96 hours for potassium sulphate synthetic salt solutions was approximately 30% and suggests that the activity was fairly low and translated to less ion interactions based on the low concentrations. In the case of 0.5 M experiments the volume loss due to the evaporation was very similar to the 0.125M experiments which are 4 times less concentrated. At specifically 1M the evaporation losses were approximately 17% lower compared to the 0.125M and 0.5M experiments. Furthermore the 4 M potassium sulphate solution which represents an extreme scenario displayed the least amount of evaporation over 96 hours.

5.1.2 Calcium sulphate

The experiments for each of the calcium sulphate salt solutions (Figure 5.2B) was over a 96 hour period and subjected to the very similar conditions in the laboratory. Experiments conducted for the 0.125 M concentrations yielded higher percentage evaporation losses. Calcium sulphate is a low soluble salt and water molecule is less restricted to evaporate. In contrast to the other salt solutions the 0.5 and 1 M experiment shows an increase of approximately 9% evaporation loss compared to the 0.125 M concentration. The insoluble calcium salt precipitated at the bottom of the container, stored excess heat and subsequently raised the water temperature which resulted in slightly higher evaporation. The 4 M experiments show more salts suspended in the container and clouded the entire brine. This clouded surface had a blanket effect on the salts solution and resulted in the lower evaporation loss.

5.1.3 Sodium sulphate

Sodium sulphate salt solutions in Figure 5.2 (C) were subjected to the same environmental conditions for 96 hours (4 days). Experiments for 0.125 M sodium sulphate solutions had a similar volume loss as the 0.5 M solution. At this stage the concentration was not significant enough to have a major impact on the evaporation loss. Sodium sulphate shows elevated volume loss over the 96 hour period based on the secondary heating source developed by the precipitation of salts which had a similar effect as $CaSO_4$ in Figure 5.2 (B). At 4 M the solution was supersaturated and lost its visible liquid quicker than the rest of the other synthetic salts.

5.1.4 Sodium nitrate

Sodium sulphate was subjected to the same controlled laboratory conditions as the other synthetic salts in Figure 5.2. The volume losses for 0.125 and 0.5 M solutions were similar, being 33.4% and 34 % respectively for the 96 hour period. At 1 M the change was slightly less at 32% but the 4 M solution had a significant reduction in the evaporation loss. The highest concentration level of 4 M shows a reduction of about 20%.

5.1.5 Magnesium sulphate

Under controlled environmental conditions, magnesium sulphate solution shows the second highest evaporation loss over the 96 hour period (Figure 5.2E). The experiments for the 0.125, 0.5 and 1 M solutions had evaporation losses between 30 and 40%. Magnesium sulphate has a valence number of +2 and has a higher state of energy than ions like sodium and potassium. The higher charge causes instability when the Mg ion interacts with the two oxygen ions from the water molecule and subsequently allows more water molecules to evaporate into the air. Magnesium sulphate yielded the greatest evaporative loss amongst the 4 M experiments for all the synthetic brines. It should be noted that, the magnesium sulphate brine is not the most abundant salt with regards to the composition of the eMalahleni brine, it only represents 6% of the total brine composition.

5.1.6 Sodium chloride

The NaCl experiments occurred over a 96 hour period for each specific molar incremental phase (Figure 5.2F). At 0.125m and 0.5 M concentrations, the evaporation levels were nearly identical. The response at low concentrations is not significant and the loss of brine volume was minimal. Experiments at 1 M yielded a different result than the two lower concentrations in Figure 5.2F. Nearly 40 % less was evaporated from the 500 cc container over a 96 hour period. A further evaporation reduction in 4 M experiments was observed (nearly 60%) in comparison with the control measure. Sodium chloride yielded the least evaporation losses amongst the synthetic salts. The total dissociation of ions for this particular salt was greater and had a greater clinging effect to water molecules and subsequently retarded the evaporation process.

5.1.7 ANALYSIS

The potassium sulphate solution shows the lowest evaporation rate during the 0.125 M experiments (in Figure 5.2). Potassium sulphate shows a 31% evaporation loss for the 0.125 M experiments while the control managed volume loss 39% over 96 hours. In Figure 5.2B, calcium sulphate projected the highest evaporation loss compared to the other synthetic salts based upon the lower solubility. The pH of the $CaSO_4$ solution was slightly alkaline (pH 8.8) and could have assisted in the low solubility, as a more acidic solution would have made more H^+ available to dissociate ions (Shukla et al.,2008).

Evaporation from brine solutions with a 0.5 M concentration in Figure 5.2B illustrate a very similar trend as described for the 0.125 M solutions in Figure 5.2 A. The solutions with sodium- and potassium sulphate show lower evaporation rates amongst the synthetic salts with a volume loss of about 30%. Calcium sulphate shows the highest evaporation rate of 39 % followed by magnesium sulphate with 36% of volume loss over a 96 hour period.

For the 1 M solution in Figure 5.2C the evaporation portrayed a slightly different pattern, especially with the higher soluble salts. Evaporation from sodium nitrate, sodium sulphate and magnesium sulphate varied roughly between 32% and 36%, while potassium sulphate and sodium chloride were much lower in the region of 22%. Magnesium sulphate shows the greatest evaporation loss (36%) during the 1 M brine experiments.

In the extreme scenario the brine concentrations of 4 M in Figure 5.2 (D) shows significant changes in the evaporation rate are noticeable. Amongst the synthetic salts, the highest evaporation loss was found in the case of calcium sulphate (31%) followed by magnesium sulphate (30.4%). Both sodium nitrate and sodium sulphate shows low evaporation losses with values of 20% and 22% respectively. As expected the NaCl shows the lowest evaporation with an overall loss of 17%.

5.1.8 SUMMARY OF THE SALINITY EXPERIMENT

The evaporation rate for 0.125 M synthetic solutions was relatively the same throughout the entire experiment. The fairly low salt concentrations had a minimum effect on the evaporation since all the synthetic salts achieved evaporation losses above 30%. The 0.5 M concentrations of salts in Figure 5.2 appear to follow the same pattern as the 0.125 M solutions but had slightly lower evaporation losses based on the concentration difference.

The 1 M experimental data in Figure 5.2 shows a more active change in evaporation losses with the sodium chloride and the potassium sulphate showing the least evaporation losses for this experimental cycle. As expected the calcium sulphate generated the highest evaporation loss over the duration of the experiment followed by magnesium sulphate.

The 4 M experiments were conducted to observe the evaporation rate of the synthetic salts solutions under highly concentrated conditions. Based on empirical evidence the 4 M experiments resembled the 0.5 M salt solutions but had higher evaporation losses for all the synthetic salts. The highly soluble salts, in particular sodium chloride, sodium nitrate and sodium sulphate had the lowest evaporation of losses.

Calcium sulphate had merely a 5% difference in volume losses between the 0.125, 0.5 and 1 M experiments. The 4 M calcium sulphate experiments show the lowest percentage of volume loss with nearly 20% difference compared to the 0.125 M experiments. The poor solubility of calcium sulphate played a significant role in evaporation along with other factors like humidity, ambient temperature and infrared radiation which will be discussed in Section 5.2

The pH tends to play a significant role in the solubility of the ions (Fatoba, 2010). In the case of $CaSO_4$, the solution was slightly alkalinea and conditions were not favourable to disssociate ions hence the low solubility. The overall trend shows the 0.125 and 0.5 M experiments have the same evaporation losses.

RESULTS AND DISCUSSION: EVAPORATION UNDER FREE AND FORCED CONVECTION

5.2 NATURAL AND FORCED CONVECTION EXPERIMENTS

This section deals with the results obtained for the evaporation of solutions (0.5 M concentration) for single salts, typically present in the eMalahleni brine, as described in Chapter 3 (section 3.2). The results for the natural convection (no wind assistance) scenario will be discussed first, followed by the results for the forced convection (with wind assistance) scenario. Temperature and humidity increments in the figures were adjusted accordingly for improved data projection.

5.2.1.1 Magnesium sulphate with natural convection

The evaporation from and temperature distribution in a 0.5 M solution of magnesium sulphate under natural convection (no wind assistance) conditions is illustrated in Figure 5.3 below.

The bold non straight-line (zigzag) curve in Figure 5.3A shows the average pressure variation of the water column above the pressure transducer located at the bottom of the container (described in section 4.3.7). It records the level changes observed over 72 hours for the experimental period. The collected data is also a good representation of the overall trend related to the sensitivity of the pressure transducer. The manual level recordings confirmed the level changes with the pressure transducer in Figure 5.3 A while the bold line shows 3 distinct wave cycles representing the day-night simulation. The rate of decrease in pressure for each 12 hour cycle is more or less uniform. At a period of 22 hours the ventilation had a slight restriction for a short period and resulted in a quick descending when freed. In total the pressure decrease was 0.117 kPa over the 72-hour period, equivalent to a level change of about 11 mm for magnesium sulphate (2750 cc). Over the same period the distilled water level showed a reduction of 15 mm (3750 cc) compared to magnesium sulphate of 0.5M (see Appendix 1).

Figure 5.3B shows the continuous temperature variation of the magnesium sulphate solution at depths of 25 mm, 50 mm, 75 mm and 125 mm below the water surface as well as at the bottom of the container over a period of 72 hours. The figure also depicts the variation in air temperature and the humidity located at 100 mm above the surface of the solution as well as the inside of the laboratory over the 72-hour period.

The temperature curves in Figure 5.3 B shows similar patterns as described above in Figure 5.3 A. The display of 3 equal day and night cycles of temperature changes for specific depths between 25 mm to 125 mm below the surface were very evident. At the bottom of the container the temperature variation was not very prominent. At 25 mm depth the temperature range was between 19°C and 30°C. The peak temperature of each cycle increased steadily from 29 °C to about 30 °C and the minimum temperature increased from 20.5°C to 21°C during the elapsed 72-hour period. The temperatures between 50 mm to 125 mm depth ranged between 23°C to 28°C. Minimum temperatures for the depths between 50-125 mm also increased over the 72-hour period, ranging from 15°C to 19°C. Temperatures at the bottom of the container show a range between 19°C and 20.5°C that resulted in a difference of 10°C between the peak surface water temperature and the bottom temperature.

The same day and night rhythmic cycles were also evident in the ambient temperature above the container (100 mm above the solution surface) although some fluctuations in temperature were visible. On average, the maximum temperature varied around 19°C although on two occasions the temperature had risen to about 25°C for short periods (about 3 hours) while minimum temperatures varied around 17°C.

The graph for the humidity of the air above the magnesium sulphate solution followed a rhythmic pattern throughout the experimental period but displayed an inverse relationship when heat was applied with the infrared lamps. Humidity decreased when ambient temperature had risen and vice versa. Maximum humidity reached figures of around 77% at 12 hours while the minimum values were reduced to about 53% at various intervals.

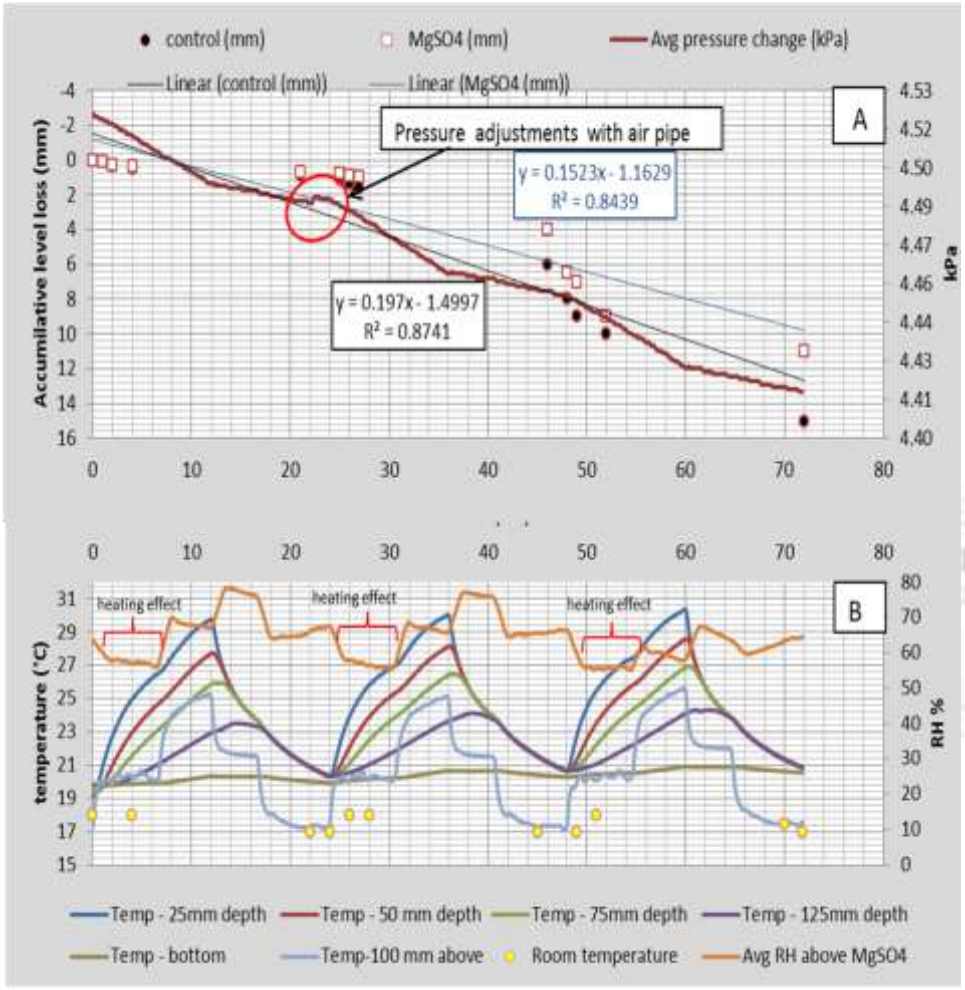

Figure 5.3 Evaporation of a magnesium sulphate solution and distilled H_2O control (A) with equations for the regression lines and temperature distribution (B) in and above the magnesium sulphate brine surface during a free convection experiment of 72 hrs.

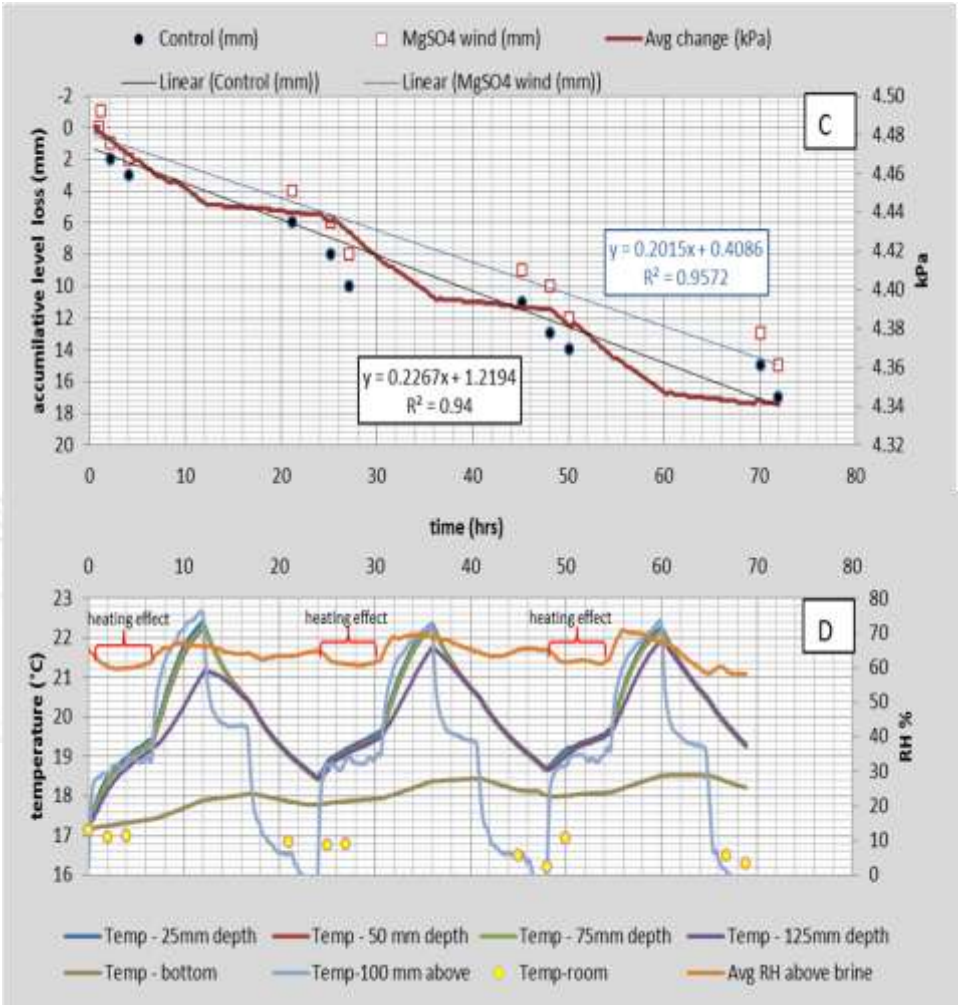

Figure 5.4 Evaporation of a magnesium sulphate solution, distilled H_2O control (C) along with equations for the regression lines and the temperature distribution (D) in and above the solution surface during a forced convection experiment of 72 hr.

5.2.1.2 Magnesium sulphate with forced convection

Figure 5.4C and Figure 5.4D shows the continuous evaporation and temperature variation in a 0.5 M solution of magnesium sulphate compared with the distilled water (control) under forced convection (wind assisted).

Figure 5.4C indicates the continuous and manually recorded evaporation levels for the magnesium sulphate solution and distilled water. The data was recorded daily over a 72-hour period under forced convection conditions (see section 4.3.3). Two trend lines representing a linear model with the respective regression equations are also shown. The magnesium sulphate solution had a reduction of about 14.5 mm over 72 hours, equivalent to about 3625 cc while the distilled water had a loss of about 17 mm (4250 cc).

The temperature curves in Figure 5.4D show the same 72 hour day and night rhythmic patterns as described above for Figure 5.4C. Fluctuations in day and night temperatures are clearly visible in the forced convection experiment and are more vigorous up to a depth of 125 mm below the surface. The temperature stratification was not very visible over the 72 hours period as a result of turbulence caused by the wind flow. The temperature at 25 mm, 50 mm and 75 mm depths are almost identical during the experimental period. The maximum range was between 21°C and the minimum was around 17.5°C. The temperature at 125 mm depth showed slightly different patterns from deeper positions of the brine as a result of the energy being dissipated throughout the depth.

Throughout the entire $MgSO_4$ experiment (with wind assistance) the rapid thermal changes were not very evident near the bottom of the container. The temperature range for the 25 mm and the 125 mm were fairly similar.

In Figure 5.4D the maximum temperature for 25 mm, 50 mm and 75 mm depth had risen to approximately 22°C below the surface of the solution. At a depth of 125 mm below the surface the peak temperatures were slightly lower, and ranged between 21°C and 21.8°C. Temperatures at the bottom of the container ranged between 17°C and 19°C had not fully resembled the rhythmic patterns described above near the surface of the brine. A difference in maximum temperatures between the surface and at a depth of 125 mm of the brine was only observed during the last 24 hours of the experiment with a difference of 3.5°C.

Rhythmic pattern changes in ambient temperature above the container clearly show the day-night cycles of the experiment. The maximum temperatures were close to 19°C during the first two days but reaching almost 23°C during the last 24 hours. The minimum room temperature reached 15.5°C and both the sensors were situated at 100 mm above the container.

A fluctuation near 65% of humidity was noted above the magnesium sulphate solution. The day-night pattern was less evident in Figure 5.4D than in Figure 5.4B. Maximum humidity for the first 48 hours was close to 68% but had risen to above 70% for a short period during the last 24 hours of the experiment.

5.2.1.3 Summary of magnesium sulphate experiments

In summary Figure 5.3 and Figure 5.4 show that the level changes in the container with magnesium sulphate decreased by 14.5 mm during the 72 hours experiment under forced convection (wind assistance) compared to the 11 mm decrease when no wind was simulated. This represents a 31.8% increase in evaporation rate when wind was added. Clear day/night temperature cycles are visible in both figures with highly visible temperature stratification expressed in the data for the free convection (no wind assistance) scenario. Daily maximum temperatures for various depths were considerably higher (about 7°C - 8°C) for the free convection simulation compared to the forced convection experiment (wind assistance).

5.2.2.1. Sodium sulphate with natural convection

The evaporation and temperature distribution in a 0.5 M sodium sulphate solution compared with distilled water under natural convection conditions (no wind assistance) is illustrated in Figure 5.5 below.

Figure 5.5E shows the average changes in the water level measured by the pressure transducer placed at the bottom of the container (discussed in paragraph 4.3.7). Day and night simulations of the sodium sulphate solution were presented by the continuous and manual level changes over 72 housr. Each 24 hour cycle shows similar rhythmic patterns over the entire experimental period. In total, the pressure decrease was approximately 0.2 kPa over the 72-hour period and equivalent to a level change of about 12 mm. The reduction in level change was a total of 3000 cc being evaporated over a 72 hour period. During the same period, the distilled water (control) experienced a water level loss of 15.5 mm (3875 cc).

Figure 5.5F represents the temperature difference of the sodium sulphate solution at depths near 25 mm, 50 mm, 75 mm, and 125 mm below the brine surface as well as at the bottom of the container. Figure 5.5F also shows the air temperature and humidity at a height of 100 mm above the solution. All these parameters were continuously recorded over a 72 hour period.

Figure 5.5F shows the same rhythmic pattern as displayed by temperature variations in the evaporation curves (Figure 5.4E). Temperature difference was clearly visible up to 125 mm depth below the surface. The same rhythmic pattern repeated itself for each experimental cycle over 24 hours. The thermal differences for the sodium sulphate brine was notable when the maximum temperature increased from 28°C to 30°C at 25 mm during the elapsed 72-hour period.

The average peak temperature at a depth of 50 mm was 27.8 °C, for 75 mm depth was 25.8 °C and at 125 mm was 22.1°C. The minimum temperatures for each 24 hour cycle increased over the 72-hour period and ranged between15°C and 19°C. Temperature changes near the bottom of the container ranged between 14.5°C to 18°C and appeared to be negligible

compared to brine levels near the surface. On average the difference in peak temperatures between the surface and at a depth of 125 mm amounted to about 8°C.

The same rhythmic cycles can also be identified in the variation of the ambient temperature above the container (100 mm above the solution surface) although some fluctuations in

temperature were not visible. The maximum temperature was around 19°C for 72 hours. Minimum temperature above the container was about 15°C for the entire experimental period.

The humidity of the air above the sodium sulphate brine followed the same temperature pattern as described in Figure 5.5F, but displays a very small suppression. The humidity responded inversely with temperature increase from the infrared lamps. The average humidity for the 72 hour period was approximately 65%.

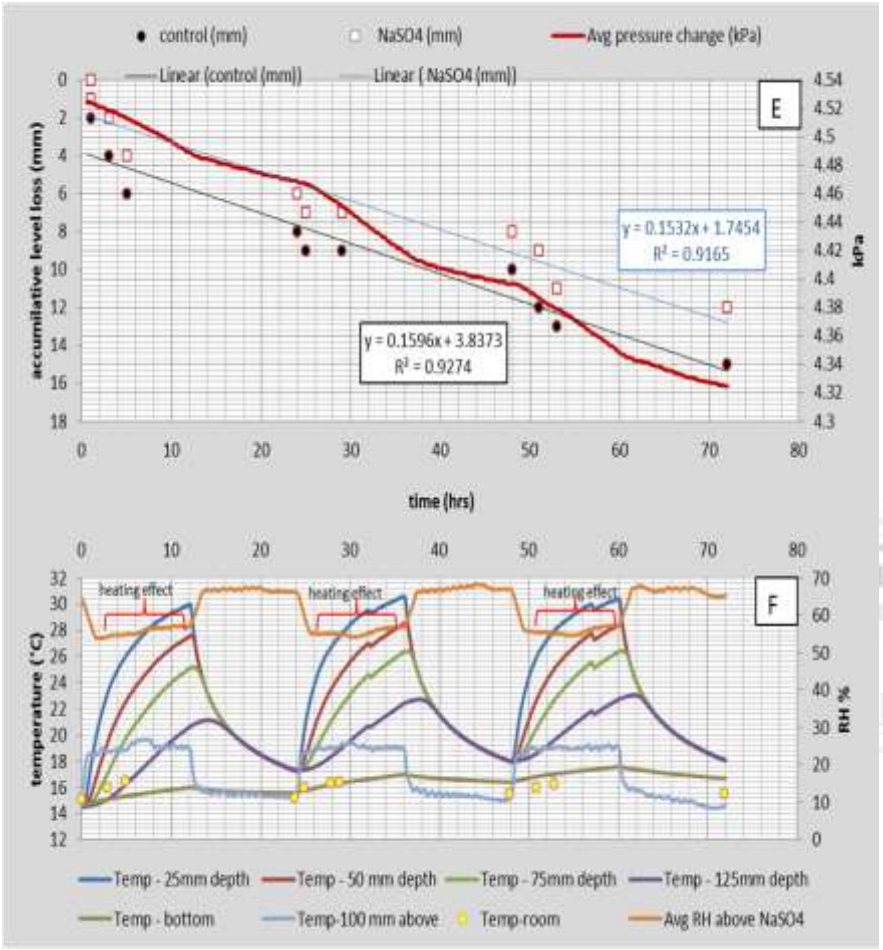

Figure 5.5 Evaporation of a sodium sulphate solution and distilled H_2O as a control along with the equations for the regression lines are also shown in Figure 5.5 (E). Figure 5.5 (F) displays the temperature distribution in and above the brine surface during a free convection experiment.

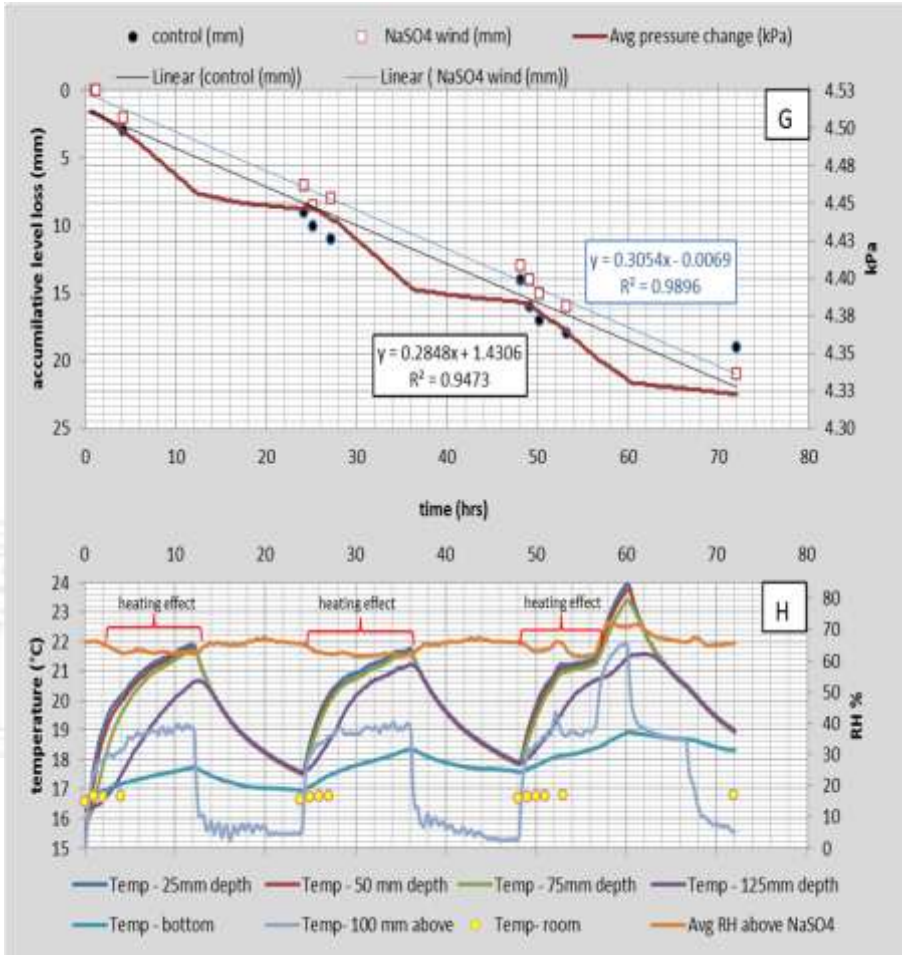

Figure 5.6 Evaporation of a sodium sulphate solution and distilled H_2O as a control along with equations for the regression lines are also shown in Figure 5.6 (G). Figure 5.6 (H) displays the temperature distribution in and above the solution surface during a forced convection experiment.

5.2.2.2 Sodium sulphate with forced convection

Figure 5.6 shows the continuous evaporation and temperature variation in a 0.5 M sodium sulphate solution under forced convection (wind assistance).

Figure 5.6G shows the manual recorded level changes for the container with sodium nitrate solution and distilled water, respectively. The experiment was recorded daily over a 72-hour period under forced convection conditions (see paragraph 4.3.3). Two linear trend lines with the equations are represented by the regression analysis.

The level changes were indicated by a broader line (red) to display the pressure changes over a 72-hour period. A pattern with 3 day-and night cycles similar to Figure 5.6G is clearly visible in Figure 5.7E. Pressure decreased from 4.534 kPa to 4.344 kPa representing a calculated reduction of about 19 mm in level change (equivalent to 4750 cc). A total of 4.5 litres therefore evaporated from the sodium sulphate solution over a period of 72 hours during wind assistance. Simultaneously the transducer placed in the distilled water shows a level change of approximately 21 mm, equivalent to 5250 cc (not shown in Figure 5.6G).

The temperature data in Figure 5.6H resembled similar patterns as described in Figure 5.6H. The fluctuation in temperature occurred over a 72-hour period are clearly visible at depths down to 125 mm below the brine surface. Very little indication of temperature stratification is visible over the first two days of the experiment compared to the last 24 hours. Temperature curves between 25 mm and 75 mm below the surface are almost identical for the first 48 hours with the maximum temperature around 21.3°C and the minimum around 17.5°C. The temperature patterns at a 125 mm depth show a significant change in comparison with depths closer to the brine surface.

The last 24 hours of the experiment showed a clear difference in temperature stratification from the previous period. The maximum temperature for the $NaSO_4$ solution had risen to 25°C at a depth of 25 mm and 23°C at 75 mm depth below the surface of the solution. At a depth of 125 mm below the surface, the maximum and minimum temperatures were similar throughout the entire experiment. Temperatures near the bottom of the sodium sulphate solution ranged between 17°C and 19°C and with a different rhythmic pattern to shallower positions from the surface. A difference in maximum temperatures between water near the surface and at a depth of 125 mm is only visible during the last 24 hours of the experiment

and amounts to about 3.5°C while the minimum temperature shows a small difference of about 2°C.

The variation in ambient temperature above the container (100 mm above the solution surface) clearly shows the day-night temperature cycles. The maximum temperatures reached almost 19°C for the first two days but increased to 23°C in the last 24 hours while the minimum temperature shows variations around the 15.5°C mark.

The humidity data of the air above the sodium nitrate solution during the forced convection experiment fluctuated around 65%. The day-night humidity pattern that was prominent in Figure 5.5 (F) is less noticeable in Figure 5.6 (H), but still visible. Maximum humidity for the first two days was about 68%, but had risen to values around 75% during the last 24 hours, while minimum values reached above 60%.

5.2.2.3 Summary of sodium sulphate experiments

In summary Figure 5.5 and Figure 5.6 show that the level of sodium sulphate solution had lowered by 19 mm under forced convection while the free convection experiment only reached 12 mm over a 72 hour period. This represents a 58% increase in evaporation with the aid of wind energy. Clear day/night temperature cycles are visible in both figures but appeared more prominent for the free convection scenario. The daily maximum temperatures of the sodium sulphate solution are considerably higher (by about 7 - 8°C) for the free convection simulation compared to the forced convection. The introduction of wind energy during the forced convection experiment caused the temperature difference as a result of the accelerated phase change.

5.2.3.1 Sodium nitrate with natural convection

The evaporation and temperature distribution in a 0.5 M solution of sodium nitrate with free convection (on wind assistance) are illustrated in Figure 5.7 below.

The graph in Figure 5.7H shows trend lines based on the manually recorded level changes for the sodium nitrate solution and distilled water, respectively. The equations for these regression lines are also included. A continuous data line (Figure 5.7I) shows the average pressure variation of the water column above the pressure transducer located at the bottom of the container (discussed in paragraph 4.3.7). The main function of the sensor is to record the level changes continuously over a 72-hour period. The prominent line in Figure 5.7I shows 3 curves representing day-night for the duration of about 12 hours. In total, the pressure difference over the 72-hour period was about 0.136 kPa and equivalent to level change of 13.5 mm (3400 cc). The distilled water used as a control measure had a level change of about 15 mm (3750 cc) based on the transducer readings (see Appendix 1).

Figure 5.7J shows the continuous temperature variation of the sodium nitrate solution. It represents depths close to 25 mm, 50 mm, 75 mm and 125 mm below the brine surface as well as at the bottom of the container over a period of 72 hours. It also shows the variation in air temperature and humidity 100 mm above the surface of the solution as well as inside the laboratory over the 72-hour period.

The temperature data in Figure 5.7J shows a more noticeable wave like pattern similar to Figure 5.7I. The 3 day and night cycles of temperature fluctuation were observed at depths between 25 mm to 125 mm below the surface. The brine temperature followed the same rhythmic changes with increased depth. However, a decline in peak temperature was clearly visible in Figure 5.7J as the depth increases.

A clear thermal stratification emerged in the sodium nitrate solution. At a depth of 25 mm below the surface, the sensor recorded the highest temperature of the sodium nitrate solution and has steadily increased from 28°C to 30°C during the elapsed 72-hour period. At depths close to50 mm and 125 mm below the surface, the maximum temperature range was between 20.5 and 28 degrees Celsius. Minimum temperatures for the specific depths also increased over the 72-hour period, ranging from 15°C to 19°C. At the bottom of the container the peak temperature has been raised from 16°C to 18°C with a small variation. The difference in

maximum temperatures between the brine surface and at a depth of 125 mm amounts to about 7°C while the minimum temperature shows differences of about 3°C.

A similar pattern emerged with the ambient temperature during the day and night experimental cycles and was notable in the variation of ambient temperature above the container. The average maximum temperature varied around 18°C although on two occasions the temperature had risen to about 21°C for short periods (about 3 hours). The minimum temperature varied around 14°C.

The humidity above the sodium nitrate solution had similar patterns as the temperature data, but shows sections of lower and irregular patterns based on the ambient temperature changes above the container caused by the infrared lamps. Maximum humidity ranged between 53% and 65% for the entire experimental period.

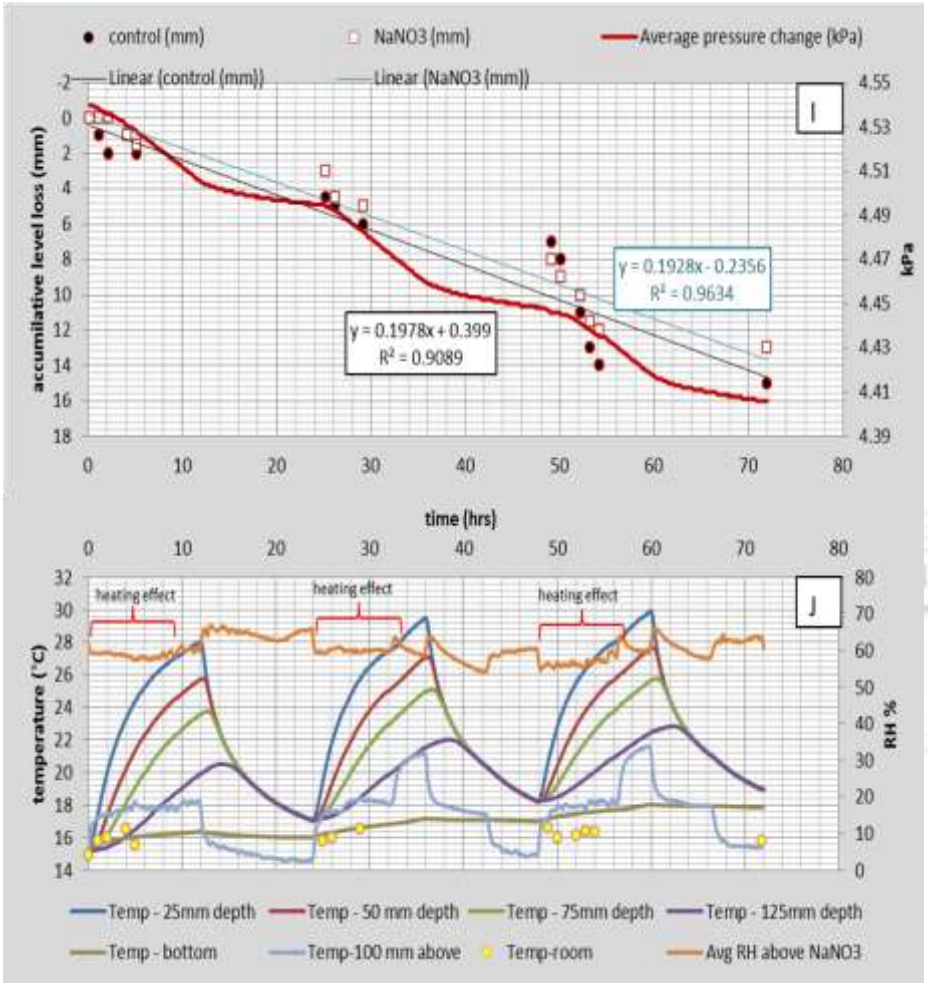

Figure 5.7 Evaporation of a sodium nitrate solution and distilled water as a control (I) and the temperature distribution (J) in and above the solution surface during a 72 hr period with no wind.

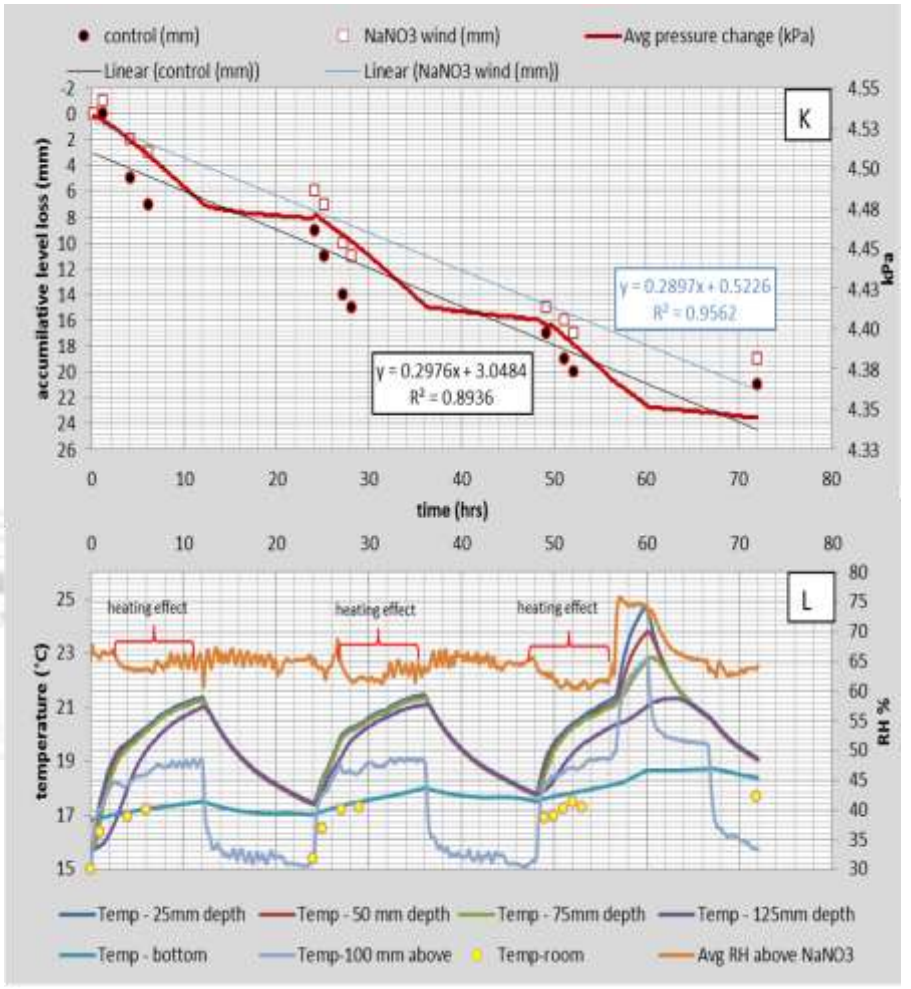

Figure 5.8 Evaporation of a sodium nitrate solution (K) and the temperature distribution (L) in and above the solution surface during a 72 hr period with wind

5.2.3.2 Sodium nitrate with forced convection.

Figure 5.8 shows the continuous evaporation from and temperature variation in a 0.5 M solution of sodium nitrate under forced convection (wind assistance).

The experiment with the sodium nitrate solution under forced convection in Figure 5.8K shows the recorded level changes of the sodium nitrate solution and distilled water respectively. The daily recorded data over a 72-hour period was obtained from a scenario where wind was applied (see paragraph 4.3.3). The linear trend lines from the sodium nitrate brine and distilled water were also shown for the data readings. The total volume over the experimental period with sodium nitrate solution was approximately 13.5 mm (equivalent to a loss of 3375 cc), and the distilled water was lowered by approximately 15 mm (equivalent 3750 cc).

The bold data line in Figure 5.8K represents the pressure changes of the $NaNO_3$ brine recorded by the pressure transducer located at the bottom of the container over a 72-hour period. Day and night rhythmic patterns, similar to Figure 5.7I emerge. Pressure decrease from 4.534 a to 4.344 kPa representing a calculated level change of about 18 mm. A total of 4320 cc evaporated from sodium nitrate solution over a period of 72 hours during the forced convection experiment. Over the same period the container with distilled water in Figure 5.8 I decreased by about 20.2 mm (equivalent to 4848 cc).

Temperature data in Figure 5.8L shows the same cyclic pattern as described above in Figure 5.8 K. The fluctuations in temperature over a 24-hour period are clearly visible to a depth of 125 mm below the surface. Very little indication of temperature stratification was visible over the first two days of the experiment. The curves represents temperature data at 25 mm, 50 mm and 75 mm, respectively are almost identical for the first 48 hours with the maximum temperature reaching around 21.3°C and the minimum at 17.5°C. The last 24 hour cycle shows partial separation of temperature differences where the sensors are located. During the last 24 hours of the experiment, temperature at a depth of 25 mm was 25°C and 23°C at 75 mm below the surface of the solution. At a depth of 125 mm below the surface, the maximum and minimum temperatures remain similar during the first 48 hours. Temperatures at the bottom of the container range from about 17°C to 19°C and mildly resemble the temperature cycles closer to surface of the brine. A small difference in maximum temperatures between surface and at a depth of 125 mm is only visible during the last 24 hours of the experiment.

The total difference amounted to about 3.5°C while the ambient temperature above the container (100 mm above the solution surface) clearly shows the day-night cycles with the maximum temperatures around 19°C during the first two days but reaching almost 23°C on the 3rd day. The minimum temperature reached variations of approximately 15.5°C.

The humidity above the sodium nitrate solution during the forced convection experiment fluctuated around 65%. The day-night pattern was more evident in Figure 5.8J when there was no wind assistance, but is less prominent in Figure 5.8L. Maximum humidity for the first two days was about 68% but had risen to values around 75% on the 3rd day while minimum values were reached about 60%.

5.2.3.3 Summary of sodium nitrate experiments

In summary, Figure 5.7 and Figure 5.8 show level changes with sodium nitrate that were reduced by 18 mm during the experimental period of 72 hours under forced convection compared to a level change of 13 mm when no wind was applied in the system. This represents a 38% increase in evaporation when wind was added. Clear day/night temperature cycles are visible with both scenarios with more prominent temperature stratification with the experiment under a free convection scenario. Daily maximum temperatures that translated into level changes are considerably higher (by about 7 - 8°C) for the no wind simulation compared to the free convection scenario.

5.2.4.1 Calcium sulphate with natural convection

The temperature distribution and evaporation from a 0.5 M solution of calcium sulphate under free convection conditions are illustrated in Figure 5.9 below.

The data (curved bold line) in Figure 5.9M shows the average brine level changes expressed in pressure by the pressure transducer located at the bottom of the container (discussed in paragraph 4.3.7). In Figure 5.9M the evaporation data shows 3 significant changes in pressure which is indicative of a day and night cycle. The rhythmic changes for each 24 hour cycle were similar throughout the experiment. In total the pressure difference was 0.156 kPa over the 72-hour period, equivalent to a level change of nearly 15.5 mm, which translates to a total volume of 3950 cc (3.9 litres) being evaporated over a period of 72 hours. Over the same period the level of the distilled water had a reduction of 16 mm (equivalent to 3800 cc).

Figure 5.9N represents the temperature data of the calcium sulphate solution at depths close to 25 mm, 50 mm, 75 mm, 125 mm respectively and at the bottom below the brine surface over a 72 hours period. The figure as also shows the changes in air temperature and humidity 100 mm above the calcium sulphate solution over the 72-hour period.

The temperature data in Figure 5.9N resonated with the same pattern as in Figure 5.9M. The 3 day and night cycles temperature data are clearly visible throughout the depth of the calcium sulphate solution. A clear thermal stratification emerged within the calcium sulphate brine. At 25 mm depth peak temperatures increased from 27.5°C to 29.5°C during the elapsed 72-hour period. The average temperatures at depths between 50 mm to 125 mm ranged between 14.3°C and 27°C. Temperatures at the bottom of the container ranged between 16°C and 18°C for the entire experiment and had subtle variation in comparison to levels closer to the surface of the brine. The maximum temperature between the surface and the bottom of the container was about 12°C while the temperature at a depth of 125 mm reached about 7°C.

The humidity of the air above the calcium sulphate solution followed similar rhythmic patterns as the brine temperature, but shows an inverse relationship with the ambient temperature. The humidity level was inversely proportional to the ambient temperature throughout the 72 hour experiment. The maximum humidity reached values around 65% while the minimum values were lowered to about 53%.

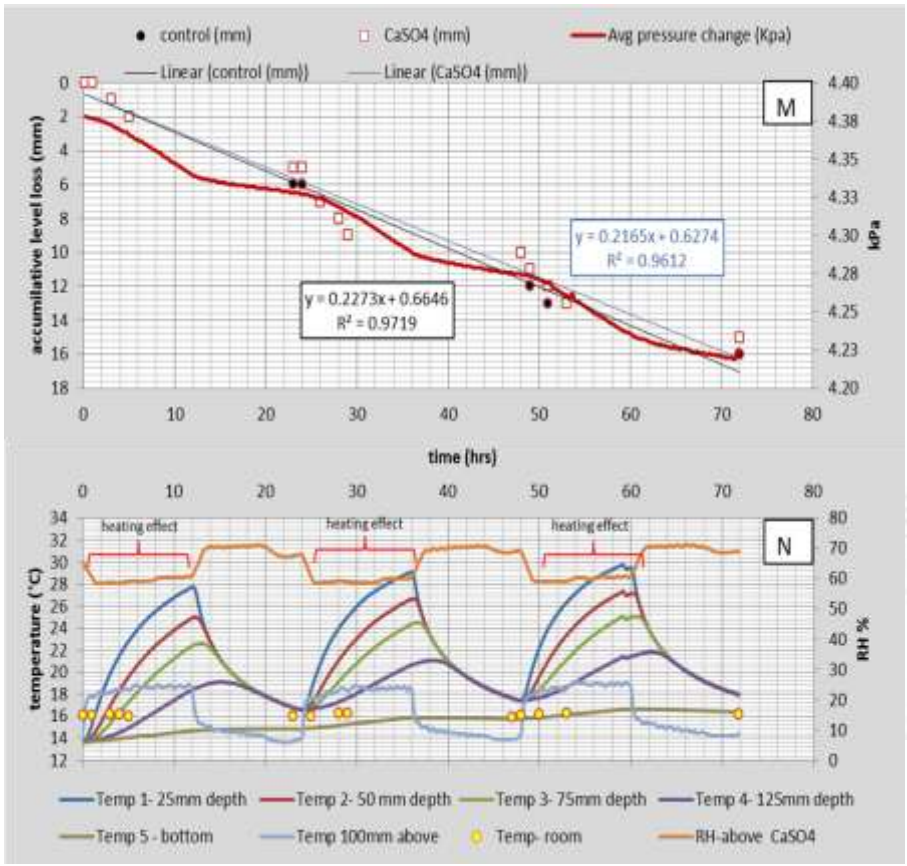

Figure 5.9 Evaporation of a calcium sulphate solution and H_2O as a control (M) and the temperature distribution (N) in and above the solution surface during a 72hr period under free convection conditions.

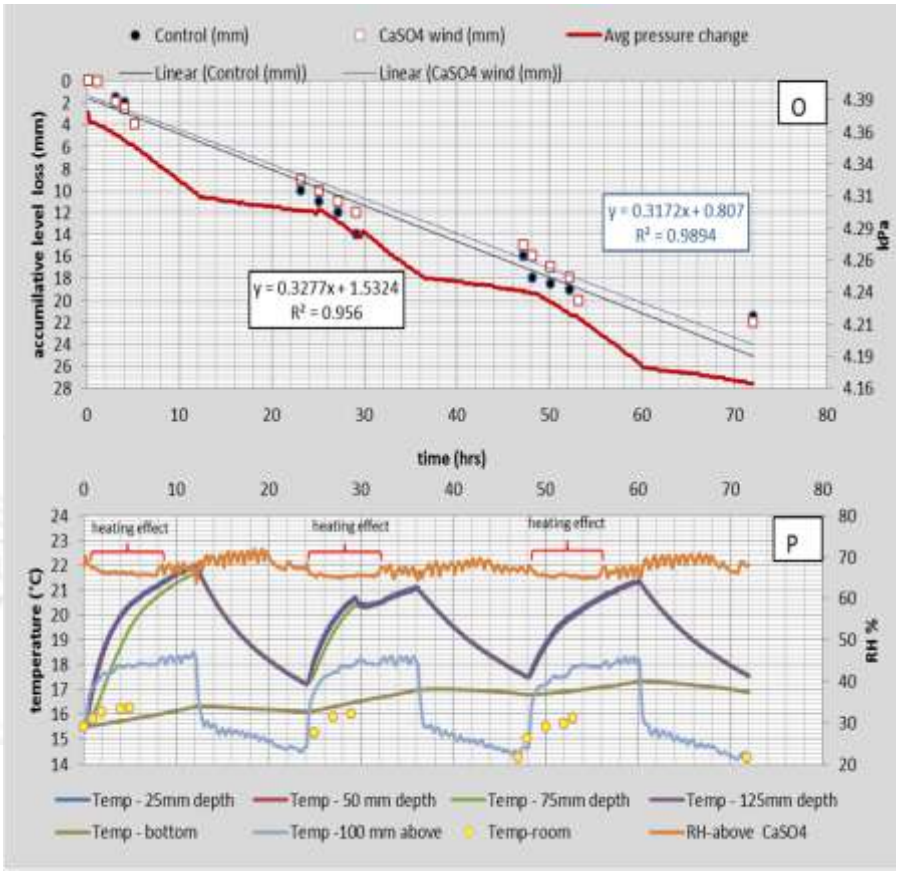

Figure 5.10 Evaporation of a calcium sulphate solution (O) and the temperature distribution (P) in and above the solution surface during a 72hr period with forced convection under forced convection conditions.

.

5.2.4.2 Calcium sulphate with forced convection

Figure 5.10 shows the continuous evaporation and temperature variation of a 0.5 M solution of calcium sulphate solution under forced convection (wind assistance).

Figure 5.10O shows the $CaSO_4$ brine level changes for the calcium sulphate solution or distilled water respectively over a 72-hour period (see paragraph 4.3.3). The linear trend lines for the calcium sulphate solution and distilled water data and their respective equations are also shown. The total evaporative loss for the calcium sulphate solution was about 20 mm (equivalent to a loss of 4950 cc), while the distilled water shows a total loss of 22.5 mm which is equivalent to 5568 cc.

The water pressure data depicted as a bold curved line was recorded by the pressure transducer located at the bottom of the container over a 72-hour period. A similar pattern is displayed in Figure 5.10O where 3 day and night cycles emerged. The pressure difference was about 0.214 kPa representing a level change of about 21.85 mm (a loss equivalent to 4500 cc). Over the same period the distilled water as a control measure had a level change of approximately 21 mm which is equivalent to 5050 cc (see Appendix 1).

The temperature data near the surface of the brine in Figure 5.10P show the same 3 day and night cycle pattern as described above for Figure 5.10O. Temperature rhythmic cycles are clearly visible at depths down to 125 mm below the surface. Very little indication of temperature stratification was visible over the first two days of the experiment. Temperature data at depths near 25 mm, 50 mm and 75 mm mark are almost identical for the first 48 hours with the maximum temperature reaching around 21.3°C and the minimum close to 17.5°C. Data for the temperature at 125 mm depth differed slightly from deeper temperature readings with the maximum at 21°C while the minimum temperature reaching 17.5°C for all the other depths. During the last 24 hours of the experiment, clear temperature stratification developed when the maximum temperature had risen to 25°C for the brine at a depth of 25 mm. In addition, 23°C is the maximum temperature for a depth close to 75 mm below the surface of the solution. At a depth of 125 mm below the surface during the same time, maximum and minimum temperatures were very similar during the first 48 hours. Temperatures at the bottom of the container range between 17°C - 19°C and mildly resembled the cycles described above for the brine surface. A difference in maximum temperatures between the brine surface and at a depth of 125 mm is only visible during the last 24 hours of the

experiment and reached temperatures of about 3.5°C while the minimum temperature had a small difference of about 2°C.

The variation in ambient temperature above the calcium sulphate solution (100 mm above the solution surface) clearly shows the day-night patterns with the maximum temperatures reaching around 19°C during the first two days but reaching almost 23°C after 72 hours. The minimum temperatures varied around 15.5°C.

Data representing the humidity above the sodium nitrate solution during the forced convection experiment fluctuated around 65%. The day-night pattern is prominent in Figure 5.10P but with a limited range. The humidity shows patterns of distortion but maintained a range between 65% and 75%.

5.2.4.3 Summary of calcium sulphate experiments

In summary Figure 5.10 indicate that the brine level of the calcium sulphate was lowered by 22 mm during the simulation period of 72 hours under the forced convection scenario. In comparison, Figure 5.9 indicates a change of 15.5 mm when no wind was simulated. This represents a 42% increase in evaporation when wind was added. Clear day/night temperature cycles are visible on both figures with bold temperature stratification in the data for the free convection scenario. Daily maximum temperatures for the entire depth of the brine is considerably higher (by about 7 - 8°C) for the no wind assistance simulation compared to the forced convection experiments.

5.2.5.1Potassium sulphate with natural convection

The evaporation from a 0.5 M solution of sodium nitrate under and temperature distribution under free convection conditions are illustrated in Figure 5.11.

The upper and lower straight-line data (curves) in Figure 5.11Q shows the linear trends based on the recorded brine levels taken daily at the containers with sodium nitrate solution and distilled water respectively. The equations for these regression lines are also shown and suggested a strong linear relationship as far as the data is concern. Depicted by the diagram in Figure 5.11Q the brine level of the sodium nitrate solution had a level changed of about 16 mm (equivalent to a loss of 4000 cc), while the distilled water shows a level change of about 19.1 mm (equivalent to an evaporation loss of 4775 cc).

The large curving line in Figure 5.11Q represents the average pressure expressed by the pressure transducer at the bottom of the container (discussed in paragraph 4.3.7). The fluctuation in pressure is directly related to the level change over 72 hours of day and night simulation. The rate of decrease in pressure for each 12 hour interval was similar for each cycle. In total the pressure decreases from 4.540 kPa to about 4.404 kPa over the 72-hour period, equivalent to a 13.6 mm level change. When converted to a volume, a total of 3400cc (3.4 litres) evaporated from the sodium nitrate solution over a period of 72 hours. Over the same period the water level in the container with distilled water lost 14.8 mm and the equivalent to 3700 cc (see Appendix 1).

Figure 5.11R shows the continuous temperature variation of the sodium nitrate solution at depths of 25 mm, 50 mm, 75 mm and 125 mm below the brine surface as well as at the bottom of the container over a period of 72 hours. It also shows the variation of the air temperature and humidity about 100 mm above the surface of the sodium nitrate solution over the experimental period.

The temperature data in Figure 5.11R displays a high level of similarity with temperature patterns in Figure 5.11Q. Three rhythmic patterns show temperature changes that were recorded by the sensors at specific depths of the brine and followed the same rhythmic pattern for each 24 hours. These represent the day-night simulation during the experiment. A clear thermal stratification with the sodium nitrate solution is evident with the maximum temperatures at 25 mm depth increasing steadily from 28°C to 30°C during the elapsed 72-hour period. Maximum temperatures increased from 26°C to 28°C at a depth for 50 mm, for

75 mm the increase is from 24°C to 26°C and 125 mm the temperature changes is from 21°C to 23°C. Minimum temperatures for the various depths also increased over the 72-hour period, ranging from 15°C to 19°C for the depths up to 125 mm below the surface. Temperature at the bottom of the container ranged between 16°C and 18°C and mildly resembled the rhythmic patterns described for depths closer to the surface of the brine. On average the difference in maximum temperatures between the brine surface and at a depth of 125 mm amounts to 7°C while the minimum temperature shows a small difference of about 3°C.

At certain times, the cycles were noticeable with the variation in ambient temperature above the container (100 mm above the solution surface) although some fluctuations in temperature were visible. On average, the maximum temperature varied around 18°C although on two occasions the temperature had risen to about 21°C for short periods (about 3 hours). The minimum temperature variations were around 15°C.

The data for the humidity above the sodium nitrate solution followed the same cycles as identified earlier, but as expected the data shows an inverse relationship with that of the ambient temperature. Humidity fluctuations are a direct result from heat energy emitted from infrared lamps. The maximum humidity reached values around 65% while minimum humidity levels were at 53%.

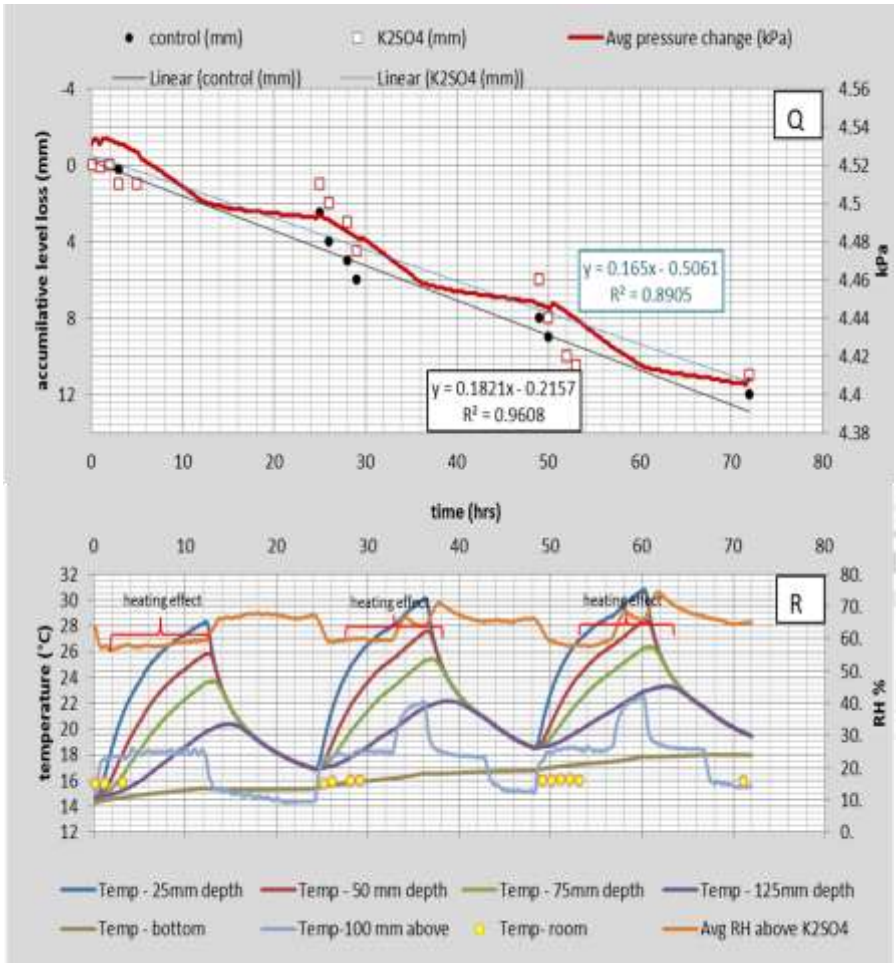

Figure 5.11 Evaporation of a potassium sulphate solution, distilled H_2O as a control (Q) and temperature distribution (R) in and above the solution surface during a 72 hr period under free convection conditions.

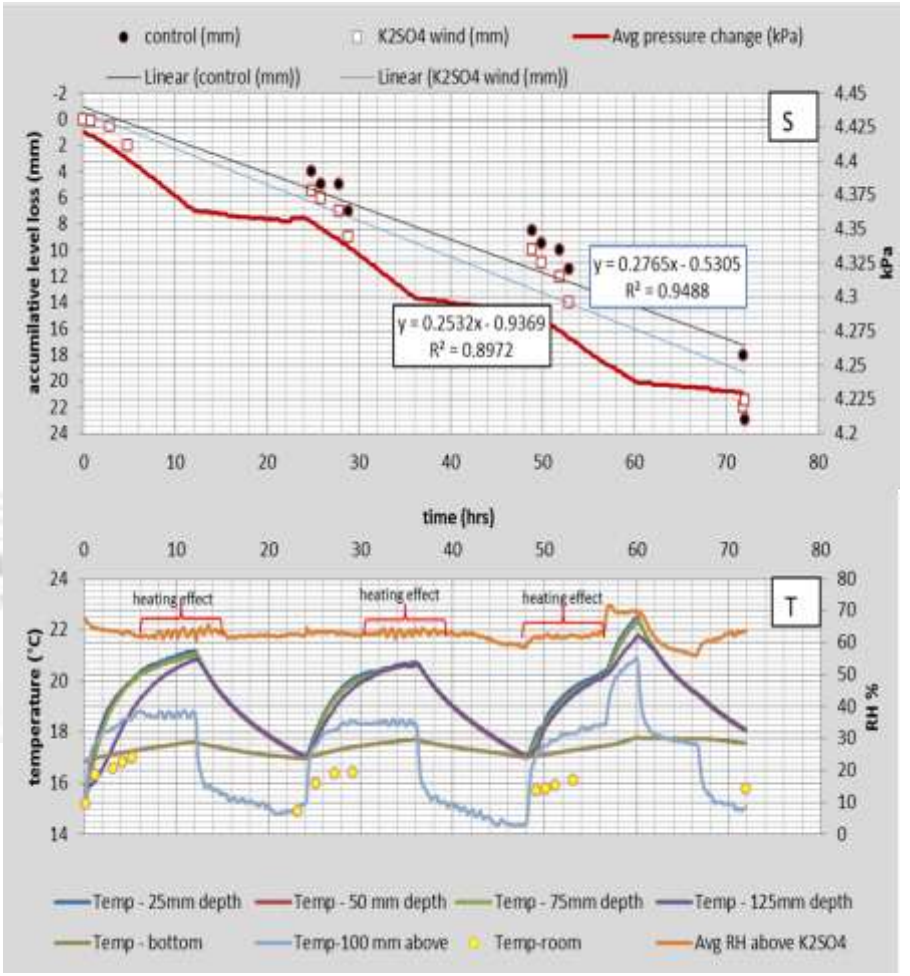

Figure 5.12 Evaporation of a potassium sulphate solution (S, distilled H_2O as a control and temperature distribution (T) in and above the solution surface during a 72 hr period under forced convection conditions.

5.2.5.2 Potassium sulphate with forced convection.

Figure 5.12 below shows the continuous evaporation and temperature variation of a 0.5 M solution of sodium nitrate under forced convection conditions (wind assistance).

Figure 5.12 shows an 18 mm brine level reductions with potassium sulphate solution during the simulation period of 72 hours under forced convection. The free convection experiment yielded 14.5 mm when no wind force was simulated. Clear day/night temperature rhythmic patterns are visible in both figures with prominent temperature stratification expressed in the data with no wind assistance. Daily maximum temperatures for free convection experiments were considerably higher (by about 9°C) compared to the forced convection.

Figure 5.11 Q shows level changes of the potassium sulphate solution taken daily over a 72-hour period. The experiment was subjected to a forced convection scenario (see paragraph 4.3.3). Two trend lines and equations representing a linear relationship are also shown.

The imposing curving line in Figure 5.11R represents the level changes over a 72-hour period. The data was recorded by the pressure transducer located at the bottom of the container. A pattern with 3 distinct rhythmic cycles is visible in Figure 5.11Q. Pressure decreased from 4.534 kPa to 4.344 kPa representing a calculated level change of about 18 mm (equivalent to 4500 cc). The water level in the container with distilled water was lowered by 20.2 mm and equivalent to 5050 cc (see Appendix 1).

The temperature data (curves) in Figure 5.11R shows the same 3 wave cycle pattern as described in Figure 5.11Q. Temperature changes emulating a day and night scenario can be easily observed down to 125 mm below the surface. A uniform temperature was observed for most of the experimental period. Temperature data near depths at 25 mm, 50 mm and 75 mm shows almost identical patterns for the first 48 hours with the maximum temperature reaching 21.3°C while minimum reached 17.5°C. Temperature data at 125 mm depth shows a slight change in comparison with the others sensors. The maximum temperature reached about 22°C while the minimum temperature reached 17.5°C during the course of the experiment. For a short period during the last 24 hours of the experiment, the peak temperatures near the surface show a difference in temperature which resembles a form of temperature stratification. The last 24 hours temperatures had peaked at 23°C for a depth of 25 mm while a depth near 75 mm below the surface reached 22.8°C. At a depth of 125 mm temperature had peaked just below 22°C and the maximum/minimum temperatures responded very

similar during the first 48 hours. Temperatures at the bottom of the container ranged between 17°C and 19°C but vaguely resembled the rhythmic cycles described closer to the surface water. A difference in maximum temperatures between surface water and at a 125 mm depth was only visible during the last 24 hours of the experiment and amounts to about 3.5°C while the difference in minimum temperature was only 2°C.

The ambient temperature above the container (100 mm above the solution surface) clearly reflected day-night cycles with maximum temperatures around 19°C during the first 48 hours but reaching almost 23°C on the 3rd day. The minimum temperature was in the region of 15.5°C.

The data displayed for the humidity above the sodium nitrate solution under forced convection fluctuated around 65%. The day-night rhythmic patterns was disrupted in by the wind force (Figure 5.12T), but can still be recognised. The relative humidity was above 60% for the first 48 hours, but had peaked above 70% on the 3rd day.

5.2.5.3 Summary of potassium sulphate experiments

In summary Figure 5.12 shows that the brine level of the potassium sulphate is lowered by 18 mm during the forced convection experiment. The free convection in Figure 5.11 evaporated 14.5 mm from the potassium sulphate solution. This represents a 24% increase in evaporation during the wind assistance experiment. Day/night temperature patterns are visible in both figures but the Figure 5.12T shows greater distortion. Peak temperatures throughout the entire depth of the free convection simulation were considerably higher near the surface than the simulation where the wind was applied.

5.2.6.1 Sodium chloride with natural convection

Evaporation and temperature distribution of a 0.5 M sodium chloride solution under free convection conditions are illustrated in Figure 5.13 below.

Data in Figure 5.13U representing the sodium chloride brine level change shows the average pressure variation of the salt solution expressed by the pressure transducer located at the bottom of the container (discussed in paragraph 4.3.7). The experiment represents level changes over 72 hours of day and night simulation. The several data recordings have confirmed the level changes of the pressure transducer located at the bottom of the container. The bold line in Figure 5.13U shows 3 wave cycles representing the day-night simulation. A similarity of fluctuation in pressure over a 12 hour period was fairly noticeable. In total the pressure decreases from 4.475 kPa to about 4.413 kPa over the 72-hour period, equivalent to 15 mm (3750 cc) of brine being evaporated. Over the same period the distilled water had a reduction of 17 mm (4250 cc).

Figure 5.13V shows the continuous temperature variation of the sodium chloride solution at depths of 25 mm, 50 mm, 75 mm, 125 mm and the bottom of the container over a period of 72 hours. It also depicts changes of the air temperature and humidity 100 mm above the surface of the brine solution and inside the laboratory over the 72-hour period.

The temperature data of the sodium chloride solution in Figure 5.13V shows similar patterns as described above in Figure 5.13U. Temperature changes between 25 mm depth below the surface and at the bottom of the container were observed daily. At the bottom of the container the temperature variation did not mimic the upper temperature ranges near the surface. At 25 mm depth the temperature range was between 19°C and 33°C. The peak temperature of each cycle increased steadily from 29°C to about 30°C while the minimum temperature had a range between 20.5°C and 21°C during the elapsed 72-hour period. The temperature between a depth of 50 mm and 125 mm ranged between 23°C and 28°C. At 75mm and 125 mm below the brine surface temperature ranged between 15°C to 19°C but also increased over the 72-hour period. At the bottom of the container, temperature ranged between 19°C and 20.5°C but the difference between the surface and the bottom temperature was close to 10 °C.

The ambient temperature of the room was recorded manually, although some fluctuations in temperature were visible as result of the day and night simulations. The maximum temperature reached around 20°C while the minimum temperature dropped to 17°C.

Humidity data of the air above the sodium chloride solution maintained a specific rhythmic pattern throughout the experimental period but displayed an inverse relationship when heat was applied with the infrared lamps. The humidity shows an inverse pattern in relation to the temperature changes, over the surface of the brine. Maximum humidity reached values of around 70% while the minimum values were reduced to about 55%.

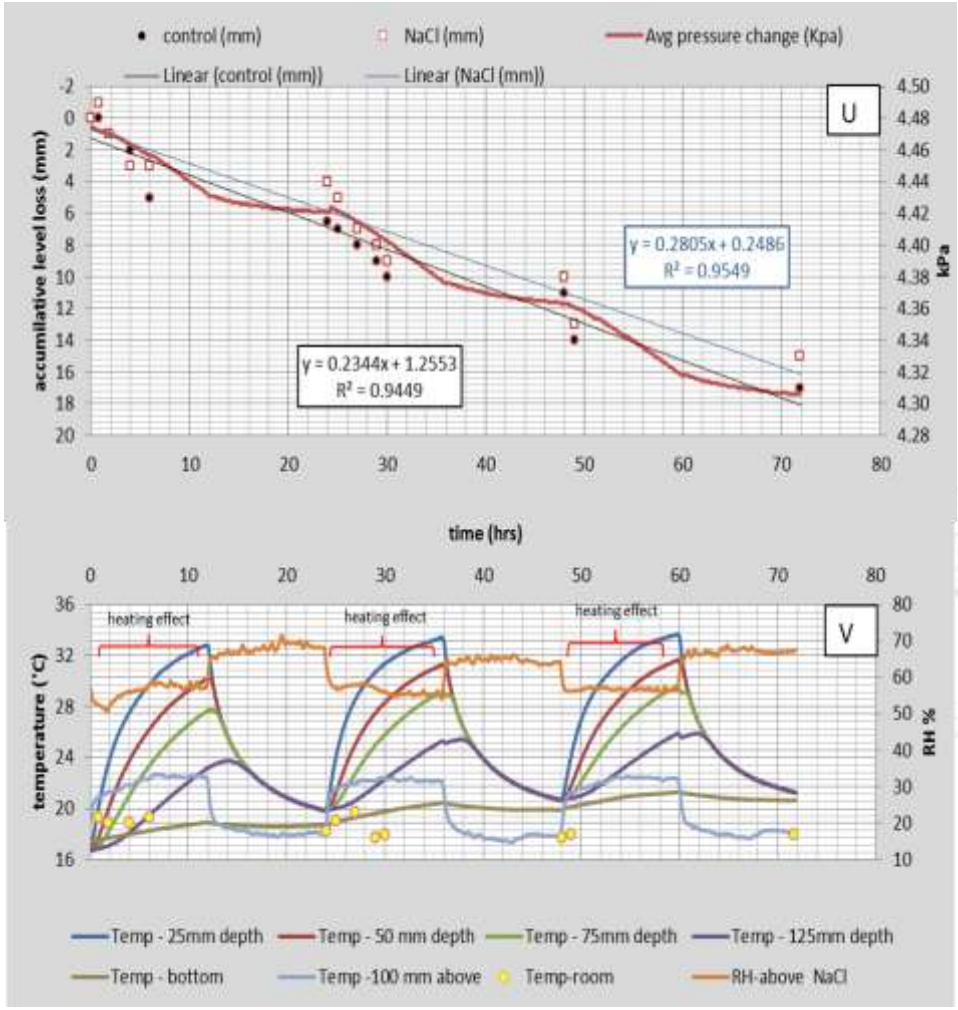

Figure 5.13 Evaporation of a sodium chloride solution, H_2O as a control (U) and the temperature distribution (V) in and above the sodium chloride solution surface during a 72hr period with a no wind scenario.

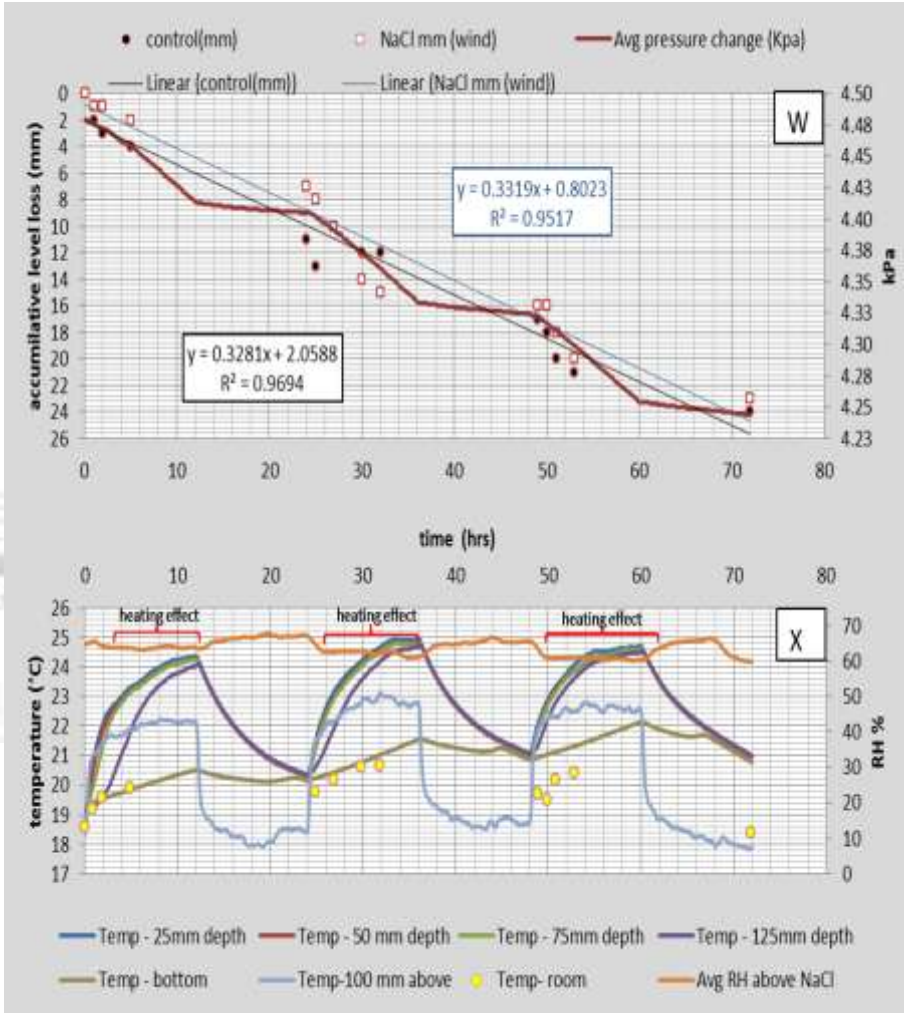

Figure 5.14 Evaporation of a sodium chloride solution, H_2O as a control (W) and the temperature distribution (X) in and above the solution surface during a 72hr period with wind

5.2.6.2 Sodium chloride with forced convection.

Figure 5.14W shows the continuous evaporation and temperature variation in a 0.5 M solution of sodium chloride under forced convection (wind assistance).

Figure 5.14W indicates the level changes of sodium chloride solution recorded on a daily basis over a 72-hour period when subjected to a wind assistance scenario (see paragraph 4.3.3). The linear trend lines and their equations are also shown.

The bold continuous data line in Figure 5.14X represents the results in level changes as pressure fluctuated above the pressure transducer over a 72-hour period A pattern with 3 day and night rhythmic patterns similar to the bold curved line in Figure 5.14 is clearly visible. The pressure difference was approximately 0.19 kPa representing a brine level change of about 15 mm (equivalent to about 3750 cc). Over the same period the water level in the container with distilled water lost approximately 17 mm (4250 cc).

The temperature data in Figure 5.14X shows the same rhythmic patterns as described above in Figure 5.14W. Temperature fluctuations are visible over a 24-hour period throughout the entire depth of the container. The temperature range is uniform throughout the 125 mm depth which lacks the temperature stratification that was evident in Figure 5.13V. The shear stress generated by the wind came into contact with the brine surface and disrupted the thermal stratification of the brine (see section 2.3.53). Temperature peaked at 21°C at depths close to 25 mm, 50 mm and 75mm for the experimental period and the minimum around 17.5°C. The temperature at 125 mm depth maintained the same rhythmic pattern but with a lower temperature, although the minimum temperature was the same for all the other sensors. Throughout the entire NaCl experiment the stratification was not very evident. The temperature range between levels of 25 mm and 125 mm shows subtle differences.

In Figure 5.14X the maximum temperature for 25 mm, 50 mm and 75 mm depth had risen to approximately above 24°C for the sodium chloride solution. At a 125 mm depth below the surface, temperatures were slightly lower during the rising phase but maintained the similar temperatures during the decrease in temperature. The ranged was between 19°C and 25°C. Temperature near the bottom of the container ranged between 19°C and 21°C and vaguely resembled similar rhythms as closer to the surface.

The variation in ambient temperature above the calcium sulphate solution (100 mm above the solution surface) clearly shows the day-night patterns with the maximum temperatures between 21°C and 24°C while minimum temperatures varied around 18°C. The variation in ambient temperature was recorded using a handheld device which shows a partial pattern of day-night cycles.

The humidity above the sodium chloride solution fluctuated between 60% and 65% during the forced convection experiment. The day-night pattern was barely noticeable in Figure 5.14X when no wind force was applied. The wind force disrupted the existing air currents and subsequently displays a suppressed data image.

5.2.6.3 Summary of sodium chloride experiments

In summary Figure 5.13 U shows that 15 mm was evaporated from the sodium chloride solution under the free convection conditions. With wind assistance (Figure 5.14 W) a change of 19 mm was observed over the 72 hour and represents a 27% increase in evaporation with the aided wind force. Clear day/night temperature cycles are evident in both figures. The difference in peak temperatures between the forced and free convection experiment was approximately 5°C. The humidity during the forced convection experiment had a smaller range than the free convection experiment based on saturated air being constantly removed above the brine surface.

5.2.7.1 eMalahleni brine with natural convection

The evaporation and temperature distribution of the eMalahleni brine under free convection scenario is illustrated in Figure 5.15 below.

Figure 5.15 Y1 shows the average pressure variation of the brine column above the pressure transducer placed at the bottom of the container (discussed in paragraph 4.3.7). These pressure fluctuations were expressed as level changes during the experimental period over a 72 hours period. The manual level recordings confirmed the level changes with the pressure transducer. The data from the pressure transducer in Figure 5.15 Y1 shows a continuous line with 3 wave patterns representing day and night simulation. The rate of decrease in pressure for each 24 hour cycle had a similar appearance. In total the pressure decreased from 4.521 kPa to about 4.404 kPa, the equivalent to 14 mm or 3500 cc. The distilled water (control) indicated a reduction of 15 mm in water level (3750 cc being evaporated).

Figure 5.15 Z1 shows the continuous temperature data variation for eMalahleni brine solution at specific depths i.e. 25 mm, 50 mm, 75 mm, 125 mm and below the brine surface as well as at the bottom of the container over a period of 72 hours. Figure 5.15 Z1 depicts variation in air temperature and humidity 100 mm above the brine surface as well as the inside of the laboratory over the 72-hour period.

The temperature data in Figure 5.15Z1 shows similar patterns as described above in Figure 5.15Z1. Three uniform day and night cycles of temperature changes were observed at depths between 25 mm to 125 mm below the surface as well as at the bottom of the container. Near the bottom of the container the temperature variation was not as vigorous as temperature fluctuation recorded nearer to the brine surface. At 25 mm depth the temperature range was between 19°C and 32°C. The peak temperature of each cycle increased steadily from 29°C to about 30°C while the minimum temperature increased from 20.5°C to 21°C during the elapsed 72-hour period. The temperature range between 50 mm and 125 mm depth was between 23°C to 28°C while the minimum temperature range was between 19°C and 20.5°C. The difference between surface and bottom temperature was close to 10 °C.

The simulation of day and night rhythmic patterns was noticeable in the temperature above the container (100 mm above the solution surface). Although temperature data in Figure 5.15 shows a certain degree of fluctuations, the greater temperature range is between 17°C and

19°C and peaked near the 26°C mark. The ambient temperature ranged between 17°C and 20°C and shows partial similarities during the entire experiment.

The data concerning the humidity above the eMalahleni brine solution followed a specific pattern throughout the experimental period but displayed an inverse relationship when heat was applied with the infrared lamps. Humidity was inversely proportional in relation to the temperature directly above the container. Maximum humidity reached values of above 70% while the minimum values were reduced just below 55%.

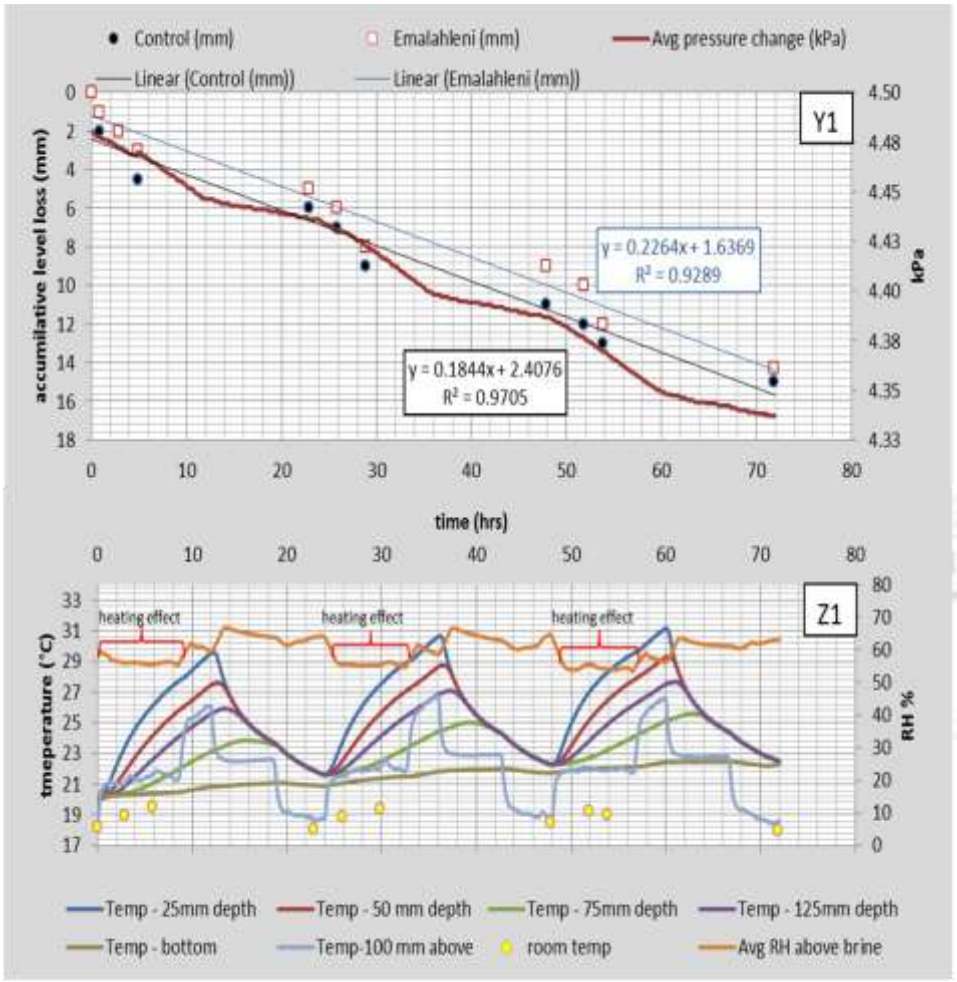

Figure 5.15 Evaporation of eMalahleni brine solution, H_2O (Y1) and the temperature distribution (Z1) in and above the eMalahleni brine surface during a 72hr period with free convection scenario.

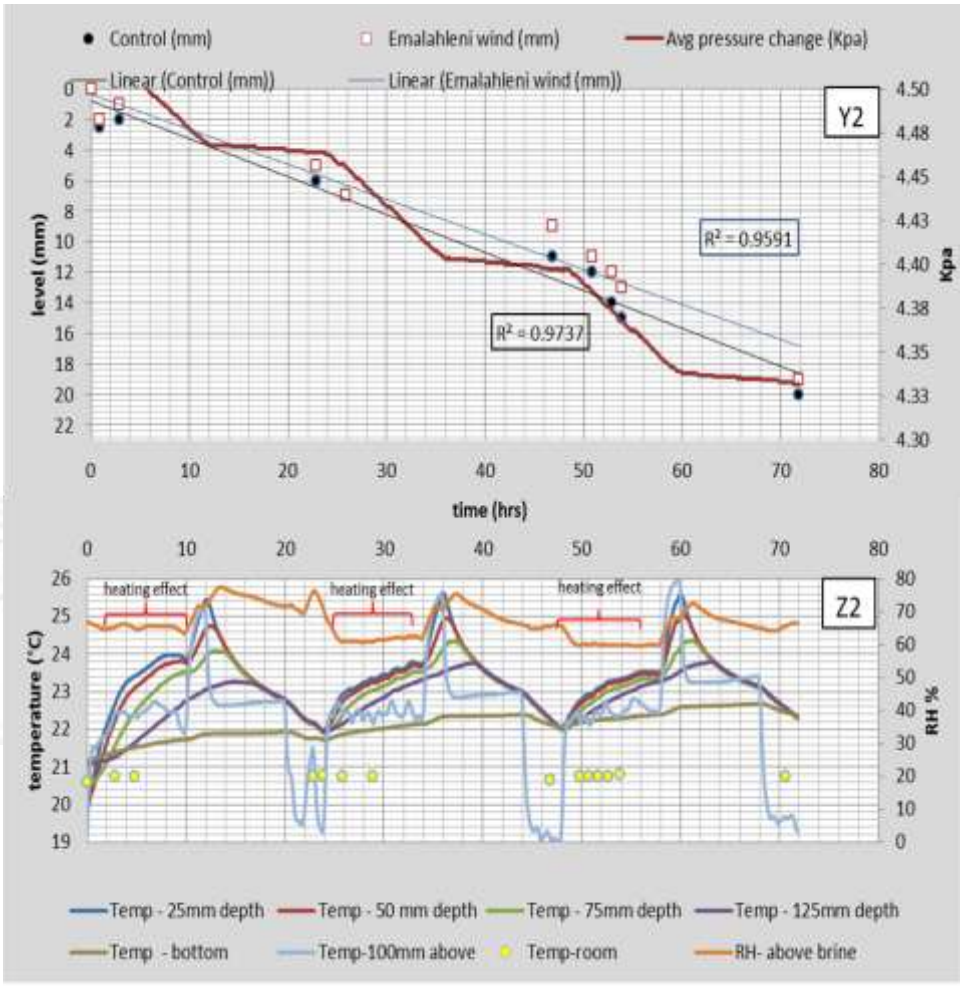

Figure 5.16 Evaporation of eMalahleni brine solution, H_2O (Y2) and the temperature distribution (Z2) in and above the eMalahleni brine surface during a 72hr period with forced convection scenario.

5.2.7.2. eMalahleni brine with forced convection

Figure 5.16 shows the continuous evaporation and temperature variation of the eMalahleni brine solution under forced convection (wind assistance).

Figure 5.16Y2 indicates the recorded level changes of the eMalahleni brine and distilled water respectively, logged on a daily basis over a 72-hour period under forced convection (see paragraph 4.3.3). Two trend lines representing a linear equation are shown in Figure 5.16Y2. As observed from the eMalahleni brine, a reduction of about 19 mm was achieved (equivalent to 4750 cc) while the distilled water shows a loss of about 20 mm (5000 cc).

The temperature data in Figure 5.16Z2 shows similar day and night rhythmic patterns as described in Figure 5.16Y2. The data shows very little temperature stratification up to a depth of 125 mm below the brine surface over most of the experimental period. Temperature near depths at 25 mm, 50 mm and 75 mm below the brine surface were almost identical during the experimental period 25°C while the minimum was around 19.5°C. Data representing temperature at 125 mm depth shows greater variations based on the low turbulent effect generated by the wind.

The stratification during the eMalahleni brine experiment was disrupted by the wind energy. The difference in temperature between the 25 mm and 125 mm depth appeared smaller with each progressive day and night cycle.

In Figure 5.16Z2 the maximum temperature at 25 mm below the brine had reached approximately 25.5°C below the brine surface. At a depth of 125 mm below the surface peak temperatures were slightly lower, and ranged between 23°C and 24°C. Temperature at the bottom of the container shows slight variations and ranged between 21°C to 22.5°C. The average difference between the depth of 25 mm and at a depth of 125 mm below the surface amounted to 3.5°C.

In Figure 5.16Z2 the ambient temperature above the container (100 mm above the solution surface) shows an irregular pattern but day-night rhythmic cycles can still be identified. The peak temperatures were in the region of around 25°C while minimum temperature dropped to about 19°C. The data recorded for the ambient temperature maintained a reading of close to 20°C.

In Figure 5.16Z2 the humidity data of the eMalahleni brine solution during forced convection was in the region of 65% during the entire experiment. The turbulent air has distorted day and night patterns but still shows subtle rhythmic patterns. The humidity data shows a greater fluctuation than the free convection experiment in Figure 5.15Z1 and ranged between 60% and 80%.

5.2.7.3 Summary of eMalahleni brine experiments

In summary, Figure 5.15 and Figure 5.16 show the level changes of the eMalahleni brine over an experimental period of 72 hours. Under free convection the level was lowered by 14 mm while the forced convection system lost nearly 20 mm. A clear distinction can be observed where the forced convection data shows more vigorous changes in Figure 5.16Y2 than the free convection experiment in Figure 5.15Y1. This represents a 42% increase in evaporation when the wind force was included in the experiment.

Clear day/night temperature cycles are evident in both figures with clearer temperature stratification expressed under the free convection scenario. Daily maximum temperatures for the free convection experiment were about 5°C higher than that with no wind scenario. The humidity data under the forced convection scenario shows greater distortion than the free convection experiment based on the turbulent air current generated by the wind force. The temperature sensor located 100 mm above the container during the forced convection container was also affected by the turbulence and is displaying more vigorous distorted data than the free convection experiment. The humidity shows clear rhythmic patterns of day and night changes in Figure 5.15Y1and ranged between 54% and 65%.The forced convection experiment ranged between 60% and 75% based on the turbulent air currents generated by the fan.

EXPERIMENTAL OVERVIEW

Several salts were subjected to very similar conditions in the laboratory during the free and forced convection experiments. Clear trends of increased evaporation can be observed from the 0.5 M salt solutions being depicted in Figure 5.17 when subjected to a wind force. Figure 5.17 depicts the total evaporation loss over 72 hrs for the synthetic and eMalahleni brine .

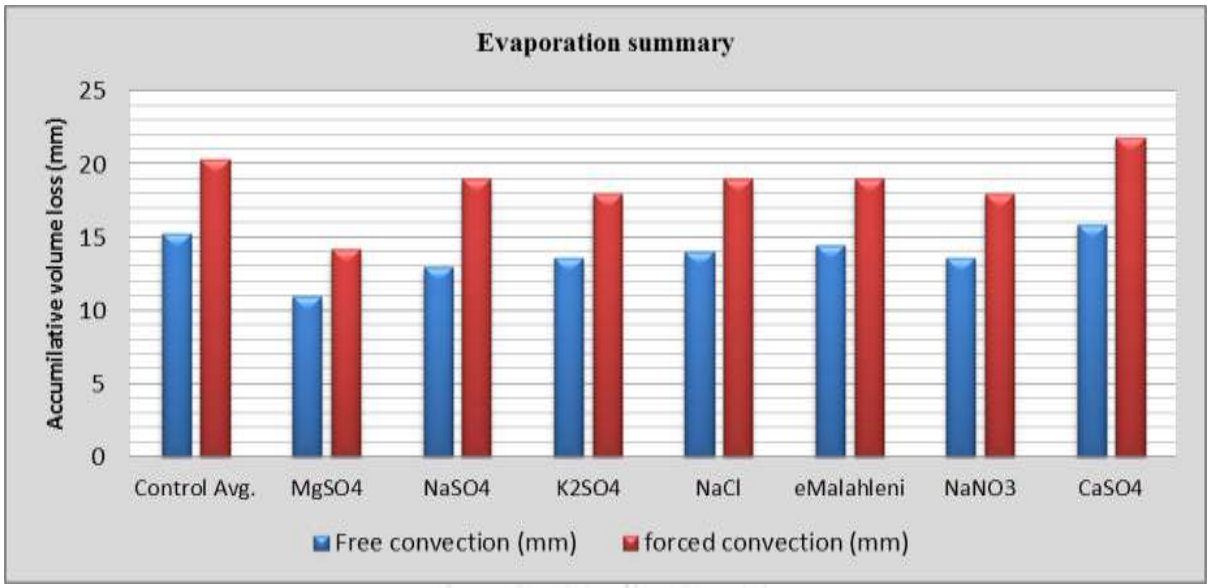

Figure 5.17 shows the total evaporation loss for the eMalahleni brine and synthetic brines over a 72 hour period for the free and forced convection scenario

Several salts were subjected to very similar conditions in the laboratory during the free and forced convection experiments. Clear trends of increased evaporation can be observed from the 0.5 M salt solutions being depicted in Figure 5.17 when subjected to a wind force.

The total percentage loss for the $MgSO_4$ solution was 2.3% for the free convection experiment. The forced convection experiment yielded a total increase in evaporation of 29% for the magnesium sulphate solution which constitutes 3.75% of the total volume. A similar trend occurred with the $NaSO_4$ solution, but the increase in evaporation is far greater with a total gain of 46% for the forced convection experiment. The overall loss is 2.71% for the sodium sulphate solution during the free convection experiment while the forced convection experiment shows a total loss of 3.95% from the total volume.

The potassium sulphate conducted under a forced convection scenario shows an increase of 28.5% in relation to the free convection experiment. The loss of approximately 3.75% of the volume was recorded for the wind assisted experiment while the free convection scenario shows a loss of only 2.92%. Figure 5.17 is showing that 19 mm has been evaporated from the sodium chloride solution during the forced convection experiment. This constitutes about 3.9% of the total volume being lost while the free convection experiment yielded a volume loss of 3%. The difference between the two NaCl brine experiments is approximately 37.5%.

The eMalahleni brine followed a similar pattern but shows a smaller volume loss of only 31% when a wind force was applied. However multi-component salts do have a tendency to retard the evaporation process especially at higher concentrations levels. Sodium nitrate shows similar evaporation losses as potassium sulphate during the forced convection experiments. The 0.5 M sodium nitrate solution did not deviate much for the forced convection and achieved 28.5% in terms of evaporation increase.

The evaporation data in Figure 5.17 shows that the calcium sulphate solution has the highest evaporation loss compared to the other salt solutions, by a large margin. The solubility product constant (Ksp) value of $CaSO_4$ is generally low hence the higher evaporation rates. The forced convection experiment for $CaSO_4$ yielded 4.5% evaporation loss from the total volume and the free convection experiment reached 3.31%. The volume loss between the forced and free convection experiment amounted to 37.5% difference in evaporation.

$MgSO_4$ data in Figure 5.17 is far below the average evaporation loss, this could possibly be based on a lower radiation delivered by faulty infrared lamps but the results from the salinity experiments (section 5.1.5) confirmed that magnesium sulphate is less soluble based on the ion interaction with the water molecules. In contrast, $CaSO_4$ solution yielded a much larger volume loss than the average free convection and forced convection experiments. The low solubility of the $CaSO_4$ allowed salts to precipitate at the bottom of the container and this could have contributed towards heat storage since the brine temperature was slightly elevated. The 0.5 M salt solutions show a slightly lower evaporation than the average control measure in Figure 5.17. This however, indicates that the 0.5 M salt concentration was not significant enough to significantly retard the evaporation rate. Overall the average loss for the free convection experiments is approximately 13.2 mm for all the salt solutions while the forced convection experiments yielded a much higher 18.5 mm. However high and low soluble salts did not follow the average trend.

5.3 DATA QUALITY ANALYSIS

5.3.1 Anthropogenic error

Human error contributed significantly as result of manual measurements during the experiments. In chapter 2 the electrostatic forces emphasised the effects of the meniscus during the experimental cycles. The electrostatic charge of the container played a significant role as for some salts it was easier to record the brine volume loss over time. Calcium sulphate indicated the least error margin as the meniscus was negligible and made the data recordings easy to read throughout the experiments.

5.3.2 Product errors

All the measuring equipment that recorded continuous data was pre- calibrated by the manufacture. The limitations of the sensors accuracies were highlighted in Chapter 4. Container failures such as leaks were fixed by the manufactures.

5.3.3 Percentage of error (absolute)

$$\frac{\text{manual recorded data} - \text{actual continous data}}{\text{actual continous data}} \text{ X } 100 \quad \text{..... (21)}$$

Table 5.1 The table represents the error margins of the different salt solutions.

Salt solution	eMalahleni brine	$CaSO_4$	NaCl	$NaSO_4$	$MgSO_4$	KSO_4	NaNO3
%error natural convection	10.3	5.6	26.6	5	29	4.4	12.6
%error forced convection	5.26	5.2	11.4	15.7	24.6	27	9

The accuracy margin was highlighted in Table 5.1 between the natural and forced convection experiments. There was a tendency of a decreased error margin when the wind energy was applied. The meniscus was diminished through the air currents hence the lower error margin.

Chapter 2 highlights this occurrence with regards to the capillary forces. The $MgSO_4$ had a greater error margin as result of the pressure above the sensor was affected by the ventilated air support was depicted in Table 5.1. The higher percentage error was also an indication of correcting or identifying potential problems that occurred during the experiments. The manual measuring system also served as a means of verifying for the digital data logging system. The higher density salts like the $MgSO_4$ showed a greater percentage of error between the manual and continuous data. The remaining residue of salts after evaporation restricted the movement of the ventilated air pipe and affected the manual measurements to a certain degree.

CHAPTER 6

MODEL APPLICATION

This section deals with all the energy balance and express the eMalahleni brine in a suggested model that will accommodate the salinity aspect for this study.

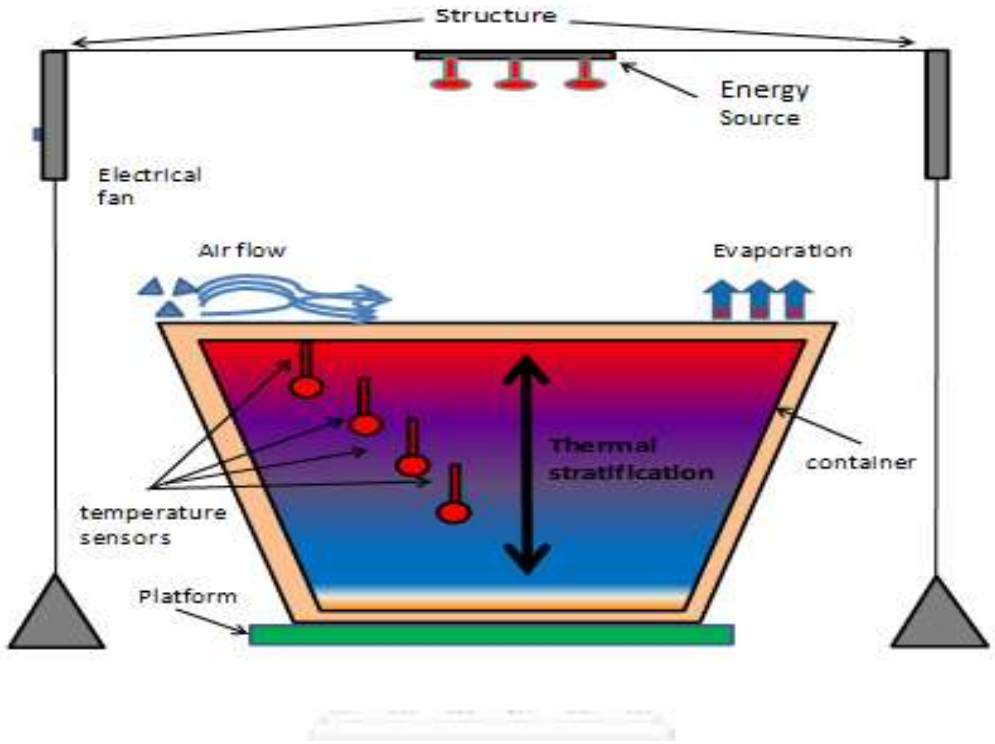

Figure 6.1 Suggested experimental setup (Adapted from Schultheis et al., 2001)

6.1 ENERGY BALANCE

The energy of the system was calculated at every 12 hour cycle in accordance with the different temperature variations (see Figure 6.1). The first segment of the energy was used to elevate the temperature and the second part to change the phase (Young, 1947). Evaporation is an endothermic process which means it requires energy to conduct the phase change. The dissipation of energy indicated that the surface level absorb a greater amount of energy from the infrared lamps.

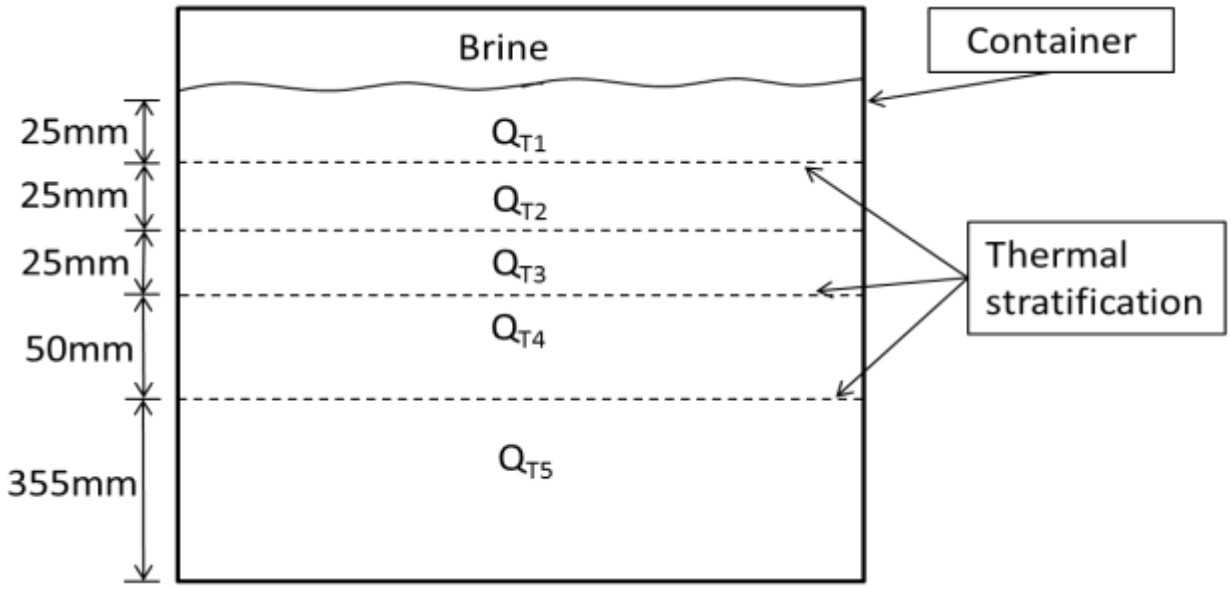

Figure 6.2 The diagram illustrates the thermal energy distribution during the eMalahleni brine experiment.

$$\boldsymbol{Q_{total} = mC\Delta t} \quad \text{..... (14)}$$

Where $\boldsymbol{Q}$ is the total energy stored in a particular layer, m is the mass, specific heat capacity; Δt is the change in time period.

Table 5.2. The table is depicting the energy distribution as a function of the different depths.

T_1= 25 mm from the surface	Q_{T1}= 8.6%
T_2= 50 mm from the surface	Q_{T2} = 8.62%
T_3= 75 mm from the surface	Q_{T3}= 7.26%
T_4 = 125 mm from the surface	Q_{T4}= 9.69%
T_5= bottom of the container	Q_{T5}= 65.89%

The energy distribution was demonstrated by the thermal stratification of the brine (Table 3). This was established by the change in the brine temperature over the experimental period. A large dissipation of heat energy was observed at the bottom of the container over the experimental period. A contributing factor was the incremental volume change at the lower section of the container. The sensor near the surface of the container covers only 25 mm while the area difference between the bottom sensor and 125mm below the surface was nearly 355m. This however suggests that large volume of brine absorbed a more significant amount of heat energy released by the infrared lamps.

$$\Delta \boldsymbol{U} = \boldsymbol{Q} + \boldsymbol{W} \quad \text{..... (15)}$$

$\Delta \ddot{\boldsymbol{U}}$= total energy

Q= temperature change

W= evaporation+ condensation

The total energy absorbed by the container was calculated for a 3 day cycle. The combination of evaporation, temperature change and condensation energy constituted towards the greater energy utilised of the experimental setup.

Wind input

$$\boldsymbol{P} = \frac{\mathbf{1}}{\mathbf{2}} \boldsymbol{\rho A v^3} \quad \text{..... (16)}$$

With P the power, ρ the density of the air, A the surface area exposed and v the velocity of the wind.

The wind energy was calculated for a 3 day experimental cycle when it was applied for 12 hour intervals. The wind energy was produced from the electric fan and propagated through the ventilated air pipes. The shear stress was not incorporated in the calculations for the above mentioned experiments since the wind velocity was approximately 2 m/s throughout the experiments.

The distribution of energy showed that a greater amount of energy was absorbed by the lower section of the container as a result of the temperature gradient and the larger volume. In addition, the upper section of the container reached a higher temperature but transferred a significant amount of energy to the lower section of the container. Approximately 30% of the energy from the system was absorbed by the surrounding area and expelled though the ventilation system. This loss of energy was a secondary effect in order to maintain the constant temperature of the experimental area during the experimental setup.

6.2 MODEL APPLICATION FOR REAL ENVIRONMENT SIMULATION

Modelling is regarded as a vital tool to expose geochemical processes, analyse laboratory experiments. In addition, it is also being used as a mechanism to predict unfolding events and monitoring plans for the future. With all the accolades associated with geochemical modelling, it remains rather a tool for research groups (Crawford,1999). The calculation for brine solution requires a different approach from the conventional Penman method (Akridge, 2008; Finch, 2001). Oroud (1999) specifically developed an energy balance model for hyper-saline solutions like the Dead Sea. The Oroud (1999) model was selected for this study because of the salinity aspect which place greater emphasis on the activity coefficient. The model was derived from the Penman equation.

Model description

A large number of models exist and it was rather important to validate the appropriate model based on the assumptions made when the model was developed (Crawford, 1999). The major ions that has been investigated for this study are Mg^{+2},Na+,K+,Ca+,Cl-,SO_4,NO_3. Using a specific computer modelling software can aid the modelling process. The activity coefficient of the eMalahleni brine which is a multi-component electrolyte solution can be very challenging to analyse in detail.

The Pitzer model is highly used and recommended to determine the activity of mixed brines (Krumgalz, 1997; Harvie et al., 1984). The ratio for combining different species in a multicomponent electrolyte was greater than the isolated ions hence it was more convenient to calculate as a collective for all the ions (Krumgalz, 1997). With the aid of the PhreeqC geochemical modelling software, the speciation of the eMalahleni brine was determined. This however, assisted with the determination of the activity coefficient which was applied in the Oroud model to calculate the evaporation rate based on the ion-ion interaction.

Oroud Model

$$\boldsymbol{E = \frac{\beta \Delta H}{\beta \Delta + \psi} + \psi f(u) \frac{\beta e_a^* - e_a}{\beta \Delta + \psi}} \quad \text{……;……} \quad (17)$$

Where $\beta\Delta$ is referred as the change in the activity coefficient, H is the energy input, ψ is the psychometric constant, $f(u)$ is the wind speed. e_a^* is the saturated air above the brine and e_a is the vapour pressure of the room.

Psychometric constant

$$\boldsymbol{\psi = \frac{C_p . P}{\varepsilon \lambda} = 0.665 \times 10^{-3}} \quad \text{……..……..} \quad (18)$$

The psychometric constant is expressed in [kPa °C^{-1}], P is expressed in atmospheric pressure [kPa]

λ latent heat of vaporisation, 2.45 [MJ kg^{-1}], *Cp* specific heat at constant pressure, 1.013x10^{-3} [MJ kg^{-1} °C^{-1}] and the ratio molecular weight of water vapour/dry air = 0.622.

$$\boldsymbol{P = 101.3 \left[\frac{293 - 0.0065z}{293}\right]^{526}} \quad \text{……..……} \quad (19)$$

Where P is the atmospheric pressure, z is the elevation from a sea level perspective.

Model validation

Data that was obtained during the eMalahleni brine experiments and applied to Oroud model to generate an output file. The output data from the Oroud model was compared to empirical data obtained from A- pans located near the study area.

Table 6.1 Actual measurements of the Emalahleni brine and the modelled brine evaporation generated by the Oroud model (1999, 2000).

Emalahleni Avg.mm/day	Oroud Model mm/day	Emalahleni Avg. mm/day (no wind)	Oroud Model mm/day (wind)	Projected monthly (no wind)	Projected monthly (with wind)
5.3333	5.330045	6.5	8.9	159.90	267.10

In Table 6.1 the daily average of the Emalahleni brine under natural convection was 5.33 mm/day. All the parameters during the experiments were applied to generate an output file to

which the Oroud model was applied. In comparison with the free convection scenario the model showed a similar result as the laboratory experiments with the eMalahleni brine. Contrary to the free convection result, the forced convection scenario showed a significant difference. Oroud (1999, 2000) suggested a very similar figure over the same period. Under the forced convection the model predicted a higher value than the actual recorded evaporation. The experiments which incorporated the wind increased the rate to about 22%. The modelled data also projected a 37% increase under forced convection being applied at 2m/s during the energy input.

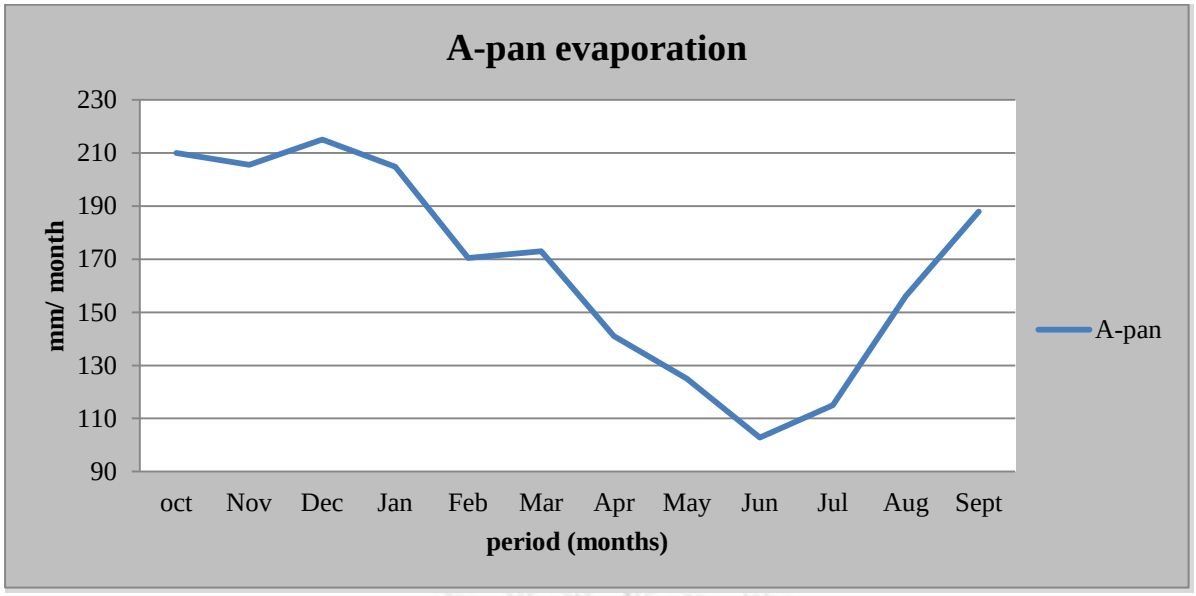

Figure 6.3.The mean monthly A-pan evaporation of the relevant secondary catchment in the Olifants Catchment (Schulze et al., 1997).

This data generated by the Oroud model (under free convection conditions) in Table 6 is within range with data presented in Figure 6.3. The month of September`s evaporation rate is in the region of 188.5 mm for this particular region in the Olifants Catchment. However the data generated by the Oroud model is suspected to have a lower value considering that (Schulze et al., 1997) projected the results without incorporating the salinity aspect. The modelled data in Table 6 suggests an even higher evaporation forecast (8.9 mm/day) under forced convection conditions compared to the monthly evaporation data in Figure 6.3. The highest evaporation rate in this secondary catchment is approximately 211 mm / month. This suggests that the model`s prediction for a forced convection scenario might be slightly higher than empirical evaporation data.

CHAPTER 7

CONCLUSION AND RECOMMENDATION

In this chapter the main conclusions are drawn from the free and forced convection experiments. This chapter also focuses on the final remarks for the model application, salinity experiments, in particular the different synthetic salts. This chapter also presents the recommendations, challenges and possible future studies.

7.1 Brine characteristics and impacts

Based on the salinity experiments, all the synthetic salts exposed to various molar concentrations have shown different volume losses. The results indicated that the greatest volume loss is with the least soluble salt amongst the synthetic salts while the higher soluble salts gained the lowest volume lost. The eMalahleni brine is mainly a sulphate-sodium based solution with a variety of major and minor ions.

7.1.1 Chemical aspect

Known as a hydroscopic constituent, sodium chloride yielded the lowest evaporation for the higher molar concentrations as a result of the high ionic strength of the solution. Sodium chloride is monatomic and as an ionic compound, it totally dissociates in water where each ion breaks apart and bonds with the water molecules. Polyatomic salts like $MgSO_4$ do not totally separate into individual ions but collectively have a single charge.

Dissociation of ions will ultimately lead to a greater solubility of the salt especially in the case of NaCl. The activity coefficient increases and subsequently leads to lower vapour pressure based on the strong ion-ion bonds. In addition, Moore and Runkles (1968) highlighted the vapour pressure as one of the main contributing factor, while Oroud (1999) identified the activity coefficient as one of the main contributing factors which influence the evaporation rates. With an increase in the salt concentration, the activity coefficient increases along with a decrease in vapour pressure. The salinity experiments confirmed this statement when a decrease in evaporation was noted with an increase in salt concentration.

7.1.2 Physical aspect

With experiments conducted in the laboratory, it was concluded that nearly all the saline solutions had lower evaporation rates than the distilled water (control). Apart from these findings, lower soluble salts such as $CaSO_4$ indicated a different result compared to other

synthetic salts. The results from the experiments show that salts that precipitated at the bottom of the container were partially beneficial towards the evaporation rate, in particular salts with a lower solubility like $CaSO_4$. It is suggested that the low solubility as a result of the small Ksp value permitted the salt to precipitate at the bottom of the container.

Findings from the molar concentration (salinity) experiments indicate that the $NaSO_4$ brine solution had a higher crystallization rate as it reached super saturation at a faster rate than other synthetic salts. Calcium sulphate brine was the least soluble but yielded high evaporation volumes followed by the $NaSO_4$ (see Figure 5.2). This indicated that salts at the bottom of the container, accumulated by means of crystallization or precipitation (crash out) may have generated a secondary heating source which could have enhanced the evaporation rates. Based on imperical evidence, $NaSO_4$ brine was the first synthetic salt to crystalize during the salinity experiments.

The highest precipitation of salts at the bottom of the container was achieved with low soluble $CaSO_4$ synthetic brine. In some cases the presence of salts elevated the temperature of brine by at least 0.5°C. According to Mao (1999) the temperature of saline solutions can be warmer but do not necessary have greater evaporation rates.

In this study the forced convection did contribute positively towards the evaporation rate. Chu (2010) suggests that, the wind factor was limited when evaporation lowered the brine level and subsequently resulted in limited wind impact on the brine surface. In this study, the floatable wind source eliminated this drawback and delivered a more consistent wind source. In this study the ambient temperature did play an important role and was more effective in the initial and later stages of the brine experiments.

Identifying the overwhelming factor which played the most significant role in the evaporation levels of the brine experiments was difficult to express. Both physical and chemical factors were observed that affected the evaporation rate and based on various research papers and brine experiments results, the brine evaporation rate was due to a combination of these factors.

7.2 Model application

PhreeqC can be used as modelling software but it has some limitations when modelling brines with high ionic strength. The application of the Oroud (1995) model had certain assumptions and was applied for arid to semi-arid regions i.e. Dead Sea and was found to be applicable to a certain extent. The estimated value that was generated from the model was limited to a specific season of the eMalahleni area. The climate for this specific region was very moderate in terms of temperatures and rainfall as described in Figure 3.2 and 3.3. Data collected in the laboratory through experiments can be compared to the real environment but it has some limitations. The assumptions for the Oroud (1995) model included that it was designed for high to moderate temperatures that resembled conditions in the Middle East. However, the summer period of the eMalahleni period can be highly compatible with meteorological conditions of the Middle East region especially maximum and minimum temperatures. Using PhreeqC and a physical model such as Oroud (1995) to determine evaporation from saline water bodies has not been previously demonstrated and documented.

7.2 RECOMMENDATIONS

Various methods can be applied to enhance the evaporation. A number of factors will predetermine the application of the method. This includes the geo-location, duration and the most important is the budget (incurring costs). In this section several factors were recommended for the improvement of solar brine pond evaporation.

Evaporation sprayers are a popular choice to enhance the evaporation rates but have two significant drawbacks. If the substance is highly toxic, the overspray into the atmosphere might potentially contaminate the soil or groundwater. The intense energy consumption to maintain the system could be another concern.

Another potential solution could be the Wind Aided Intensified Evaporation (WAIV) system which has a great variety of applications. This method increases the surface area by means of an erected structure above the brine solution which leads to exposure to a wind force while the brine flows down the structure. This can be either a passive or active system depending on the material and application. The study of Petrik et al (2015) suggested a dual application for the WAIV system to also make use of nanofibres to function as a separator for the divalent cations.

The optical appearance of the brine pond can be altered to increase the radiation absorption. Darker shades can assist with the radiation absorption by adding Methylene Blue as a

colorant to enhance the evaporation. However the drawback for dye application might be the exorbitant costs of the dyes and colour might be compromised when subjected to other substances. In terms of energy storage capacity, this can be enhanced to increase the heat storage of a brine pond by covering the bottom with a coal cinder where it serves as a secondary heating source. It could elevate the brine temperature and subsequently increase the evaporation.

7.2.2 The usage of brine as a by-product

The eMalahleni water reclamation project was a major advancement in the coal mining industry where several traditional mitigation practices were excluded. One of the methods is controlled discharge which still contributed towards higher saline levels in the water resources. New technology improving the usage of by-products from brine could be beneficial provided that the toxic levels are deemed to be safe for humans and the environment. The feasibility is in question for the usage of Gypsum as a by-product because of large quantities readily available for the market (Petrik et al., 2015).

7.3 Future work

To improve the evaporation rate a number of avenues are available in the industry but a few are cost effective. With soaring costs to maintain good governance and compliance, the industry is always poised for new technologies to improve the efficiency of their respective practices. The concept of zero discharge is fast becoming a major component in the design model of modern day practices where a waste product is viewed as a viable resource in the quest to minimize the environmental concern. The process where a brine waste product can be used to substitute a toxic element like cadmium in the solar cell manufacture is a good example.

Further investigation is needed to establish the endo-exothermic characteristics of the eMalahleni brine in its stratified form. It is highly plausible that the optimum amount of precipitated salts can enhance the evaporation rate and act as a secondary energy source. In the laboratory, $CaSO_4$ brine with accumulated salts that precipitated out at the bottom and show improvements in the evaporation rate. It reached competitive evaporation rates with distilled water at certain intervals.

REFERENCES

Adler, N. 2007. An Assessment of the Relationship between the Government, *The Mining Industry and the Role of Science.* CSIR, Pretoria.: WRC.

Ahmed, M., Shayya.W.H, Hoey.D, Mahendran,A. 2000. Use Of Evaporation Ponds For Brine Disposal In Desalination Plants. *Desalination*. Pp.155-168.

Ahmed, M,Shayyab,W.H.,Hoey,D.,Al-Handaly,J. 2001. Brine Disposal from Reverse Osmosis Desalination Plants In Oman and the United Arab Emirates. Desalination., Pp.135-147.

Ai-Shammiri, M. 2002. Evaporation Rate As A Function Of Water Salinity. *Desalination*., Pp.189-203.

Al-Jibbouri, S. Strege, C., Ulrich, J. (2002). Crystallization kinetics of epsomite influenced by pH-value andimpurities. *Journal of Crystal Growth* (236), 400-406.

Al-Khlaifat, L.A., (2008). Dead Sea rate of evaporation. *American Journal of Applied Sciences, Volume 5*(Issue 8), 934-942.

Arya, S.P 1998. Introduction to Micrometeorology. London: Academic Press.

Asmar, B.N., Ergenzinger, P. 1999. Estimation Of Evaporation From The Dead Sea. Hydrological Processes. Pp.2743–2750.

Atkins, P.W. 1978. *Physical Chemistry*. Bristol: Oxford University Press.

Awerbuch, L. (1990). Disposal of concentrates from brackish water desalting plants by means of evaporation technology. *Desalination, 1*(78), 71-79.

Barrie Johnson, D., Hallberg,K.B. 2005. Acid mine drainage remediation options: a review. *Science of the Total Environment*. 1(338), pp.3-14.

Bell, F.G., Bullock,S.E.T., Halbich ,T.F,Lindsay,J. 2001. Environmental Impacts Associated With An Abandoned Mine In The Witbank Coalfield, South Africa. International Journal Of Coal Geology., Pp.195-216.

Beran, J. A. 2014. Laboratory manual for principles of general chemistry / Jo Allan Beran, Regents Professor, Texas A&M University System, Texas A & M University—Kingsville.—Tenth edition.

Brutsaert, W. 1982. Evaporation Into The Atmosphere. Dordrecht: Kluwer Academic Publishers.

Bradshaw, A. W. (1982). Mine waste reclamation. *Mining, 299,* 75-80.

Calder, I.R., Neal, C.1984. Evaporation From Saline Lakes: A Combination Equation Approach. Hydrological Sciences Journal. 29(1), Pp.89-97.

Calver, A., Finch, J. 2008. Methods For The Quantification Of Evaporation From Lakes. Oxfordshire: *World Meteorological Organization's* Commission for Hydrology.

Chu, C., Li,M.,Chen,Y., Kuo,Y. 2010. A Wind Tunnel Experiment On The Evaporation Rate Of Class A Evaporation Pan. Journal Of Hydrology. 381 , Pp.221–224.

Cobaner, M. 2013. *Reference Evapotranspiration Based On Class A Pan Evaporation Via Wavelet Regression Technique. Irrigation Science*., Pp.119-134.

Coleman, M. 2000. *Review and discussion of the evaporation rate of brines, Actis Environmental Services.* Mundijong: Actis Environmental Services.

Comrie, W.P. 2011. Development Of A Reconciliation Strategy For The Olifants River Water Supply System. Aueron.

Connell, D. 2005. *Basic Concepts of Environmental Chemistry* (2nd ed.). Boca Raton: CRC Press.

Crawford, J. 1999. Geochemical Modelling – *A Review Of Current Capabilities And Future Directions.* Stockholm.

Dalton, J. 1802. *Experimental Essays On The Constitution Mixed Gases; On The Force Of Steam Or Vapor From Water And Other Liquids In Different Temperatures, Both In A Torricellian Vacuum And In Air; On Evaporation And On The Expansion Of Gases By Heat. Manch Lit Philos* Soc. 5(11), Pp.535–602.

Dama-Fakir, P., Wurster, A. Toerien, A. 2012. Field Testing To Determine The Evaporation Rate Of Brine Solutions Formed During The Membrane Treatment Of Mine-Water. Pretoria: Water Research Commission.

Du Plessis, Burger,J.A., A.J,Swartz,C.D.,Museev,N. 2006. A Desalination Guide For South African Municipal Engineers. WRC.

Duan, Z., Martin, J.L., Mcanally, W.H., Stockstill, R.L. 2009. Combined Effects Of Wind And Streamflow On Gas-Liquid Transfer Rate. *Journal Of Environmental Engineering.*

El-Naas, M. H. (2011). *Reject Brine Management, Desalination.* (M. S. (Ed.), Ed.) Trends and Technologies: InTech.

Fatoba, O.O., 2010. *Chemical interactions and mobility of species in fly ash-brine co-disposal systems,* University of the Western Cape, Cape Town, South Africa.

Ferguson. 1952. The Rate Of Natural Evaporation From Shallow Ponds. Austral. Austral. J. Science. Research., Pp.315-330.

FAO, 1992. *Expert consultations on revision of FAO methodologies for crop water requirements*. Land and Water Development Division, Food and Agriculture Organization of the United Nations, Rome: Italy.

Finch, J.W. 2001. A Comparison Between Measured And Modeled Open Water. Hydrological Processes. 15, Pp.2771-2778.

Furumai, H.2008. Rainwater and reclaimed wastewater for sustainable urban water use. *Furumai, H 2008, 'Rainwater and reclaimed wastewa Physics and Chemistry of the Earth*(33), 6-340.

Giwa, A. D.2017. Brine management methods: Recent innovations and current status. *Desalination* (407), 1-23.

Glueckstem, P., Priel, M. 1996. Optimized Brackish Water Desalination Plants With Minimum Impact On The Environment. Desalination.

Günther, P., Mey, W. 2006. Selection Of Mine Water Treatment Technologies For The eMalahleni (Witbank) Water Reclamation Project. In: In Proc. Water Institute Of South Africa Conf., Pp.21-25.

Günther, P., Naidu,T. 2008. Mine Water Reclamation – Towards Zero Disposal. Johannesburg, South Africa: Water Institute Of South Africa Biennial Conference.

Halder, B.K.,Tandon,V.,Chintalapalle, R.V, Roy,D., Tarquin,A. 2015. A Potential Biological Approach for Sustainable Disposal of Total Dissolved Solid of Brine In Civil Infrastructure. Construction And Building Materials., Pp.51-60.

Harbeck jr, G.E. 1955. The Effect of Salinity on Evaporation. Usgs Prof. Pap. A(272), Pp.1-6.

Harbeck Jr, G. E., Kohler,M.A.,Koberg, G.E.(1958). Water Loss Investigations:Lake Mead studies. *U.S.,Geol.Surv.,Profess.Paapers, 298*, 100.

Hassani, A., Tajrishi, M., Abrishamchi, A. 2008. Comparison Of Several Evaporation Models Applied To Reservoir Of The Saveh Dam, Iran. In: The 3rd International Conference on Water Resources And Arid Environments And1st Arab Water Forum. Comparison Of Several Evaporation Models Applied.

Hobbs, P.,Oelofse,S.H.H., Rascher,J. September 2008. Management of Environmental Impacts from Coal Mining in the Upper Olifants River Catchment as a Function of Age and Scale. Water Resources Development. 3(24), Pp.417-431.

Houas, A.,Lachheb,H.,Ksibi,M., Elaloui,E. ,Guillard,C., Herrmann,J. 2001. Photocatalytic Degradation Pathway of Methylene Blue in Water. Applied Catalysis B: Environmental., Pp.145-157.

Ipcc, 2007a. 2007. Climate Change 2007: The Physical Science Basis. In: Solomon, S., Qin. Cambridge, United Kingdom and New York, NY, USA: Cambridge University Press.

Itier, B., Brunet, Y.,Camp, C.R., Sadler,E.J., Yoder, R.E. 1996. Recent Developments and Present Trends in Evaporation Research: A Partial Survey. In: Evapotranspiration and Irrigation Scheduling. In: Proceedings of the International Conference. ASAE.

Jodat, A. 2012a. An Experimental Study of Ability of Similarity Theory to Predict Water Evaporation Rate for Different Convection Regimes. *International Journal of Multidisciplinary Sciences and Engineering*. 3 (2).

Jodat, A., Moghiman,M.,Morteza Anbarsooz,M. 2012b. Experimental Comparison of the Ability of Dalton Based and Similarity Theory Correlations to Predict Water Evaporation Rate in Different Convection Regimes. Heat Mass Transfer., Pp.1397-1406.

Kane, R.P., 2009. Periodicities, Enso Effects and Trends of some South African Periodicities, 2009 Enso Effects and Trends of Some South African Rainfall Series – An Update. South African Journal of Science. P.105.

Karimi-Googhari.S. 2012. Daily Pan Evaporation Estimation Using a Neuro-Fuzzy-Based Model. Journal of Agricultural Science and Technology. B(2), Pp.223-228.

Khordagui, H. 1997. Environmental Aspects Of Brine Reject From Desalination Industry In The Escwa Region. Beirut.

Kirabira, J. K. (2015). Phase Developments during Natural Evaporation Simulation of Lake Katwe Brine Based on Pitzer's Model. *British Journal of Applied Science & Technology, 4*(11), 1-7.

Koening, L. (1958). *R&D Progress Report No 20.* Washington, DC, 1958: Office of Saline Solutions.

Knox, J.W., Rodriguez-Diaz, J.A., Hess,T. M. 2011. Estimating Evapotranspiration by Using Atmometers for Irrigation Scheduling in a Humid Environment. England: Journal of Irrigation and Drainage Engineering.

Kokya, B.A., Kokya, T.A. 2008. Proposing a Formula for Evaporation Measurement from Salt Water Resources. Hydrol. Process., Pp.2005-2012.

Kondo., J. 1975. Air-Sea Bulk Transfer Coefficients in Diabatic Conditions. Sendai, Japan: Geophysical Institute, Faculty of Science, Tohoku University, Sendai, Japan.

Kusangaya, S.,Warburton,M.L.,Van Garderen, E.A., Jewitt, G.P.W. 2014. Impacts of Climate Change on Water Resources in Southern Africa: A Review. Physics and Chemistry of the Earth 67–69., Pp.47-54.

Lee, C.H. 1927. Discussion of 'Evaporation On Reclamation Projects. Transactions of the American Society of Civil Engineers., Pp.340–343.

Lewis, A.,Nathoo,J.,Reddy,T., Randall,D.,Zibi,L.,Jivanji,R. 2010. Novel Technology for Recovery of Water and Solid Salts from Hypersaline Brines:Eutectic Freeze Crystallization. Pretoria: Water Research Commission.

Maas, E.V, Tanji, K.K.1990. Crop Salt Tolerance, In: Agricultural Salinity Assessment and Management. American Society of Civil Engineers., Pp.262–303.

Macedonio, F., Katzir, L., Geisma, N., Simone, S., Drioli, E., Gilron, J. 2011. Wind-Aided Intensified eVaporation (WAIV) and Membrane Crystallizer (MCr). *Desalination.*, pp.127-135

Malisawa, M.S., Rautenbach, C.J.. 2012. Evaluating Water Scarcity in the Southern African Development Community (SADC) Region by Using a Climate Moisture Index (Cmi) Indicator. Water Science & Technology: Water Supply. 1(12).

Mao, Y.S. 1999. Effect of Chemical Composition on Saline Water. Msc.Thesis.Mcgill University.

Marek, R., Straub, J. 2001. Analysis of the Evaporation Coefficient and the Coefficient Condensation of Water. *International Journal of Heat and Mass Transfer*. Pp.39-53.

Mazvimavi, D., 2011. Climate Change, Water Availability and Supply. In: Kotecha, P. 2011. Climate Change, Water Availability and Supply. Climate Change, Adaptation and Higher Education: Securing Our Future. 2(4), Pp.81-100.

McGuinness, J.L,. Bordine, E.F. (1972). A comparison of lysimeter-derived potential evaporation with computed values. *Tech.Bull*, 71.

Mickley, M. (1995). Proc. *Intemational Desalination Association Conference, 7*, p. 351. Abu Dhabi.

Mickley, M. (2006). *Membrane Concentrate Disposal: Practices and Regulation, Second Edition.* U.S. Department of the Interior, Bureau of Reclamation, Technical Service Center.

Moghiman, M., Aslani, B. 2013. Influence of Nanoparticles on Reducing and Enhancing Evaporation Mass Transfer and Its Efficiency. International Journal of Heat and Mass Transfer. Pp.114–118.

Mohamed, A.M.O, Maraqa, M., Al Handhaly, J. 2005. Impact of Land Disposal of Reject Brine from Desalination. Desalination 182. Pp.411-433.

Molenda, M.,Stengler,J., Linder,M.,Wörner,A (2013). Reversible hydration behavior of CaCl2 at high H_2O partial pressures for thermochemical energy storage. *Thermochimica Acta*(560), 76-81.

Monteith, J.L., Unsworth, M.H. 2008. Principles Of environmental Physics. London: Elsevier.

Moore, J., Runkles, J.R. 1968. Evaporation from Brine Solutions under Controlled Laboratory Conditions. Texas Water Development Board. P.138.

Morishima, W., Akasaka, M. 2010. Seasonal Trends of Rainfall and Surface Temperature over Southern Africa. African Study Monographs 40, 67–76. African Study Monographs., Pp.67-76.

O'Connor, D. J. 1983. Wind Effects on Gas-Liquid Transfer Coefficients. J. Environ. Eng. 3(109), Pp.731-752.

Oroud, I.M. 1995. Effect of Salinity upon Evaporation from Pans and Shallow Lakes near The Dead Sea. Theor. Appl. Climatol., P.231±240.

Oroud, I.M. 1999. Temperature and Evaporation Dynamics of Saline Solutions. *Journal of Hydrology*, Pp.2-10.

Parkhurst, D.L., Appelo, C.A.J. 2013. Description of Input and Examples for PhreeqC Version 3. A Computer Program for Speciation, Batch-Reaction, One-Dimensional Transport, and Inverse geochemical Calculations. U.S. Geological Survey Techniques And Methods, Book 6, Chap. A43.

Penman, H.L. 1948. Natural Evaporation from Open Water, Bare and Grass. And Grass. Proc. R Soc. Lond. Ser., Pp.120–145.

Petrik, L. F. Fatoba.O.O, Fey.M.V., Ndlovu.N.Z.N ., Omoniyi.E.O., Bent.D., Nel.J. (2015). *Evaporation Rates On Multi-Component Hyper-Saline Effluents.* Pretoria: Water Research Commission.

Randall D.R., Nathoo, J., Lewis, A.E. 2011. A Case Study for Treating Reverse Osmosis Brine Using Eutectic Freeze Crystallization—Approaching a Zero Waste Process. Desalination. Pp.256–262.

Rayner, D.P. 2009. Wind Run Changes: The Dominant Factor Affecting Pan Evaporation Trends in Australia. Queensland Department Of Natural Resource Queensland Department Of Natural Resources, Mines, And Water, Indooroopilly, Australia.

Risacher, F. Clement,A. (2001). A computer program for the simulation of evaporation of natural waters to high concentration. *Computers & Geosciences , 27*, 191-201.

Rohwer, C. 1931. Evaporation from Free Water Surface. Technical Bulletin No. 271.

Rose, P.D. 2002. Integrated algal ponding systems and the treatment of domestic and industrial wastewaters. Part 1: Mesosaline wastewaters – the Spirulina model. Pretoria: *Water Research Commission* (2002).

Rosegrant, M.W. 1997. Water Resources in the Twenty-First Century: Challenges and Implications. International Food and Policy.

Ruffini, A. (2009). Uranium plays in Africa. *Engineering and mining journal*, 210(10), 76 - 78.

Salhotra, M. A. Adams, E.E., Harleman, D.R.F. (1985). Effects of salinity and ionic composition on evaporation: analysis of Dead Sea evaporation pans. *Water Resources Research* (21), 1336-1344.

Salhorta, M. A., Adams,E.E., Harleman, D.R.F. (1987). The alpha, beta, gamma of evaporation from saline water bodies. *Water Resources Research* (23), 1769-1774.

Sandler, S.I., 1989. Chemical and Engineering Thermodynamics. Singapore: Wiley Series in Chemical Engineering.

SANS 241: 2011. SANS 241: 2011,2013. [Online]. [Accessed 14 August 2015]. Available fromWorldWideWeb:<HYPERLINK"https://www.dwa.gov.za/dir_ws/dwqr/subscr/ViewComDoc.asp?Docid=594"

Sartori, E., 2000. A Critical Review On Equations Employed For The Calculation Of The Evaporation Rate From Free Water Surfaces. Solar Energy Vol. 68, No. 1, Pp. 77–89, 2000. 1(68), Pp.77-89.

Schultheis, B., Bach, J., Scherzberg, H., Sondershausen, K-U. 2001. Reproduction Of Solar Evaporation Processes In An Indoor Pilot Examination Plant For An Assessment Of The Usability Of Natural Brines. [Online]. [Accessed 4 June 2011]. Available From World Wide Web:<Hyperlink"Www.K-Utec.Com/Download/Solporteng.Pdf"Www.K Utec.Com/Download/Solporteng.Pdf >

Shaw, E.M. 1983. *Hydrology in Practice*. London: Chapman & Hall.

Shukla, J., Mohandas, V.P., Kumar, A. 2008. Effect of Ph. On The Solubility Of CaSO4 •2h2O In Aqueous NaCl Solutions And Physicochemical Solution Properties At 35 °C. J. Chem. Eng. Data., Pp.2797-2800.

Singh, V. P. (1989). Hydrologic Systems. *Watershed Modelling*.

Stewart,R. B.,Rouse,W.R. (1976). A simple method for determining the evaporation from shallow lakes and ponds. *12*(4), 623-627.

Stanhill, G. (1994). Changes in the rate of evaporation from the Dead Sea. *International Journal of Climatology*(14), 465-471.

Schulze, R.E.; Maharaj, M.; Lynch, S.D.; Howe, B.J.; Melvil-Thomson, B. 1997. *South African atlas for agrohydrologyand climatology*. University of Natal, Pietermaritzburg.

Tanny, J., Cohen, S., Assouline, S., Lange, F., Grava, A., Berger, D., Teltch, B., Parlange, M.B. 2008. Evaporation from a Small Water Reservoir: Direct Measurements and Estimates. Journal of Hydrology. Pp.218-229.

UNESCO. 2005. UNESCO SCIENCE REPORT 2005. *Norwich: United Nations Educational, Scientific and Cultural Organization.*

Van Veelen.M., Dhemba, N. 2011. Water Quality Report. Development of a Reconciliation Strategy.

Wåhlin, A.K., Johansson, A.M., Aas, E., Broström, G., Weber, J.E.H., Grue, J. 2010. Horizontal Convection in Water Heated By Infrared Radiation and Cooled By Evaporation: Scaling Analysis and Experimental Results. Tellus. A (62), Pp.154-169.

Wang, H., Zou, J., Cortina, J.L., Kizito, J. 2015. Experimental and Theoretical Study on Temperature Distribution of Adding Coal Cinder to Bottom of Salt Gradient Solar Pond. *Solar Energy*. Pp.756-767.

Wang, J., Song, J., Huang, Y., Fan, C. 2013. On The Parameterization of Drag Coefficient Over Sea Surface. *Acta Oceanol. Sin*. 32(5), Pp.68-74.

Warburton, M.L., Schulze, R.E., 2005. Detection of Climate Change: A Review Of. 2005. Detection of Climate Change: A Review of Literature on Changes in Temperature, Rainfall and Streamflow, On Detection Methods and Data Problems. Climate Change and Water Resources in Southern Africa: Studies on Scenarios, Impacts, Vulnerabilities and Adaptation. Pp. 257–274 (Chapter 15).

Williamson, N.A., Johnson, M.S, Bradshaw, A.D. 1982. Mine Waste Reclamation: The Establishment of Vegetation on Metal Mine Wastes. Desalination. 299, Pp.75-80.

Xu, C.Y. Sing,V.P., (1997). Evaluation And Generalization Of 13 Mass-Transfer Equations For Determining Free Water Evaporation. *Hydrological Processes* (11), 311-323.

Young, A.A. 1947. Some Recent Evaporation Investigations. Transactions American Geophysical Union. Pp.279–284.

Yu, H. T. (2010). Chemical and thermal stratification in lakes. *The Japanese Society of Limnology*(11), 251–257.

Zayani, L., Rokbani, R., Trabelsi-Ayedi, M. 1999. Study Of The Evaporation Of A Brine Involving The System Na+, Mg2+, K+, Cl–, So4 2--H2o. Journal of Thermal Analysis and Calorimetry. 1(57), pp.575-585.

Zhu, C., Anderson, G. 2002. Environmental Applications of Geochemical Modelling. Cambridge: Cambridge University Press.

APPENDIX 1

MgSO4 Brine (free convection)	**started**	**Ended**	**Difference**
Pressure	4.521 (kPa)	4.413 (kPa)	
Height	448 (mm)	431(mm)	10.63 (mm)
Peaks temp (°C)	29.36;29.8;29.99		
Low temp (°C)	19.38;20.54;20.83;21.18		
H_2O control (free convection)	started	ended	Difference
Pressure	4.521 (kPa)	4.413 (kPa)	
Height difference	4.484 (kPa)	4.357 (kPa)	15 (mm)
Peaks temp (°C)	29.83; 30.23; 30.4		
Low temp (°C)	19.1;20.29;20.49;20.72		

MgSO4 brine (forced convection)	**started**	**ended**	**Difference**
Pressure	4.484(kPa)	4.342 (kPa)	
Height difference			14.5 (mm)
Peaks temp (°C)	22.24; 22.1;21.94;19.55		
Low temp (°C)	17.14;18.69;18.92,19.51		
H_2O control (wind)			
Pressure	4.357(kPa)	4.191 (kPa)	
Height difference			17 (mm)
Peaks temp (°C)	22.88;22.99;22.85		
Low temp (°C)	17.22;1804;18.21;19.02		

NaSO4 brine Free convection	started	ended	Difference
Pressure	4.525 (kPa)	4.325 (kPa)	
Height difference			12 (mm)
Peaks temp (°C)	29.68;30.41;30.21		
Low temp (°C)	14.51;17.48;18.11;18.41		
H_2O control (no wind)			
Pressure	4.369 (kPa)	4.218 (kPa)	
Height			16 (mm)
Peaks temp (°C)	29.39;30.29;30.6		
Low temp (°C)	14.48;17.04;17.34;18.01		

NaSO4 brine Forced convection	started	ended	Difference
Pressure	4.511(kPa)	4.323 (kPa)	
Height difference			19 (mm)
Peaks temp (°C)	22.69;22.54;23.81		
Low temp (°C)	15.56;17.66;17.63;19.17		
H_2O control (wind)			
Pressure	4.375(kPa)	4.167 (kPa)	
Height difference	(mm)	(mm)	21.2 (mm)
Peaks temp (°C)	29.39;30.29;30.6		
Low temp (°C)	14.48;1704;17.34;15.423		

K2SO4 brine Free convection	started	ended	Difference
Pressure	4.531 (kPa)	4.408 (kPa)	
Height difference			12 (mm)
Peaks temp (°C)	28.08;29.68;30.4		
Low temp (°C)	14.7;17.15;18.85;19.89		
H_2O control (no wind)			
Pressure	4.339 (kPa)	4.235 (kPa)	
Height			11 (mm)
Peaks temp (°C)	29.18;31.21;32.05		
Low temp (°C)	13.75;16.47;18.14;19.24		

K2SO4 brine Forced convection	started	ended	Difference
Pressure	4.421(kPa)	4.23 (kPa)	
Height difference			18 (mm)
Peaks temp (°C)	20.85;20.63;22.24		
Low temp (°C)	16.27;16.98;17.2418.25		
H_2O control (wind)			
Pressure	4.382(kPa)	4.185 (kPa)	
Height difference	(mm)	(mm)	20.22 (mm)
Peaks temp (°C)	20.72;20.81;22.62		
Low temp (°C)	15.62;17.13;16.9;17.86		

NaCl brine Free convection	started	ended	Difference
Pressure	4.475 (kPa)	4.413 (kPa)	
Height difference	448 (mm)	431(mm)	14 (mm)
Peaks temp (°C)	32.64, 32.32;32.55		
Low temp (°C)	19.09; 19.99;20.32		
H_2O control (no wind)	started	ended	Difference
Pressure	4.368(kPa)	4.223 (kPa)	
Height difference	446 (kPa)	431(kPa)	17 (mm)
Peaks temp (°C)	32.5; 32.26; 32.48		
Low temp (°C)	17.34; 19.91;20.36		

NaCl brine Forced convection	started	ended	Difference
Pressure	4.48 (kPa)	4.244 (kPa)	
Height difference			19 (mm)
Peaks temp (°C)	24.37; 24.97;24.97		
Low temp (°C)	19.14;20.481;20.18		
H_2O control (wind)			
Pressure	4.374 (kPa)	4.172 (kPa)	
Height difference	(mm)	(mm)	23.63 (mm)
Peaks temp (°C)	23.56; 23.28,23.61		
Low temp (°C)	17.34; 19.91;20.36		

eMalahleni brine Free convection	started	ended	Difference
Pressure	4.48 (kPa)	4.337 (kPa)	
Height difference			14.3 (mm)
Peaks temp (°C)	29.30;30.33;30.72		
Low temp (°C)	20.04;20.92;21.77;22.21		
H_2O control (no wind)			
Pressure	4.369 (kPa)	4.222 (kPa)	
Height			15 (mm)
Peaks temp (°C)	30.88;31.28;31.5		
Low temp (°C)	19.73;21.3;18.22;22.36		

eMalahleni brine Forced convection	started	ended	Difference
Pressure	4.527 (kPa)	4.332 (kPa)	
Height difference			19 (mm)
Peaks temp (°C)	25.34;25.39;25.4		
Low temp (°C)	19.93;22.16;22.24.22.49		
H_2O control (wind)			
Pressure	4.386 (kPa)	4.192 (kPa)	
Height difference	(mm)	(mm)	19.82 (mm)
Peaks temp (°C)	25.35;25.18;25.62		
Low temp (°C)	20.26;21.77;21.86;2209		

NaNO3 brine Free convection	started	ended	Difference
Pressure	4.54 (kPa)	4.404 (kPa)	
Height difference			13.6 (mm)
Peaks temp (°C)	28.73;30.29;30.55		
Low temp (°C)	16.18;16.63;18.48;19.16		
H_2O control (no wind)			
Pressure	4.366 (kPa)	4.222 (kPa)	
Height			14.8 (mm)
Peaks temp (°C)	28.71;30.73;30.13		
Low temp (°C)	14.01;16.56;17.95;18.79		

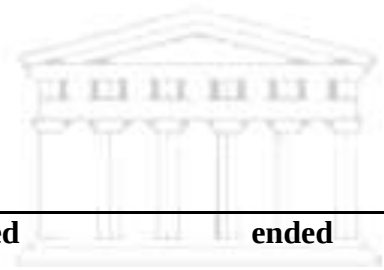

NaNO3 brine Forced convection	started	ended	Difference
Pressure	4.534(kPa)	4.344 (kPa)	
Height difference			18 (mm)
Peaks temp (°C)	21.4;21.34;24.6		
Low temp (°C)	15.56;17.54;17.6;19.22		
H_2O control (wind)			
Pressure	4.373(kPa)	4.175 (kPa)	
Height difference	(mm)	(mm)	20.22 (mm)
Peaks temp (°C)	21.1;21.3;24.5		
Low temp (°C)	15.67;16.6;17.05;18.53		

CaSO4 (no wind)	started	ended	Difference
Pressure	4.378 (kPa)	4.222 (kPa)	
Height difference	4.348 (kPa)	4.203kPa)	14.89 (mm)
Peaks temp (°C)	27.32;28.84;29;62		
Low temp (°C)	13.65;16.66;17.62;18.16		
H2O control (no wind)			
Pressure	4.348 (kPa)	4.203 (kPa)	
Height			15.81 (mm)
Peaks temp (°C)	29.08;29;84;30.29		
Low temp (°C)	13.45;16.43;17.21;17.95		

CaSO4 (wind)	started	ended	Difference
Pressure	4.376(kPa)	4.162 (kPa)	
Height difference			21.85(mm)
Peaks temp (°C)	21.87;20.9;21.42		
Low temp (°C)	15.45;16.94;17.63;17.72		
H2O control (wind)			
Pressure	4.354(kPa)	4.151 (kPa)	
Height difference	(mm)		21.73 (mm)
Peaks temp (°C)	21.57;21.38;21.32		
Low temp (°C)	15.5;16.36;16.57;16.64		

APPENDIX 2

eMalahleni brine analysis input and output with PheerC

	1019000	
units mg/l	7.32	
pH		
Alkalinity	325	
Ca	1154.78	
Mg	466.02	
Na	6159.31	
K	691.78	
N(5)	400	
S(6)	17893.12	
Cl	450	
Elements	Molality	Moles
Alkalinity	6.61E-03	6.61E-03
Ca	2.93E-02	2.93E-02
Cl	1.29E-02	1.29E-02
K	1.80E-02	1.80E-02
Mg	1.95E-02	1.95E-02
N(5)	6.57E-03	6.57E-03
Na	1.40E-01	1.40E-01
S(6)	1.15E-01	1.15E-01

Distribution of of species							
	Log Species	Log Molality	Log Activity	mole Molality	V Activity	Gamma	cm³/mol
	OH-	3.11E-07	2.10E-07	-6.507	-6.677	-0.17	-3.31
	H+	6.11E-08	4.79E-08	-7.214	-7.32	-0.106	0
	H2O	5.55E+01	9.95E-01	1.744	-0.002	0	18.07
C(4)	6.97E-03						
	HCO3-	5.78E-03	4.18E-03	-2.238	-2.379	-0.14	25.83
	CO2	4.23E-04	4.52E-04	-3.373	-3.345	0.029	29.09
	CaHCO3+	3.17E-04	2.33E-04	-3.5	-3.633	-0.133	9.9
	NaHCO3	2.05E-04	2.19E-04	-3.689	-3.66	0.029	1.8
	MgHCO3+	1.85E-04	1.28E-04	-3.732	-3.893	-0.161	5.75
	CaCO3	2.81E-05	3.01E-05	-4.551	-4.522	0.029	-14.6
	CO3-2	1.49E-05	4.10E-06	-4.826	-5.388	-0.562	-3.22
	NaCO3-	9.67E-06	7.10E-06	-5.015	-5.149	-0.134	0.81
	MgCO3	9.57E-06	1.02E-05	-5.019	-4.99	0.029	-17.09
Ca	2.93E-02						
	Ca+2	1.50E-02	4.37E-03	-1.825	-2.36	-0.535	-17.07
	CaSO4	1.40E-02	1.50E-02	-1.853	-1.824	0.029	7.5
	CaHCO3+	3.17E-04	2.33E-04	-3.5	-3.633	-0.133	9.9
	CaCO3	2.81E-05	3.01E-05	-4.551	-4.522	0.029	-14.6
	CaOH+	2.05E-08	1.51E-08	-7.688	-7.822	-0.134	0
	CaHSO4+	6.42E-09	4.71E-09	-8.193	-8.327	-0.134	0
Cl	1.29E-02						
	Cl-	1.29E-02	8.89E-03	-1.889	-2.051	-0.162	18.54
H(0)	3.03E-26						
	H2	1.52E-26	1.62E-26	-25.819	-25.79	0.029	28.61
K	1.80E-02						
	K+	1.60E-02	1.09E-02	-1.797	-1.962	-0.165	9.42
	KSO4-	2.04E-03	1.48E-03	-2.689	-2.83	-0.14	34.58
Mg	1.95E-02						
	MgSO4	1.11E-02	1.18E-02	-1.956	-1.927	0.029	5.84
	Mg+2	8.25E-03	2.62E-03	-2.084	-2.582	-0.499	-20.79
	MgHCO3+	1.85E-04	1.28E-04	-3.732	-3.893	-0.161	5.75
	MgCO3	9.57E-06	1.02E-05	-5.019	-4.99	0.029	-17.09
	MgOH+	2.65E-07	1.97E-07	-6.577	-6.705	-0.128	0
N(5)	6.57E-03						
	NO3-	6.57E-03	4.34E-03	-2.183	-2.362	-0.179	29.99
Na	1.40E-01						
	Na+	1.27E-01	9.31E-02	-0.895	-1.031	-0.136	-0.82

	NaSO4-	1.24E-02	9.00E-03	-1.905	-2.046	-0.14	18.43
	NaHCO3	2.05E-04	2.19E-04	-3.689	-3.66	0.029	1.8
	NaCO3-	9.67E-06	7.10E-06	-5.015	-5.149	-0.134	0.81
	NaOH	1.83E-18	1.96E-18	-17.737	-17.708	0.029	0
O(0)	0.00E+00						
	O2	0.00E+00	0.00E+00	-40.834	-40.805	0.029	30.4
S(6)	1.15E-01						
	SO4-2	7.59E-02	1.93E-02	-1.12	-1.715	-0.595	16.43
	CaSO4	1.40E-02	1.50E-02	-1.853	-1.824	0.029	7.5
	NaSO4-	1.24E-02	9.00E-03	-1.905	-2.046	-0.14	18.43
	MgSO4	1.11E-02	1.18E-02	-1.956	-1.927	0.029	5.84
	KSO4-	2.04E-03	1.48E-03	-2.689	-2.83	-0.14	34.58
	HSO4-	1.22E-07	8.98E-08	-6.913	-7.047	-0.134	40.73
	CaHSO4+	6.42E-09	4.71E-09	-8.193	-8.327	-0.134	0

Saturation indices

Phase	SI**	log	IAP	log K(298 K1 atm)
Anhydrite	0.2	-4.07	-4.28	CaSO4
Aragonite	0.59	-7.75	-8.34	CaCO3
Calcite	0.73	-7.75	-8.48	CaCO3
CO2(g)	-1.88	-3.34	-1.46	CO2
Dolomite	1.37	-15.72	-17.09	CaMg(CO3)2
Gypsum	0.5	-4.08	-4.58	CaSO4:2H2O
H2(g)	-22.69	-25.79	-3.1	H2
H2O(g)	-1.51	0	1.5	H2O
Halite	-4.65	-3.08	1.57	NaCl
O2(g)	-37.91	-40.8	-2.89	O2
Sylvite	-4.91	-4.01	0.9	KCl

****For a gas, SI = log10(fugacity). Fugacity = pressure * phi / 1 atm.**
For ideal gases, phi = 1.